Developmental control of Drosophila olfactory projection neurons by TALE-class transcription factors

Developmental Control of *Drosophila* Olfactory Projection Neurons by TALE-Class Transcription Factors

A Dissertation Submitted to
the Graduate School of Life and Environmental Sciences,
the University of Tsukuba
in Partial Fulfillment of the Requirements
for the Degree of Doctor of Philosophy in Science
(Doctoral Program in Structural Biosciences)

Mai ANDO

Table of Contents

Abbreviations

TALE,	Three Amino Acid Loop Extension
Hth,	Homothorax
Exd,	Extradenticle
Ems,	Empty spiracles
Mira,	Miranda
Fas II,	Fasciclin II
ORNs,	Olfactory Receptor Neurons
AL,	Antennal Lobe
PNs,	Projection Neurons
MB,	Mushroom Body
LH,	Lateral horn
Ad,	Anterodorsal
Lat,	Lateral
Ven,	Ventral
NB,	Neuroblast
MARCM,	Mosaic Analysis with a Repressive Cell Marker
LOF,	Loss-of-Function
GOF,	Gain-of-Function
AEL ,	After Egg Laying
APF,	After Puparium Formation

Abstract

Precise neuronal connectivity in the nervous system depends on specific axonal and dendritic targeting of individual neurons. In the *Drosophila* brain, olfactory projection neurons convey odor information from the antennal lobe to higher order brain centers such as the mushroom body and the lateral horn. Here, I show that Homothorax (Hth), a TALE-class homeodomain transcription factor, is expressed in many of the antennal lobe neurons including projection neurons and local interneurons. In addition, HTH is expressed in the progenitors of the olfactory projection neurons, and the activity of *hth* is required for the generation of the lateral but not for the anterodorsal and ventral lineages. MARCM analyses show that the *hth* is essential for correct dendritic targeting of projection neurons in the antennal lobe. Moreover, the activity of *hth* is required for axonal fasciculation, correct routing and terminal branching of the projection neurons. I also show that another TALE-class homeodomain protein, Extradenticle (Exd), is required for the dendritic and axonal development of projection neurons. Mutation of *exd* causes projection neuron defects that are reminiscent of the phenotypes caused by the loss of the *hth* activity. Double immunostaining experiments show that Hth and Exd are coexpressed in olfactory projection neurons and their progenitors, and that the expressions of Hth and Exd require the activity of each other gene. These results thus demonstrate the functional importance of the TALE-class homeodomain proteins in cell-type specification and precise wiring of the *Drosophila* olfactory network.

Introduction

The precise specification and wiring of a large number of neurons are crucial processes for the construction of the functional brain network. Owing to the remarkable conservation in the organization and connectivity with the vertebrate brain, the *Drosophila* olfactory system provides an ideal model to investigate the molecular mechanisms that underlie the wiring specificity in the nervous system (Masse et al., 2009; Vosshall and Stocker, 2007). As in vertebrate olfactory systems, each of the *Drosophila* olfactory receptor neurons (ORNs) expresses only a single type receptor, and projects their axons to a specific olfactory glomerulus in the antennal lobe (AL), the first order relay station of olfactory information in the fly brain (Fig. 1). The *Drosophila* AL consists of only ~50 glomeruli, which can be identified by their location and shape (Laissue et al., 1999). Each of the glomeruli is contributed by the neural processes of four cell types: the axonal terminals of ORNs, the dendritic processes of projection neurons (PNs), multi-glomerular processes of local interneurons, and glia processes ensheathing the glomeruli (Jhaveri et al., 2000; Lai et al., 2008; Laissue et al., 1999; Stocker et al., 1990). Axons of ~50 classes of ORNs and dendrites of ~50 classes of PNs converge to form specific connectivity in each of the AL glomeruli (Couto et al., 2005; Fishilevich and Vosshall, 2005; Laissue et al., 1999). The PN axons convey olfactory information from the AL to higher brain centers by targeting stereotypic locations in the mushroom body (MB) and lateral horn (LH) (Jefferis et al., 2007; Lin et al., 2007; Marin et al., 2002; Wong et al., 2002).

Specific glomerular targeting of ORNs and PNs proceeds in multi-step processes. Before the arrival of ORNs at the developing AL, neuronal processes of PNs independently form a prototypic map by selective dendritic arborization, based on information cues external to the ALs (Jefferis et al., 2001). The specification of individual PN types is therefore thought to be controlled by intrinsic programs that, in turn, regulate the expression of different cell surface molecules on different PNs to instruct dendritic and axonal targeting specificity (Hong et al., 2009; Komiyama et al., 2007; Zhu et al., 2006a; Zhu and Luo, 2004). Accordingly, PNs are pre-specified by lineage and birth order to form synaptic connections with specific incoming ORN axons (Jefferis et al., 2001). A BTB-Zn-finger protein, Chinmo, regulates the birth order-dependent wiring of PNs, and a loss of *chinmo* causes early-born PNs to adopt the targeting specificity of late-born PNs within the same cell lineage (Zhu et al., 2006b). In addition, several transcription factors have been identified that control the dendritic connectivity of the *Drosophila* olfactory PNs (Komiyama and Luo, 2007; Komiyama et al., 2003; Spletter et al., 2007).

homothorax (*hth*) and *extradenticle* (*exd*) were originally identified as mutations that cause homeotic transformation of specific body segments in *Drosophila*, without altering the expression patterns of the homeotic genes themselves (reviewed in Mann and Affolter, 1998; Mann et al., 2009; Moens and Selleri, 2006). Along with their vertebrate homologs, Meis /Prep and Pbx proteins, Hth and Exd comprise the PBC subclass of the TALE (Three Amino Acid Loop Extension) homeodomain proteins based on the presence of the conserved PBC motif N-terminal to the homeodomain. Hth and Exd form a heterocomplex to regulate developmental and DNA binding specificity of homeotic proteins. Nuclear localization and/or stability of the two proteins often

depends on the Hth/Exd protein-protein interaction, making them obligate partners that work together as a functional complex regulating a number of downstream target genes. Furthermore, Hth/Meis/Prep and Exd/Pbx function as partners for a variety of transcription factors other than the homeotic proteins (Mann and Affolter, 1998; Mann et al., 2009; Moens and Selleri, 2006).

In addition to metameric development, *hth* and *exd* are required for the development of neuronal systems such as the ventral nerve cord (Aspland and White, 1997; Kurant et al., 1998; Rauskolb et al., 1993; Rieckhof et al., 1997) and the eyes (Lopes and Casares, 2010; Peng et al., 2009; Wernet et al., 2003). Furthermore, *exd* and *hth* are required for the development of the primary axonal scaffolds in the embryonic *Drosophila* brain, controlling other transcription factors, such as *orthodenticle, empty spiracles* (*ems*) and *eyeless,* these are essential for patterning the embryonic brain (Nagao et al., 2000). Recent study also shows that *hth* is required for the specification of the neuronal subtypes in the optic lobe by regulating various targets including *Brain-specific-homeobox* and *N-cadherin* (Hasegawa et al., 2011).

In this study, I investigated the functions of *hth* and *exd* in the development of *Drosophila* olfactory PNs. I show that Hth and Exd are coexpressed in the AL neurons including postmitotic PN and their progenitor cells. Mutations of *hth* cause marked dendritic targeting defects of olfactory PNs with concomitant axonal fasciculation and targeting defects. In the olfactory PNs, Hth is co-expressed with Exd, and loss of *exd* activity phenocopies the dendritic and axonal defects caused by loss of *hth* activity. Moreover, expression of Hth and Exd depend on the activity of each other gene in both developing and mature PNs. These results demonstrate the importance of the evolutionary conserved TALE-class homeodomain proteins in cell-type specification

and wiring in the olfactory network of the fly brain.

Materials and Methods

Fly stocks

Three *hth* alleles were used: hth^{P2}, $hth^{P1\text{-}K6\text{-}1}$ and $hth^{P1\text{-}\Delta15\text{-}3}$ (Kurant et al., 1998). hth^{P2} is a lethal P-element insertion allele while $hth^{P1\text{-}K6\text{-}1}$ and $hth^{P1\text{-}\Delta15\text{-}3}$ are lethal excision alleles (Kurant et al., 1998). No protein expression was detected for hth^{P2} and $hth^{P1\text{-}K6\text{-}1}$ while weak signals were detected for $hth^{P1\text{-}\Delta15\text{-}3}$ presumably due to its truncated product (data not shown). exd^{1} also is a protein null allele with strong phenotypes (Rauskolb et al., 1993). In addition, following *Drosophila* strains were used: *UAS-En-Hth* (Inbal et al., 2001), $acj6^{6}$ (Ayer and Carlson, 1991), and $lola^{ore76}$ (Spletter et al., 2007). *UAS-hth* (Pai et al., 1998) was used for rescue and overexpression experiments. *GH146-GAL4* (Stocker et al., 1997) and *MZ19-GAL4* (Ito et al., 1998) were used for the visualization of PNs. A ubiquitous driver, *tubP-GAL4* (Lichtneckert et al., 2008), and a pan neural driver, $elav^{c155}$*-GAL4* (Lin and Goodman, 1994), were also used to visualize clones in some of the experiments. MZ699 (Ito et al., 1997) and GH298 (Stocker et al., 1997) were used to label ventral PNs and AL local interneurons, respectively. Unless otherwise noted, flies were raised at 25°C.

MARCM mosaic analysis

Clones were generated using Mosaic Analysis with a Repressive Cell Marker (MARCM) method (Lee and Luo, 1999).

The following genotypes were examined for loss-of-function (LOF),

overexpression and rescue analyses using *GH146-GAL4*: (1) Wild type: *hs-FLP UAS-mCD8::GFP; GH146-GAL4/+; FRT82B GAL80/FRT82B*. (2) *hth* LOF: *hs-FLP UAS-mCD8::GFP; GH146-GAL4/+; FRT82B GAL80/FRT82B hth*. (3) *hth* overexpression: *hs-FLP UAS-mCD8::GFP; GH146-GAL4/UAS-hth; FRT82B GAL80/FRT82B*. (4) *hth* rescue: *hs-FLP UAS-mCD8::GFP; GH146-GAL4/UAS-hth; FRT82B GAL80/FRT82B* hth^{P2}. (5) *acj6* LOF: $acj6^{6}$ *FRT19A/FRT19A GAL80 hs-FLP; FRTG13 GH146-GAL4 UAS-mCD8::GFP/UAS-mCD8::GFP.* (6) *lola* LOF: *hs-FLP UAS-mCD8::GFP/+; FRT42D* $lola^{ore76}$ *GH146-GAL4 UAS-mCD8::GFP/FRT42D GAL80.* (7) *exd* LOF: *FRT19A* exd^{1} */FRT19A GAL80 hs-FLP; FRTG13 GH146-GAL4 UAS-mCD8::GFP/* +. Egg collection was performed for 6 hours on standard food. For the induction of mitotic recombination, newly hatched larvae were heat shocked at 37°C for 1-1.5h at 24 hours after the end of egg collection.

The following genotypes were examined for LOF analyses using *MZ19-GAL4*: (1) Wild type: *yw, hs-FLP, UAS-mCD8::GFP; MZ19-GAL4, UAS-mCD8::GFP/+; FRT82B GAL80/FRT82B*. (2) *hth* LOF: *yw, hs-FLP, UAS-mCD8::GFP; MZ19-GAL4, UAS-mCD8::GFP/+; FRT82B GAL80/FRT82B* $hth^{P1\text{-}K6\text{-}1}$. Egg collection was performed for 24 hours on standard food. For the induction of mitotic recombination, larvae were heat shocked at 37°C for 1h at 48 hours after egg collection.

The following genotypes were examined for *hth* or *p35* rescue using *tubP-GAL4*: (1) Wild type: *hs-FLP; tubP-GAL4, UAS-mCD8::GFP/+; FRT82B GAL80/FRT82B.* (2) *hth* LOF, *hs-FLP; tubP-GAL4, UAS-mCD8::GFP/+; FRT82B GAL80/FRT82B* $hth^{P1\text{-}K6\text{-}1}$. (3) *hth* rescue*: hs-FLP; tubP-GAL4, UAS-mCD8::GFP/UAS-hth; FRT82B GAL80/FRT82B* $hth^{P1\text{-}K6\text{-}1}$. (4) *p35* rescue*:*

hs-FLP; tubP-GAL4, UAS-mCD8::GFP/UAS-p35; FRT82B GAL80/FRT82B hth$^{P1\text{-}K6\text{-}1}$. Egg collection was performed for 24 hours on standard food. For the induction of mitotic recombination, newly hatched larvae were heat shocked at 37°C for 30 min at 24 hours after egg collection.

The following genotypes were examined for *hth* rescue using *elav*^{C155}*-GAL4*: (1) Wild type: *hs-FLP UAS-mCD8::GFP/+; elav*^{C155}*-GAL4 UAS-mCD8::GFP/+; FRT82B GAL80/FRT82B*. (2) *hth* LOF, *hs-FLP UAS-mCD8::GFP/+; elav*^{C155}*-GAL4 UAS-mCD8::GFP/+; FRT82B GAL80/FRT82B hth*^{P2}. *(3) hth* rescue*: hs-FLP UAS-mCD8::GFP/+; elav*^{C155}*-GAL4 UAS-mCD8::GFP/UAS-hth; FRT82B GAL80/FRT82B hth*^{P2}. Egg collection was performed for 6 h on standard food. For the induction of mitotic recombination, newly hatched larvae were heat shocked at 37°C for 1h at 24 h after the end of egg collection.

Immunocytochemistry and confocal microscopy

Immunostaining and confocal imaging were performed as described in Kurusu et al. (Kurusu et al., 2002). The following antibodies were used: mouse anti-nc82 (Wagh et al., 2006) at 1:20; rat anti-mCD8α (Caltag) at 1:100; chick anti-GFP (Abcam) at 1:500; rabbit anti-Hth (Kurant et al., 1998) at 1:1000; rat anti-Hth (gift from Stephen M. Cohen) at 1:500; mouse anti-Exd (Aspland and White, 1997) at 1:5; mouse anti-Acj6 (Certel et al., 2000) at 1:5, rabbit anti-Lola (common region) at 1:50 (Spletter et al., 2007), rat anti-EMS (U. W. unpublished) at 1:20, and rabbit anti-Miranda (Ikeshima-Kataoka et al., 1997) at 1:200. Alexa-546, 633 or 433-conjugated secondary antibodies (Jackson ImmunoResearch) were used at dilution

of 1:1000. Confocal images were captured using a Zeiss LSM510 and processed with Adobe-Photoshop.

Results

Hth is expressed in AL neurons

Previous studies demonstrated that the Hth protein is expressed in several cell clusters in the developing deuto- and tritocerebrums that pioneer the axonal tract between the AL and the dorsal brain regions (Nagao et al., 2000). To extend this observation into postembryonic stages, I analyzed Hth expression in the larval and the adult brains, and found that Hth was expressed in many of the cells that surround the AL (Fig. 2). Expression analysis using an AL driver, *GH146-GAL4* (Stocker et al., 1997), which is expressed in ~60% of the olfactory PNs (Jefferis et al., 2001), confirmed that Hth was expressed in the antero dorsal (ad) and the lateral PNs (Figs. 3A-E), the two major olfactory PN lineages in the *Drosophila* brain (Jefferis et al., 2001; Lai et al., 2008; Marin et al., 2002). In the lateral lineage, Hth was also expressed in the GH298-positive interneurons (Figs. 4A and 4C; summary diagram in Fig. 5). Moreover, expression of Hth was observed in a small group of ventral cells that in part overlapped with the *GH146*-positive PNs (Fig. 3E; summary diagram in Fig. 5). These ventral Hth neurons also overlapped with a subset of the ventral PNs labeled with MZ699 in the adult brain (Figs. 4B and 4D). In addition to these expressions in postmitotic AL neurons, examination of the developing larval brain showed that Hth was expressed in the neurobrasts (NBs) of the anterodorsal and lateral AL lineages (Fig. 6).

Hth is required for the generation of the lateral NB lineage

Prompted by the expression of Hth in the anterodorsal and the lateral AL-NBs, I examined its functions in the generation of the two major AL lineages using the MARCM technique (Lee and Luo, 1999). Wild-type and mutant clones were induced with heat-shock in the 1st instar stage using *tubP-GAL4*, a ubiquitous driver, in conjunction with a membrane-targeted *mCD8::GFP* reporter. Whereas the heat-shock scheme generated NB clones of the three olfactory lineages for wild type, only the anterodosal and the ventral NB clones were recovered for $hth^{P1\text{-}K6\text{-}1}$, a protein null allele (Kurant et al., 1998) (Table 1). Moreover, expression of *UAS-hth* in the $hth^{P1\text{-}K6\text{-}1}$ mutant background restored the recovery of the lateral NB clones, suggesting that *hth* was essential for the generation of the lateral lineage. To determine whether the loss of the lateral NB clones was caused by apoptosis, I induced expression of a pan-caspase inhibitor, p35, in $hth^{P1\text{-}K6\text{-}1}$ mutant background. Intriguingly, blocking of cell death in the mutant background resulted in recovery of lateral NB clones in the developing brain at an efficacy comparable to the wild type (Table 2), suggesting that the loss of lateral NB lineage in *hth* mutant was caused by apoptosis.

The result that *hth* was essential for the generation of the lateral lineage is reminiscent of the proliferation phenotype of *ems* AL clones (Lichtneckert et al., 2008). Ems is transiently expressed in the progenitors of the anterodorsal and the lateral lineages at the larval stages, and its expression is essential for the generation of the lateral but not the ad-NB clones (Lichtneckert et al., 2008). To determine whether *hth* is required for the expression of *ems*, I analyzed Ems expression in the *hth* mutant clones at the larval stage. Despite that Hth was expressed in both the anterodorsal and the lateral progenitors at the corresponding stage (Figs. 6A, B), the expression of Ems

in the ad-NB was not altered by the loss of the *hth* activity (Fig. 7A). Moreover, Ems was detected in the lateral NBs of the $hth^{P1\text{-}K6\text{-}1}$ mutant clones rescued with p35 (Fig. 7B). These results thus suggest that, although *hth* and *ems* are similarly required for the generation of the lateral AL lineage, *hth* dose not regulate *ems* expression in either the anterodorsal and the lateral lineages.

Loss of *hth* suppresses *GH146* expression in a subset of olfactory PNs

The results that Hth was expressed not only in the progenitors but also in many of the postmitotic PNs suggested that Hth might have important functions in the specification of olfactory PNs. To investigate *hth* functions in the differentiation of the olfactory PNs, I then generated $hth^{P1\text{-}K6\text{-}1}$ mutant clones using the olfactory PN driver *GH146*. While only the lateral mutant lineage was missing with the ubiquitous driver *tubP-GAL4* (Table 1), both the lateral and the ventral NB clones were missing with the *GH146-GAL4* driver (Table 3). In addition, this driver resulted in anterodorsal PN-NB clones with markedly reduced sizes; the numbers of the *GH146*-labeled cells were significantly reduced at the adult stage in the $hth^{P1\text{-}K6\text{-}1}$ (8.0 ± 0.7 cells, n=8) and $hth^{P1\text{-}\Delta15\text{-}3}$ (10.8 ± 3.4 cells, n=8) clones, compared to the wild clones (26.6 ± 1.3 cells, n=9, $p < 0.001$).

Although both the reduction in the cell numbers of the mutant ad-PN clones and the failure of the recovery of the ventral *hth* mutant clones with the *GH146* driver could be caused by proliferation defect, it was also plausible that the loss of the *hth* activity suppressed the expression of the *GH146-GAL4* driver in the anterodorsal and the ventral PNs. Contrary to the apparent reduction in the numbers of GFP-labeled PNs, neither $hth^{P1\text{-}K6\text{-}1}$ nor $hth^{P1\text{-}\Delta15\text{-}3}$ ad-PN mutant clones affected the overall AL size, with

most of the glomeruli, including those innervated by the ad-PNs, remaining identifiable (see Fig. 8C). Moreover, no reduction in the numbers of labeled cells was detected at the adult stage for another allele, hth^{P2} (25.1 ± 1.2 cells, n=14, compared to the wild clones, 26.6 ± 1.3 cells, n=9), though this allele exhibited a significant reduction in the numbers of the labeled cells at the mid-pupal stage (11.5 ± 2.4 cells, n=8, 50 h after puparium formation (APF)), compared to wild type at the corresponding stage (28.7 ± 0.9 cells, n=7, $p < 0.001$, 50 h APF).

In order to clarify the effect of *hth* mutations on the proliferation of the anterodorsal and the ventral PNs, I examined exact cell numbers using the ubiquitous driver *tubP-GAL4*. No significant reduction was observed even for the $hth^{P1\text{-}K6\text{-}1}$ mutation both at the adult stage ($hth^{P1\text{-}K6\text{-}1}$, 53.7 ± 2.0 cells, n=18, compared to wild type, 50.8 ± 1.5 cells, n=14) and at the mid-pupal stage (50 h APF) ($hth^{P1\text{-}K6\text{-}1}$, 51.0 ± 2.0 cells, n=9, compared to wild type, 51.9 ± 1.3 cells, n=11). Moreover, no reduction was observed for the ventral *hth* clones as well ($hth^{P1\text{-}K6\text{-}1}$, 45.3 ± 1.9 cells, n=8, compared to wild type, 43.8 ± 1.5 cells, n=10, at the adult stage). These results thus suggest that *hth* is not necessary for the generation of the correct number of cells in both the anterodorsal and the ventral lineages. Rather, it is more likely that *hth* regulates the expression of the *GH146-GAL4* driver in a subset of the anterodorsal and the ventral PNs.

Loss of *hth* causes dendritic targeting defects

Although hth^{P2} clones exhibited reduced number of *GH146*-labeled ad-PNs at the mid pupal stage, the result that the correct number of ad-PN labeling was resumed at the adult stage allowed us to further investigate the functions of *hth* in dendritic

targeting of olfactory PNs using this allele. For this aim, I focused on the ad-PNs, which is one of the two major olfactory PN groups and the only *hth* mutant PNs identifiable with the *GH146-GAL4* diver (Table 3). For a systematic evaluation of the dendritic defects of the ad-PNs, I focused on 13 landmark glomeruli. In the wild type, nine of the landmark glomeruli (VA1d, VA1lm, VA3, VM2, DM6, D, DC3, DL1, and VM7) are innervated by the *GH146* ad-PNs, whereas four glomeruli (VA2, DA1, DM5, DM2) are never or rarely innervated by the *GH146* ad-PNs (Fig. 8A, Figs. 9A and 9D). Instead, they are innervated either by the embryonic (VA2) or by the lateral PNs (Jefferis et al., 2001; Komiyama et al., 2003).

I also excluded mutant ALs of reduced sizes that were recovered along with the samples of the normal AL size. Histochemical examination with an anti-Hth antibody revealed loss of a large group of lateral AL neurons for the reduced ALs (Figs. 10A-C), suggested dual induction of *hth* mutant clones to both the anterodorsal and the lateral AL lineages. Many of the lateral-type glomeruli, such as DM5 and DA1, were missing in the reduced ALs accordingly.

In contrast to distinctive dendritic targeting by the wild type clones (Fig. 8A), hth^{P2} ad-NB clones exhibited reduction or loss of targeting on many of the on-target glomeruli (Fig. 8B). Marked innervation defects were particularly evident for VA1lm, VA3, and D (Fig. 9B). Furthermore, hth^{P2} ad-NB clones exhibited ectopic innervation in the off-target landmark glomeruli (Fig. 9E). A previous study (Zhu and Luo, 2004) suggested that N-cadherin is essential for olfactory PNs to restrict their dendrites in the AL. However, no alternation in the expression of N-Cadherin was found in the hth^{P2} ad-NB clones (Figs. 11A-C).

To further examine the functions of *hth* in dendritic targeting, I also examined

hth$^{P1\text{-}K6\text{-}1}$ NB clones, and found that, consistent with the reduced numbers of the labeled cells, *hth*$^{P1\text{-}K6\text{-}1}$ PN clones showed more prominent under-innervation than the *hth*^{P2} clones in many of the on-target glomeruli (Fig. 8C and Fig. 9C). On the other hand, despite under-labeling of the *GH146* ad-PNs, *hth*$^{P1\text{-}K6\text{-}1}$ PN clones exhibited ectopic innervation in DA1 (white arrows in Figs. 8C1, C2; quantification in Fig. 9F), confirming *hth* functions in the restriction of dendritic targeting of the olfactory PNs. Similar results were obtained with *hth*$^{P1\text{-}\Delta 15\text{-}3}$ PN clones (data not shown).

Although the innervation defects of the mutant ad-NB clones suggested functional significance of *hth* in precise dendritic targeting, it was difficult to determine whether the apparent dendritic input in a given glomerulus was contributed by normal or ectopic targeting because of mixed innervation by multiple mutant PNs involved in the NB clones. This was particularly the case with irregularly or partially innervated glomeruli such as DL1, VA1d and DC3. In order to analyze PN targeting at a higher resolution, I examined single-cell clones, which represented post-mitotic neurons. While the wild-type single-cell clones induced at the early 1st instar always innervated DL1 (Figs. 12A and D) (Jefferis et al., 2001; Komiyama et al., 2003), the majority of the *hth*^{P2} single-cell clones failed to innervate the target glomeruli (Figs. 12B and D). Instead, all of the *hth*^{P2} single-cell clones innervated nearby ectopic glomeruli, such as DC3, which were never innervated by the wild-type clones (Figs. 12B and E). These results were also confirmed with the *hth*$^{P1\text{-}K6\text{-}1}$ single-cell clones (Figs. 12C, D and E).

To further analyze the functions of *hth* in dendritic targeting, I utilized another PN driver, *MZ19* (Ito et al., 1998), which labels only two types of ad-PNs that innervate either VA1d or DC3 along with a lateral PN that innervates DA1 (Jefferis et

al., 2004). While wild-type *MZ19* single-cell clones innervated either VA1d or DC3 (Figs. 13A and C), *hth*$^{P1\text{-}K6\text{-}1}$ mutant ad-PNs failed to innervate these target glomeruli and exhibited ectopic innervation in nearby glomeruli (Figs. 13B, D-F). Furthermore, I recovered post-mitotic single-cell clones of the lateral DA1-type PN, and found dendritic mistargeting by the mutant DA1-type PN (Figs. 14A-D). These results thus suggest that *hth* is required for correct targeting of both anterodorsal and lateral PNs such as DA1-type PN. The recovery of the lateral DA1-type PN also implies that, although *hth* is required for the generation of the lateral lineage, it is not required for the survival of postmitotic lateral neurons at least for the DA1-type PN once they are generated.

Loss of *hth* causes axonal defects

In addition to the glomerular targeting defects, mutations of *hth* caused severe defects in axonal patterns. The axons of wild-type PNs were bundled in a single fascicle and exhibited a stereotype projection that targets the LH via the MB calyx (Fig. 15A). In contrast, both the *hth*^{P2} and *hth*$^{P1\text{-}K6\text{-}1}$ clones exhibited marked defasciculation of their axons (Figs. 15B-D). Expression of Fasciclin II (Fas II), a cell adhesion molecule important for axonal fasciculation (Kurusu et al., 2002; Lin et al., 1994), was detected only faintly on the mutant axons (Fig. 16). Axonal routing via the MB calyx was perturbed in many of the mutant clones (Fig. 15E). Moreover, although most *hth* mutant axons still converged in the LH, aberrant extensions in the ventrolateral brain (arrowhead in Figs. 15B, and C) were induced for the majority of the *hth*^{P2} and *hth*$^{P1\text{-}K6\text{-}1}$ mutant clones (Fig. 15F). Similar results were obtained with *hth*$^{P1\text{-}\Delta 15\text{-}3}$ PN clones (data not shown).

In contrast to the NB clones, single-cell clones of the *hth* mutants exhibited wild-type like axonal targeting (Figs. 17A-D) with normal number of boutons on the MB calyx (Fig. 17E). However, consistent with the loss of DL1 innervation, they exhibited altered branching pattern in the LH region (arrows in Figs. 17B and C) and increase in the numbers of the terminal branches (Fig. 17F). Similar alteration in PN identity was observed for the single-clones of the lateral PN lineage labeled with *MZ19-GAL4* (Fig. 18). While retaining wild type-like axonal targeting via the MB calyx, the mutant DA1-type PNs exhibited alterations in the terminal branching patterns with a significant increase in the maximum branch length (Fig. 18E). The numbers of the boutons in the MB calyx were also altered (Fig. 18D).

These data demonstrate that, in addition to its functions in dendritic targeting, *hth* is required for the normal fasciculation and targeting of the olfactory PN axons.

Developmental rescue of dendritic and axonal defects with *hth* expression

To confirm the importance of *hth* in PN development, I tried to rescue the dendritic and axonal defects of *hth* mutant clones by driving a *UAS-hth* transgene in hth^{P2} mutant background. I first used the *GH146-GAL4* driver for the rescue experiments but failed to obtain satisfactory rescue results; only 27% of the clones driving *UAS-hth* (3/11) showed restoration of the normal axonal projection pattern (Fig. 19C), with the other clones (8/11) suffering from mild to severe axonal defects (Fig. 19D). Rescue efficacy in dendritic targeting was also variable; wild-type like innervation was restored only for a subset of the on-target glomeruli (Figs. 20A-E). Aberrant dendritic innervation in ectopic glomeruli was in part suppressed but still observed for many of the off-target glomeruli (Fig. 20F). Analysis of single-cell clones

showed that half of the clones (3/6) restored dense or moderate DL1 targeting. Wild-type like axonal projection and LH terminal branching were also restored in such clones (Figs. 21C and F).

Whereas Hth was expressed in most ad-PNs and their progenitor cells, *GH146-GAL4* was expressed in only a subset of the post-mitotic ad-PNs (Lai et al., 2008; Lichtneckert et al., 2008), and might not be suitable for effective restoration of the normal dendritic and axonal patterns in the *hth* mutant background. I therefore tried to rescue *hth* mutant defects using *elav-GAL4*, a pan-neuronal driver expressed in both pre- and postmitotic cells (Dumstrei et al., 2003; Kurusu et al., 2002, 2009). Despite that *elav-GAL4* was expressed in all PNs, wiled-type clones induced at the early 1st instar exhibited prominent labeling of the DL2dv glomerulus (Figs. 22A and D). As in the *GH146* clones, loss of *hth* caused severe axonal and dendrite defects in *elav-GAL4* marked PN clones (Figs. 22B and E). Notably, *hth* expression driven by the *elav-GAL4* driver effectively restored wild type-like axonal and dendritic patterns (Figs. 22C and F). the majority of the *hth* ad-NB clones restored not only the normal axonal projection pattern (Figs. 22C and G) but also the correct dendritic targeting of the DL2dv glomerulus (Figs. 22F and H). Aberrant innervation in the nearby DL1 glomerulus was also suppressed by this driver (Figs. 22F and I). Thus, these results confirmed that the axonal and dendritic defects in the *hth* mutant clones were indeed caused by the loss of the *hth* function.

Dendritic and axonal phenotypes of *hth* overexpression in ad-PNs

Having examined loss-of-function (LOF) phenotypes of *hth*, I then examined gain-of-function (GOF) phenotypes by overexpressing *hth* in the wild-type background.

In contrast to the multi glomerular defects with LOF NB clones, dendritic targeting by the GOF NB clones was normal for most of the on-target glomeruli except for VA3 (arrow in Fig. 23B2; quantification in Fig. 23C). Mild ectopic innervation was caused in DA1, one of the off-target glomeruli (Fig. 23D). On the other hand, all the GOF single-cell clones induced at the early 1st instar innervated the correct target DL1 (Figs. 24A-D).

The PN axons of the GOF-NB clones remained fasciculated, correctly targeting the LH via the MB calyx (Fig 25). However, the arborization patterns in the LH region were slightly altered (arrow in Fig. 25) with an increase in the number of the terminal branches whereas the number of boutons on the MB calyx was not affected (Fig. 26). These data suggest that precise control of the *hth* expression level is critical for correct dendritic targeting and terminal branching only in a select group of PNs.

hth interacts with exd in PN development

Exd is another TALE-class homeodomain transcription factor that acts as a cofactor of homeotic proteins (Kurant et al., 1998; Mann and Affolter, 1998; Mann and Chan, 1996; Pai et al., 1998; Rauskolb et al., 1993; Rieckhof et al., 1997). In the specification of segmental identity, Exd forms a heterocomplex with Hth to confer regulatory specificity to homeotic proteins (Kurant et al., 1998; Mann and Affolter, 1998; Mann and Chan, 1996; Pai et al., 1998; Rauskolb et al., 1993; Rieckhof et al., 1997). In addition, Exd is co-expressed with Hth in the embryonic brain to regulate primary axonal patterning (Nagao et al., 2000).

In order to determine functional interaction between *hth* and *exd* in PN

development, I analyzed PN phenotypes of *exd*^{1} mutant clones using *GH146-GAL4* as a driver. As was the case with *hth*, loss of *exd* resulted in the loss of the lateral lineage while recovering the ad-PN clones at a normal efficacy (Table 3). The mutation of *exd*^{1} also caused loss of the ventral PN clones when labeled with the *GH146-GAL4* driver. Moreover, similar to *hth*$^{P1\text{-}K6\text{-}1}$ and *hth*$^{P1\text{-}\Delta 15\text{-}3}$, *exd*^{1} showed a significant reduction in the number of the GFP labeled cells in the *GH146*-driven ad-PN clones at the adult stage (4.1±0.5 cells per clone, n=11, compared to the wild type, 26.6±1.3 cells per clone, n=9, $p<0.001$).

The dendritic phenotype of *exd*^{1} mutant PNs was reminiscent of the *hth*$^{P1\text{-}K6\text{-}1}$ PNs (Fig. 27B). Because of the reduction in the number of the GFP labeled cells, *exd*^{1} mutant clones showed severe loss of dendritic targeting in many of the on-target glomeruli (Fig. 27C). Yet, as with the *hth*$^{P1\text{-}K6\text{-}1}$ and *hth*$^{P1\text{-}\Delta 15\text{-}3}$ mutant clones, *exd*^{1} PN clones exhibited ectopic innervation in DA1 (white arrows in Figs. 27B1 and B2; quantification in Fig. 27D). Analysis of single-cell clones demonstrated that the majority of the *exd*^{1} clones failed to innervate DL1, with ectopic innervation in nearby glomeruli, such as DC3 (Figs. 28A-D).

As was the case with loss of *hth*, loss of *exd* caused severe defects in axonal fasciculation and routing (Figs. 29B–D). In addition, many of the *exd*^{1} ad-NB clones also exhibited ectopic ventrolateral extensions (arrowhead in Fig. 29B; quantification in Fig. 29E). Moreover, *exd*^{1} single-cell clones showed aberrant arborization in the LH region with significant increase in the numbers of the terminal branches (Figs. 30A, B and E). Although axonal routing was unaffected (Fig. 30C), the number of boutons on the MB calyx was reduced in the *exd*^{1} single-cell clones (Fig. 30D). This calyx phenotype was not observed in *hth*^{P2} and *hth*$^{P1\text{-}K6\text{-}1}$ DL1 clones (Fig. 17E) but was

similar to that of *hth*$^{P1\text{-}K6\text{-}1}$ DA1 clones (Fig. 18D).

Double immunostaining using anti-Exd and anti-Hth antibody revealed that Exd and Hth were co-expressed in the ad-PNs of both developing and adult brains (Figs. 31A–D). Exd and Hth were also expressed in the anterodorsal and lateral progenitors at the larval stage (Fig. 32). The expression of Exd was abolished in the *hth*^{P2} ad-NB clones (Figs. 33A and B) and the *hth*^{P2} single-cell clones (Figs. 33C and D). Conversely, expression of Hth was abolished in the *exd*^{1} ad-NB clones (Figs. 34A and B) and the *exd*^{1} single-cell clones (Figs. 34C and D). These results thus demonstrate that expressions of Hth and Exd depend on the activity of each other gene in ad-PNs.

Loss of *hth* alters expression of neither Acj6 nor Lola

Prompted by the results that *hth* plays a critical role in olfactory PN development, I examined expression of other transcription factors that were known to be important for olfactory PN specification. A POU domain protein, Acj6, is one of the best-studied transcription factors that control precise connectivity of olfactory PNs (Ayer and Carlson, 1991, Ayer and Carlson, 1992, Certel et al., 2000, Clyne et al., 1999 and Komiyama et al., 2003). Double immunolabeling experiments demonstrated that Hth and Acj6 were co-expressed in most of the ad-PNs at the larval, early pupal and adult stages (Figs. 35A–C). However, the expression of Acj6 was not altered in the *hth*^{P2} mutant clones (Fig. 36A). Conversely, the expression of Hth was not altered in the *acj6*^{6} mutant clones (Fig. 36B). These results suggest that *hth* and acj6 are independently controlled in ad-PNs.

The BTB-Zinc-finger transcriptional factor, Lola, is another transcription

factor required for precise dendrite and axonal targeting of olfactory PNs (Spletter et al., 2007). Double immunolabeling experiments using anti-Hth antibody and anti-Lola antibody (raised against the common region) (Goeke et al., 2003) demonstrated that the two proteins were co-expressed in ad-PNs at the larval, early pupal and adult stages (Figs. 37A–C). However, the expression of Lola was not altered in the hth^{P2} mutant clones (Fig. 38A), and, conversely, the expression of Hth was not altered in the $lola^{ore76}$ mutant clones (Fig. 38B). These results thus suggest that *hth* and *lola* are independently controlled in ad-PNs.

Discussion

Precise connectivity of neural circuits in the nervous system depends on the generation of diverse cell types and specific wiring of individual neurons. Temporal and spatial regulation of gene expression by transcription factors has a central role in determining axonal and dendritic targeting specificity in the brain (Dasen and Jessell, 2009 , Komiyama and Luo, 2006 , Komiyama and Luo, 2007 and Skeath and Thor, 2003). In this study, I have shown that two of the evolutionary conserved TALE-class homeodomain transcription factors, Hth and Exd, have important functions in the development of *Drosophila* olfactory PNs.

hth and *exd* control the development of AL-PNs

In addition to the regulatory functions as homeotic cofactors, *hth* and *exd* have important functions in the determination of the developmental identity of the antennal segment (Casares and Mann, 1998, Dong et al., 2000, Dong et al., 2002 and Mann et al., 2009); removing the function of *exd* or *hth* transforms the antenna into leg-like structures, and ectopic expression of *hth* can trigger antennal development elsewhere in the fly. In addition, the activities of *hth* and exd are required for the development of the embryonic axonal tracts that pioneer the projections between the deutocerebrum and the dorsal parts of the protocerebrum (Nagao et al., 2000). Consequently, loss of *hth* or exd results in marked perturbations of the axonal scaffolds in the developing brain (Nagao et al., 2000).

In this study, I have shown that Hth is expressed in many of the AL neurons

including local interneurons and PNs. Hth and Exd are coexpressed not only in postmitotic neurons but also in the progenitors of the anterodorsal and lateral AL lineages. Loss of either *hth* or *exd* causes loss of the lateral lineage, in which *hth* plays an essential role in suppression of apoptosis. Moreover, we have shown that *hth* and *exd* are required for precise dendritic and axonal targeting of olfactory PNs. Mutations of *hth* result in profound targeting defects in many of the on-target glomeruli such as VA1lm, VA3 and D. They also cause ectopic innervation in many of the off-target glomeruli (Figs. 8, 9, 12, 13, and 14). The dendritic defect of exd^{1} mutation is reminiscent of the phenotype of *hth* mutations, with reduced number of *GH146*-expressing cells yet exhibiting selective ectopic innervation in the off-target DA1 glomeruli (Figs. 27 and 28). The functional importance of *hth* and *exd* was further confirmed in post-mitotic neurons by the analyses of single-cell clones of the anterodorsal DL1 and the lateral DA1 neurons. Apart from dendritic defects, *hth* and *exd* mutations cause severe axonal defasciculation, misrouting and aberrant ventrolateral extensions. As with *hth* mutant clones, *exd* mutant clones exhibit an increase in the numbers of the LH terminal branches. Moreover, I have shown that coexpression of Hth and Exd is essential for efficient expression of either protein in the olfactory PNs, recapitulating the interdependence of the expression of the two proteins in the embryonic brain (Nagao et al., 2000). These results suggest that *exd* and *hth* could positively regulate each other expression in the olfactory PNs. Alternatively, stability of Hth and Exd in the olfactory PNs could depend on the interaction of the two proteins as suggested in the antennal and leg discs (Abu-Shaar and Mann, 1998 , Casares and Mann, 1998 , Dong et al., 2000 , Dong et al., 2002 , Mann et al., 2009 and Stevens and Mann, 2007).

Dendritic phenotypes of *hth*, *acj6*, and *lola* mutants

Although Hth is co-expressed with Acj6 and Lola in both developing and adult ad-PNs, loss of *hth* function fails to alter Acj6 and Lola expression. Conversely, mutation of neither *acj6* nor *lola* abolishes Hth expression. In agreement with independent regulatory mechanisms, the dendritic phenotype of *hth* PNs diverges from the phenotypes of either *acj6* or *lola* mutant PN clones. Thus, in contrast to the severe innervation defects in VA1lm, VA3, and D of the *hth* mutant clones (Figs. 8 and 9), $acj6^{6}$ mutant clones show only mild defects for VA1lm and D (Komiyama et al., 2003), and only VA3 is severely affected (Komiyama et al., 2003). Similar differences can be noted for single-cell clones, in which *hth* but not *acj6* mutant clones exhibit complete switching of DL1 specificity (Fig. 12) (Komiyama et al., 2003).

With partial commonality with *hth* mutant PNs, *lola* mutant PNs exhibit severe defects in multiple glomeruli (Spletter et al., 2007). Nonetheless, *lola* and *hth* mutant clones exhibit different degree and spectra of glomerular mistargeting. While both hth^{P2} and $hth^{P1\text{-}K6\text{-}1}$ ad-NB clones fail to innervate the VA1lm glomerulus (Figs. 6 and 7), most of the *lola* ad-NB clones completely innervate VA1lm (Spletter et al., 2007). In addition, only 23% of the *lola* single-cell clones lack dendritic innervation in DL1 (Spletter et al., 2007) while the majority of the *hth* single-cell clones fails to innervate the correct target (Fig. 12). It is also noteworthy that, unlike the mutations of *hth* or *exd*, loss of the *lola* activity dose not eliminate the lateral PN lineage (Spletter et al., 2007). In addition to these LOF phenotypes, GOF mistargeting phenotypes are also different between *hth*, *acj6*, and *lola* mutations (Figs. 23-26) (Komiyama et al., 2003 and Spletter et al., 2007). Similar differences in dendritic phenotypes can be noted with

mutations of other transcription factors that have been shown to be involved in PN specification (Komiyama and Luo, 2007 and Tea et al., 2010). These results are thus consistent with the notion that different transcription factors control the targeting specificity of olfactory PNs via distinct intrinsic programs that regulate diverse repertoires of downstream genes, even though they are coexpressed during development.

Molecular functions of Hth and Exd in olfactory PN specification

In the development of vertebrate spinal motor neurons, homeodomain transcription factors play important roles in the generation and determination of diverse neuronal subtypes (Dasen and Jessell, 2009 and Dasen et al., 2005). In particular, Hox proteins act as central mediators of the intrinsic programs that shape motor neuron subtype identity and target muscle specificity (Dasen and Jessell, 2009). Hox proteins not only influence the identity of motor neuron columns but also control the initial specificity of motor axon projections via specific transcriptional cascades that determine the expression profiles of the cell surface guidance receptors such as Eph family proteins. Combinatorial expression of Hox proteins and a cofactor, Meis 1, the vertebrate homolog of Hth, determine the specificity of the motor neuron pool subtypes (Dasen et al., 2005).

The result that Hth and Exd are expressed in many of the *Drosophila* AL neurons suggests that Hth and Exd are unlikely candidates as lineage specific or cell-type specific regulators by themselves. Rather, it is more likely that these TALE-class homeodomain transcription factors control the identity of the AL neuromere in collaboration with other transcription factors that regulate the wiring

specificity of individual neurons. In the development of antenna, *hth* and *exd* genetically interact with Distalless, which encodes another homeodomain transcription factor (Casares and Mann, 1998 , Dong et al., 2000 and Dong et al., 2002). Although Distalless is expressed in the antennal olfactory neurons that innervate the AL glomeruli, it is expressed neither in the olfactory PNs nor in the local interneurons (M. A., Y. T and K. F. T., unpublished observation). Unlike the more posterior parts of the central nervous system, none of the homeotic proteins are expressed in the *Drosophila* deuto- and protocerebrum neuromeres except for Probosipedia that is expressed in a small number of cells at the posterior deutocerebrum (Hirth et al., 1995 and Hirth et al., 1998). On the other hand, studies on the embryonic brain have shown that Ems plays an essential role in the development of the deutocerebrum primordia that give rise to the ALs (Hirth et al., 1995 and Younossi-Hartenstein et al., 1997). In addition, the activity of ems is required for the generation of the lateral PNs and for precise dendritic targeting of the ad-PNs (Lichtneckert et al., 2008). Intriguingly, the amino acid sequence Tyr-Pro-Trp, located in the immediate upstream of the Ems homeodomain, partially matches the YPWM motif of the homeotic proteins that are bound by Exd/Pbx proteins (Mann and Affolter, 1998 and Mann et al., 2009). Although our data demonstrate that Ems expression is independent of the *hth* activity, the phenotypic commonality that both *hth* and *ems* are required for the generation of the lateral but not the ad-PNs suggests a cooperative interaction of the Hth, Exd and Ems proteins in the regulation of down stream programs that regulate the proliferation of the lateral progenitors. In addition, Hth and Exd could cooperatively function with non-homeodomain transcription factors in the AL neurons as demonstrated by the ternary interaction between the Pbx1, Meis1 and MyoD proteins on the downstream

target genes that regulate myogenic differentiation (Berkes et al., 2004).

Hth/Exd functions in the vertebrate brain

Four Exd-related proteins (Pbx1, Pbx2, Pbx3, and Pbx4) and five Hth-related proteins (Meis1, Meis2, Meis3, Prep1 and Prep2) are found in vertebrates. Mutations of the Pbx/Meis genes cause homeotic transformations in the hindbrain, mimicking the LOF phenotypes of the Hox genes expressed in the anterior neuromeres (Moens and Selleri, 2006). In addition, as with the *Drosophila* homologs (Nagao et al., 2000; this study), these vertebrate TALE-class homeodomain proteins are expressed in more anterior brain structures during development. In the mouse brain, Meis1/2 and Pbx1/2/3 are expressed in the developing telencephalon (Toresson et al., 2000), and Meis2 and Pbx1/2 are expressed in the entire dorsal mesencephalon, regulating the expression of the cell-surface EphA8 receptor to a specific subset of cells (Shim et al., 2007). In zebrafish development, Pbx4 functionally interacts with Engrailed to pattern the midbrain–hindbrain and diencephalic–mesencephalic boundaries (Erickson et al., 2007). Moreover, Pbx3 and Meis1 are coexpressed with Rnx, an orphan Hox protein, in the ventral medullary respiratory center to regulate the development and/or functions of inspiratory neurons (Rhee et al., 2004). Given the cross-phylum commonality in the glomerular organization and neuronal connectivity between the *Drosophila* and vertebrate olfactory systems (Masse et al., 2009 and Vosshall and Stocker, 2007), it would be important to determine the functional significance of the TALE-class homeodomain transcription factors in the control of the cell type specificity in the vertebrate brain.

Acknowledgments

I am grateful to Prof. Katsuo Furukubo-Tokunaga for his supervision and critical advices through the period of my doctoral study. I thank Ms. Y. Totani, Dr. H. Mochizuki, Ms. K. Kondo and the members of the Furukubo-Tokunaga laboratory for assistance and discussion. I also thank Drs. U. Walldorf, L. Luo, T. Komiyama, T. Chihara, M. Kurusu, A. Nose, R. Stocker, H. Reichert, E. Giniger, H. Sun, A. Salzberg, R. Mann, C. Desplan, A. Hofbauer, S. M. Cohen, A. L. Kolodkin, and R. White, as well as the Bloomington Stock Center and the Developmental Studies Hybridoma Bank for generous sharing of the fly stocks and antibodies.

References

Abu-Shaar, M., Mann, R. S., 1998. Generation of multiple antagonistic domains along the proximodistal axis during *Drosophila* leg development. Development. 125, 3821-3830.

Aspland, S. E., White, R. A., 1997. Nucleocytoplasmic localisation of extradenticle protein is spatially regulated throughout development in *Drosophila*. Development. 124, 741-747.

Ayer, R. K., Jr., Carlson, J., 1991. acj6: a gene affecting olfactory physiology and behavior in *Drosophila*. Proc Natl Acad Sci U S A. 88, 5467-5471.

Ayer, R. K., Jr., Carlson, J., 1992. Olfactory physiology in the *Drosophila* antenna and maxillary palp: acj6 distinguishes two classes of odorant pathways. J Neurobiol. 23, 965-982.

Berkes, C. A., Bergstrom, D. A., Penn, B. H., Seaver, K. J., Knoepfler, P. S., Tapscott, S. J., 2004. Pbx marks genes for activation by MyoD indicating a role for a homeodomain protein in establishing myogenic potential. Mol Cell. 14, 465-477.

Casares, F., Mann, R. S., 1998. Control of antennal versus leg development in *Drosophila*. Nature. 392, 723-726.

Certel, S. J., Clyne, P. J., Carlson, J. R., Johnson, W. A., 2000. Regulation of central neuron synaptic targeting by the *Drosophila* POU protein, Acj6. Development. 127, 2395-2405.

Clyne, P. J., Certel, S. J., de Bruyne, M., Zaslavsky, L., Johnson, W. A., Carlson, J. R., 1999. The odor specificities of a subset of olfactory receptor neurons are governed by Acj6, a POU-domain transcription factor. Neuron. 22, 339-347.

Couto, A., Alenius, M., Dickson, B. J., 2005. Molecular, anatomical, and functional organization of the *Drosophila* olfactory system. Curr Biol. 15, 1535-1547.

Dasen, J. S., Jessell, T. M., 2009. Hox networks and the origins of motor neuron diversity. Curr Top Dev Biol. 88, 169-200.

Dasen, J. S., Tice, B. C., Brenner-Morton, S., Jessell, T. M., 2005. A Hox regulatory network establishes motor neuron pool identity and target-muscle connectivity. Cell. 123, 477-491.

Dong, P. D., Chu, J., Panganiban, G., 2000. Coexpression of the homeobox genes Distal-less and homothorax determines *Drosophila* antennal identity. Development. 127, 209-216.

Dong, P. D., Dicks, J. S., Panganiban, G., 2002. Distal-less and homothorax regulate

multiple targets to pattern the *Drosophila* antenna. Development. 129, 1967-1974.

Dumstrei, K., Wang, F., Hartenstein, V., 2003. Role of DE-cadherin in neuroblast proliferation, neural morphogenesis, and axon tract formation in *Drosophila* larval brain development. J Neurosci. 23, 3325-3335.

Erickson, T., Scholpp, S., Brand, M., Moens, C. B., Waskiewicz, A. J., 2007. Pbx proteins cooperate with Engrailed to pattern the midbrain-hindbrain and diencephalic-mesencephalic boundaries. Dev Biol. 301, 504-517.

Fishilevich, E., Vosshall, L. B., 2005. Genetic and functional subdivision of the *Drosophila* antennal lobe. Curr Biol. 15, 1548-1553.

Goeke, S., Greene, E. A., Grant, P. K., Gates, M. A., Crowner, D., Aigaki, T., Giniger, E., 2003. Alternative splicing of lola generates 19 transcription factors controlling axon guidance in *Drosophila*. Nat Neurosci. 6, 917-924.

Hasegawa, E., Kitada, Y., Kaido, M., Takayama, R., Awasaki, T., Tabata, T., Sato, M., 2011. Concentric zones, cell migration and neuronal circuits in the *Drosophila* visual center. Development. 138, 983-993.

Hirth, F., Hartmann, B., Reichert, H., 1998. Homeotic gene action in embryonic brain development of *Drosophila*. Development. 125, 1579-1589.

Hirth, F., Therianos, S., Loop, T., Gehring, W. J., Reichert, H., Furukubo-Tokunaga, K., 1995. Developmental defects in brain segmentation caused by mutations of the homeobox genes orthodenticle and empty spiracles in *Drosophila*. Neuron. 15, 769-778.

Hong, W., Zhu, H., Potter, C. J., Barsh, G., Kurusu, M., Zinn, K., Luo, L., 2009. Leucine-rich repeat transmembrane proteins instruct discrete dendrite targeting in an olfactory map. Nat Neurosci. 12, 1542-1550.

Ikeshima-Kataoka, H., Skeath, J. B., Nabeshima, Y., Doe, C. Q., Matsuzaki, F., 1997. Miranda directs Prospero to a daughter cell during *Drosophila* asymmetric divisions. Nature 390, 625-629.

Inbal, A., Halachmi, N., Dibner, C., Frank, D., Salzberg, A., 2001. Genetic evidence for the transcriptional-activating function of Homothorax during adult fly development. Development. 128, 3405-3413.

Ito, K., Sass, H., Urban, J., Hofbauer, A., Schneuwly, S., 1997. GAL4-responsive UAS-tau as a tool for studying the anatomy and development of the *Drosophila* central nervous system. Cell Tissue Res. 290, 1-10.

Ito, K., Suzuki, K., Estes, P., Ramaswami, M., Yamamoto, D., Strausfeld, N. J., 1998. The organization of extrinsic neurons and their implications in the functional roles of the mushroom bodies in *Drosophila* melanogaster Meigen. Learn Mem. 5, 52-77.

Jefferis, G. S., Marin, E. C., Stocker, R. F., Luo, L., 2001. Target neuron prespecification in the olfactory map of *Drosophila*. Nature. 414, 204-208.

Jefferis, G. S., Potter, C. J., Chan, A. M., Marin, E. C., Rohlfing, T., Maurer, C. R., Jr., Luo, L., 2007. Comprehensive maps of *Drosophila* higher olfactory centers: spatially segregated fruit and pheromone representation. Cell. 128, 1187-1203.

Jefferis, G. S., Vyas, R. M., Berdnik, D., Ramaekers, A., Stocker, R. F., Tanaka, N. K., Ito, K., Luo, L., 2004. Developmental origin of wiring specificity in the olfactory system of *Drosophila*. Development. 131, 117-130.

Jhaveri, D., Sen, A., Rodrigues, V., 2000. Mechanisms underlying olfactory neuronal connectivity in *Drosophila*-the atonal lineage organizes the periphery while sensory neurons and glia pattern the olfactory lobe. Dev Biol. 226, 73-87.

Komiyama, T., Luo, L., 2006. Development of wiring specificity in the olfactory system. Curr Opin Neurobiol. 16, 67-73.

Komiyama, T., Luo, L., 2007. Intrinsic control of precise dendritic targeting by an ensemble of transcription factors. Curr Biol. 17, 278-285.

Komiyama, T., Johnson, W. A., Luo, L., Jefferis, G. S., 2003. From lineage to wiring specificity. POU domain transcription factors control precise connections of

Drosophila olfactory projection neurons. Cell. 112, 157-1567.

Komiyama, T., Sweeney, L. B., Schuldiner, O., Garcia, K. C., Luo, L., 2007. Graded expression of semaphorin-1a cell-autonomously directs dendritic targeting of olfactory projection neurons. Cell. 128, 399-410.

Kurant, E., Pai, C. Y., Sharf, R., Halachmi, N., Sun, Y. H., Salzberg, A., 1998. Dorsotonals/homothorax, the *Drosophila* homologue of meis1, interacts with extradenticle in patterning of the embryonic PNS. Development. 125, 1037-1048.

Kurusu, M., Awasaki, T., Masuda-Nakagawa, L. M., Kawauchi, H., Ito, K., Furukubo-Tokunaga, K., 2002. Embryonic and larval development of the *Drosophila* mushroom bodies: concentric layer subdivisions and the role of fasciclin II. Development. 129, 409-419.

Kurusu, M., Maruyama, Y., Adachi, Y., Okabe, M., Suzuki, E., Furukubo-Tokunaga, K., 2009. A conserved nuclear receptor, Tailless, is required for efficient proliferation and prolonged maintenance of mushroom body progenitors in the *Drosophila* brain. Dev Biol. 326, 224-236

Lai, S. L., Awasaki, T., Ito, K., Lee, T., 2008. Clonal analysis of *Drosophila* antennal lobe neurons: diverse neuronal architectures in the lateral neuroblast lineage. Development. 135, 2883-2893.

Laissue, P. P., Reiter, C., Hiesinger, P. R., Halter, S., Fischbach, K. F., Stocker, R. F., 1999. Three-dimensional reconstruction of the antennal lobe in *Drosophila* melanogaster. J Comp Neurol. 405, 543-552.

Lee, T., Luo, L., 1999. Mosaic analysis with a repressible cell marker for studies of gene function in neuronal morphogenesis. Neuron. 22, 451-461.

Lichtneckert, R., Nobs, L., Reichert, H., 2008. Empty spiracles is required for the development of olfactory projection neuron circuitry in *Drosophila*. Development. 135, 2415-2424.

Lin, D. M., Fetter, R. D., Kopczynski, C., Grenningloh, G., Goodman, C. S., 1994. Genetic analysis of Fasciclin II in *Drosophila*: defasciculation, refasciculation, and altered fasciculation. Neuron. 13, 1055-1069.

Lin, D. M., Goodman, C. S., 1994. Ectopic and increased expression of Fasciclin II alters motoneuron growth cone guidance. Neuron. 13, 507-523.

Lin, H. H., Lai, J. S., Chin, A. L., Chen, Y. C., Chiang, A. S., 2007. A map of olfactory representation in the *Drosophila* mushroom body. Cell. 128, 1205-1217.

Lopes, C. S., Casares, F., 2010. hth maintains the pool of eye progenitors and its downregulation by Dpp and Hh couples retinal fate acquisition with cell cycle exit. Dev Biol. 339, 78-88.

Mann, R. S., Affolter, M., 1998. Hox proteins meet more partners. Curr Opin Genet Dev. 8, 423-429.

Mann, R. S., Chan, S. K., 1996. Extra specificity from extradenticle: the partnership between HOX and PBX/EXD homeodomain proteins. Trends Genet. 12, 258-262.

Mann, R. S., Lelli, K. M., Joshi, R., 2009. Hox specificity unique roles for cofactors and collaborators. Curr Top Dev Biol. 88, 63-101.

Marin, E. C., Jefferis, G. S., Komiyama, T., Zhu, H., Luo, L., 2002. Representation of the glomerular olfactory map in the *Drosophila* brain. Cell. 109, 243-255.

Masse, N. Y., Turner, G. C., Jefferis, G. S., 2009. Olfactory information processing in *Drosophila*. Curr Biol. 19, R700-713.

Moens, C. B., Selleri, L., 2006. Hox cofactors in vertebrate development. Dev Biol. 291, 193-206.

Nagao, T., Endo, K., Kawauchi, H., Walldorf, U., Furukubo-Tokunaga, K., 2000. Patterning defects in the primary axonal scaffolds caused by the mutations of the extradenticle and homothorax genes in the embryonic *Drosophila* brain. Dev Genes Evol. 210, 289-299.

Pai, C. Y., Kuo, T. S., Jaw, T. J., Kurant, E., Chen, C. T., Bessarab, D. A., Salzberg, A., Sun, Y. H., 1998. The Homothorax homeoprotein activates the nuclear localization of another homeoprotein, extradenticle, and suppresses eye development in *Drosophila*. Genes Dev. 12, 435-446.

Peng, H. W., Slattery, M., Mann, R. S., 2009. Transcription factor choice in the Hippo signaling pathway: homothorax and yorkie regulation of the microRNA bantam in the progenitor domain of the *Drosophila* eye imaginal disc. Genes Dev. 23, 2307-2319.

Rauskolb, C., Peifer, M., Wieschaus, E., 1993. extradenticle, a regulator of homeotic gene activity, is a homolog of the homeobox-containing human proto-oncogene pbx1. Cell. 74, 1101-1112.

Rhee, J. W., Arata, A., Selleri, L., Jacobs, Y., Arata, S., Onimaru, H., Cleary, M. L., 2004. Pbx3 deficiency results in central hypoventilation. Am J Pathol. 165, 1343-1350.

Rieckhof, G. E., Casares, F., Ryoo, H. D., Abu-Shaar, M., Mann, R. S., 1997. Nuclear translocation of extradenticle requires homothorax, which encodes an extradenticle-related homeodomain protein. Cell. 91, 171-183.

Shim, S., Kim, Y., Shin, J., Kim, J., Park, S., 2007. Regulation of EphA8 gene expression by TALE homeobox transcription factors during development of the mesencephalon. Mol Cell Biol. 27, 1614-1630.

Skeath, J. B., Thor, S., 2003. Genetic control of *Drosophila* nerve cord development. Curr Opin Neurobiol. 13, 8-15.

Spletter, M. L., Liu, J., Liu, J., Su, H., Giniger, E., Komiyama, T., Quake, S., Luo, L., 2007. Lola regulates *Drosophila* olfactory projection neuron identity and targeting specificity. Neural Dev. 2-14.

Stevens, K. E., Mann, R. S., 2007. A balance between two nuclear localization sequences and a nuclear export sequence governs extradenticle subcellular localization. Genetics. 175, 1625-1636.

Stocker, R. F., Lienhard, M. C., Borst, A., Fischbach, K. F., 1990. Neuronal architecture of the antennal lobe in *Drosophila* melanogaster. Cell Tissue Res. 262, 9-34.

Stocker, R. F., Heimbeck, G., Gendre, N., de Belle, J. S., 1997. Neuroblast ablation in *Drosophila* P[GAL4] lines reveals origins of olfactory interneurons. J Neurobiol. 32, 443-456.

Tea, J. S., Chihara, T., Luo, L., 2010. Histone deacetylase Rpd3 regulates olfactory projection neuron dendrite targeting via the transcription factor Prospero. J Neurosci. 30, 9939-9946.

Toresson, H., Parmar, M., Campbell, K., 2000. Expression of Meis and Pbx genes and

their protein products in the developing telencephalon: implications for regional differentiation. Mech Dev. 94, 183-187.

Vosshall, L. B., Stocker, R. F., 2007. Molecular architecture of smell and taste in *Drosophila*. Annu Rev Neurosci. 30, 505-533.

Wagh, D. A., Rasse, T. M., Asan, E., Hofbauer, A., Schwenkert, I., Durrbeck, H., Buchner, S., Dabauvalle, M. C., Schmidt, M., Qin, G., Wichmann, C., Kittel, R., Sigrist, S. J., Buchner, E., 2006. Bruchpilot, a protein with homology to ELKS/CAST, is required for structural integrity and function of synaptic active zones in *Drosophila*. Neuron. 49, 833-844.

Wernet, M. F., Labhart, T., Baumann, F., Mazzoni, E. O., Pichaud, F., Desplan, C., 2003. Homothorax switches function of *Drosophila* photoreceptors from color to polarized light sensors. Cell. 115, 267-279.

Wong, A. M., Wang, J. W., Axel, R., 2002. Spatial representation of the glomerular map in the *Drosophila* protocerebrum. Cell. 109, 229-241.

Younossi-Hartenstein, A., Green, P., Liaw, G. J., Rudolph, K., Lengyel, J., Hartenstein, V., 1997. Control of early neurogenesis of the *Drosophila* brain by the head gap genes tll, otd, ems, and btd. Dev Biol. 182, 270-283.

Zhu, H., Luo, L., 2004. Diverse functions of N-cadherin in dendritic and axonal

terminal arborization of olfactory projection neurons. Neuron. 42, 63-75.

Zhu, H., Hummel, T., Clemens, J. C., Berdnik, D., Zipursky, S. L., Luo, L., 2006a. Dendritic patterning by Dscam and synaptic partner matching in the *Drosophila* antennal lobe. Nat Neurosci. 9, 349-355.

Zhu, S., Lin, S., Kao, C. F., Awasaki, T., Chiang, A. S., Lee, T., 2006b. Gradients of the *Drosophila* Chinmo BTB-zinc finger protein govern neuronal temporal identity. Cell. 127, 409-422.

Tables

Table 1

Recovery of *hth* mutant AL-NB clones

	WT		*hth*$^{P1\text{-}K6\text{-}1}$		*hth*$^{P1\text{-}K6\text{-}1}$ *; UAS-hth*	
Anterodorsal	**19**	**(9.3%)**	**8**	**(13%)**	**3**	**(4.4%)**
Lateral	**23**	**(11%)**	**0**	**(0 %)**	**15**	**(22%)**
Ventral	**15**	**(7.4%)**	**10**	**(17%)**	**8**	**(12%)**
Total	**204**		**60**		**68**	

AL-NB clones were induced at the 1st instar stage using *tubP-GAL4* and examined at the adult stage.

Table 2

Rescue of the *hth* mutant lateral NB clones with *p35.*

	WT		***hth*$^{P1\text{-}K6\text{-}1}$**		***hth*$^{P1\text{-}K6\text{-}1}$ *; UAS-p35***	
Anterodorsal	**18**	**(6.3%)**	**15**	**(13%)**	**9**	**(7.7%)**
Lateral	**15**	**(5.2%)**	**0**	**(0%)**	**6**	**(5.1%)**
Total	**288**		**114**		**117**	

AL-NB clones were induced at the 1st instar stage using *tubP-GAL4*, and analyzed at the late third instar stage. Ventral clones were not included from the analysis because of the difficulty in unequivocal identification at the larval stage.

Table 3

Recovery of *hth* and *exd* mutant NB clones with *GH146*

	WT		*hth*$^{P1\text{-}K6\text{-}1}$		*hth*$^{P1\text{-}\Delta15\text{-}3}$		*hth*^{P2}		*exd*^{1}	
Anterodorsal	**38**	**(7.1%)**	**9**	**(13%)**	**16**	**(13%)**	**108**	**(12%)**	**19**	**(9.7%)**
Lateral	**24**	**(4.5%)**	**0**	**(0%)**	**0**	**(0%)**	**0**	**(0%)**	**0**	**(0%)**
Ventral	**18**	**(3.4%)**	**0**	**(0%)**	**0**	**(0%)**	**0**	**(0%)**	**0**	**(0%)**
Total	**533**		**70**		**126**		**924**		**196**	

AL-NB clones were induced at the 1st instar stage using the *GH146-GAL4* driver and examined at the adult stage.

Figures

Figure 1. The *Drosophila* olfactory system.

ORNs expressing the same receptor (shown in the same color) target their axons to the same glomerulus in the antennal lobe (AL). PNs are grouped into three lineages: anterodorsal (ad), lateral (lat) and ventral (ven) PNs. The dendrites of projection neurons target to specific glomeruli, and their axons project to specific parts of higher olfactory centers such as the calyx of the mushroom body (MB) and lateral horn (LH).

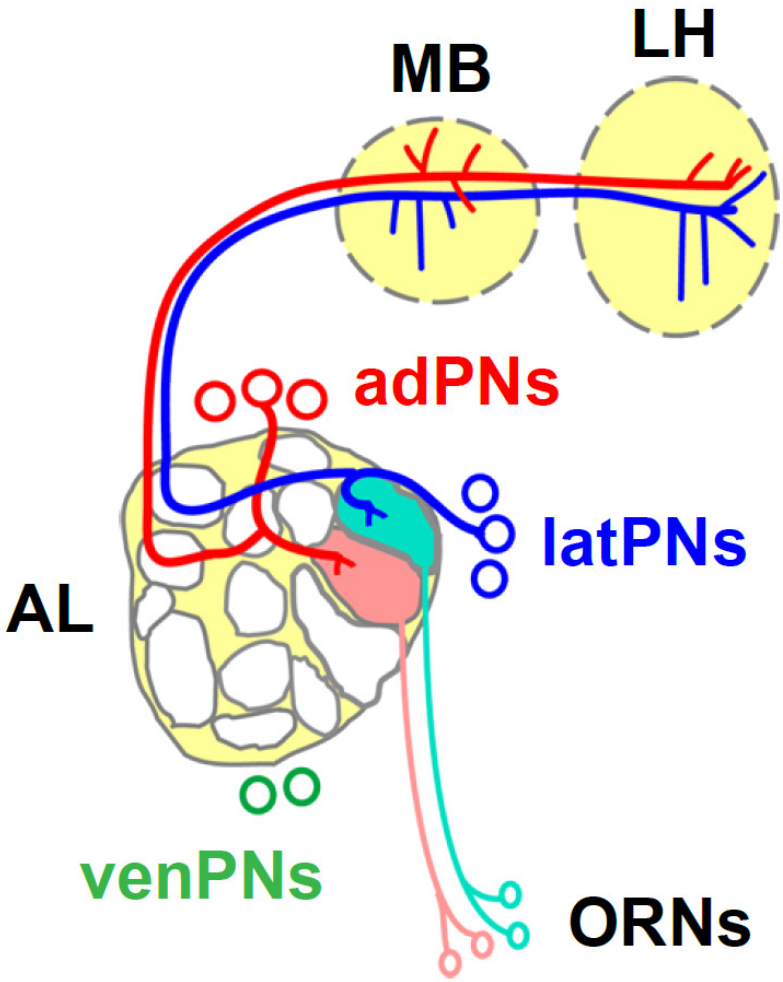
MB
LH
adPNs
latPNs
AL
venPNs
ORNs

Figure 2. Hth expression in the adult brain.

Anti-Hth immunostaining (magenta) showing Hth expression in the adult brain. Green, *GH146*-positive PNs labeled with *UAS-mCD8::GFP*. Note the large clusters of Hth-positive neurons around the margins of the ALs. Scale bar: 100 μm.

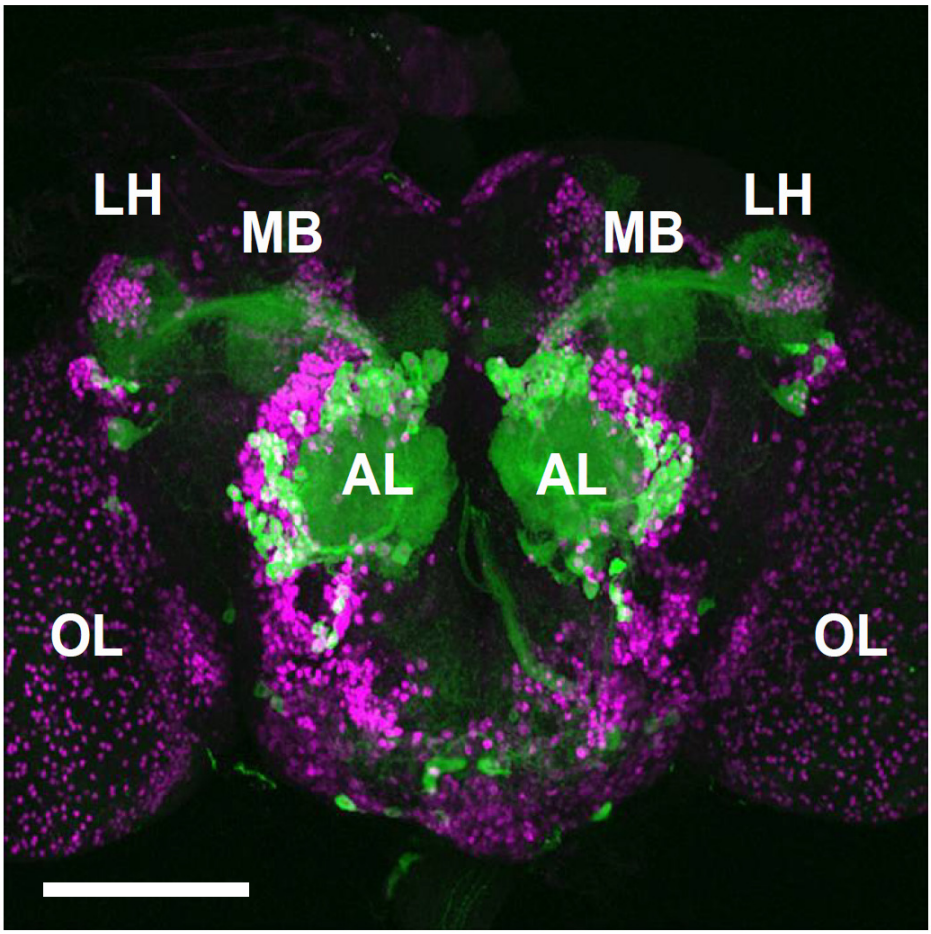
LH
MB
MB
LH
AL
AL
OL
OL

Figure 3. Hth is expressed in *GH146*-positive PNs.

Anti-Hth immunostaining (magenta) showing Hth expression in the 48 h after egg laying (AEL) (A), 72 h AEL (B), 3rd instar (C), 20 h after puparium formation (APF) (D), and adult (E) brain. Green, *GH146*-positive PNs labeled with *UAS-mCD8::GFP*. Note that Hth is expressed in the three PN lineages (ad-, lat- and ven-PNs) in the adult brain. The right side of the brain is shown. Medial is to the left, and dorsal is up. Antennal lobe is demarcated with a thin yellow line. White dot boxes show the regions zoomed in (F-J). Note strong expression of Hth in the PN nuclei. Scale bars: 20 μm for A-D, 20 μm for E, and 10 μm for F-J.

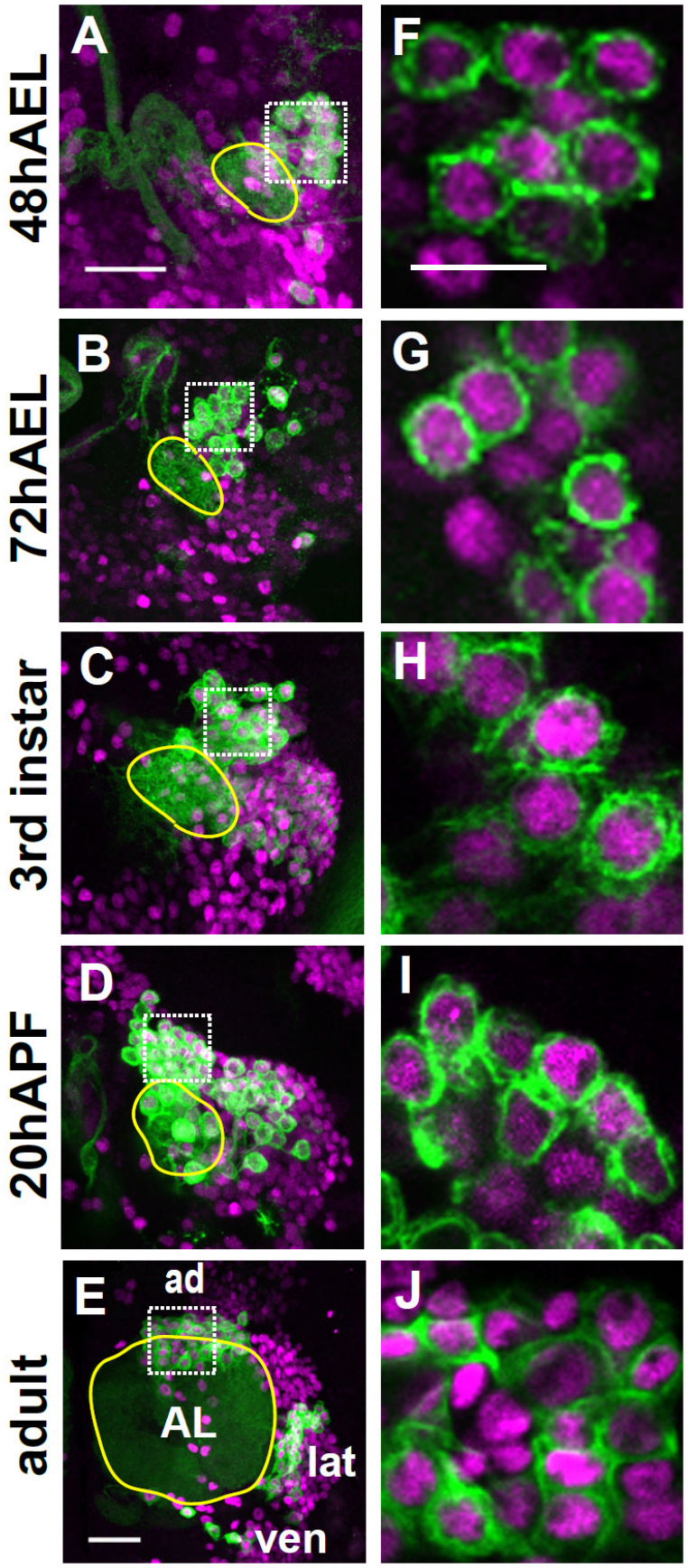
48hAEL
72hAEL
3rd instar
20hAPF
adult
A
B
C
D
E
F
G
H
I
J
ad
AL
lat
ven

Figure 4. Hth is expressed in GH298-positive lateral local interneurons and MZ699-positive ventral PNs.

Anti-Hth immunostaining (magenta) showing Hth expression in the adult brain. (A) Hth expression in lateral local interneurons labeled with GH298 and *UAS-mCD8::GFP*. (B) Hth expression in ventral PNs labeled with MZ699 and *UAS-mCD8::GFP*. The right side of the brain is shown. Medial is to the left, and dorsal is up. Antennal lobe is demarcated with a thin yellow line. White dot boxes show the regions zoomed in (C and D). Single optical sections of adult brains. White arrowheads, Hth-negative neurons. Yellow arrowheads, Hth-positive neurons. Scale bars: 20μm.

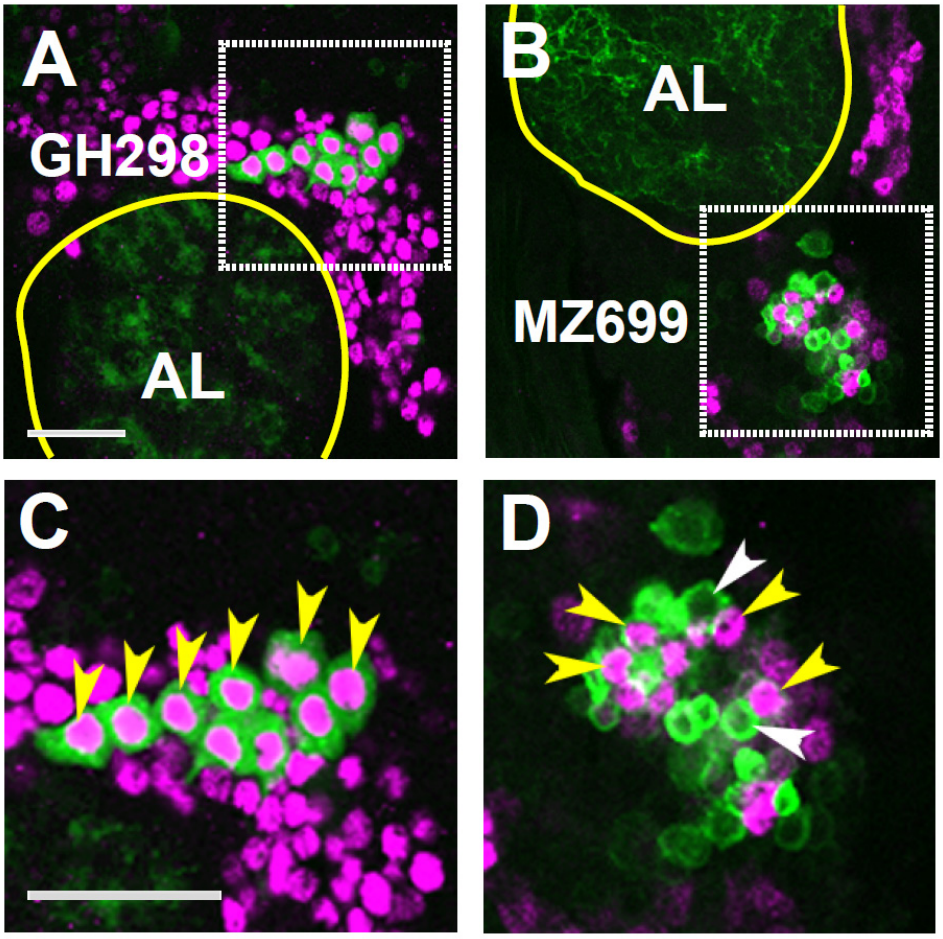
A
GH298
AL
B
AL
MZ699
C
D

Figure 5. Summary diagram of Hth expression in the adult AL neurons.

Magenta showing Hth expression. Green circle, *GAL4* marker expression. Hth was expressed in many of the cells that surround the AL. Expression analysis using an AL driver, *GH146-GAL4*, which is expressed in ~60% of the olfactory PNs, confirmed that Hth was expressed in the antero dorsal (ad) and the lateral PNs, the two major olfactory PN lineages in the *Drosophila* brain. In the lateral lineage, Hth was also expressed in the GH298-positive interneurons. Moreover, expression of Hth was observed in a small group of ventral cells that in part overlapped with the *GH146*-positive PNs.

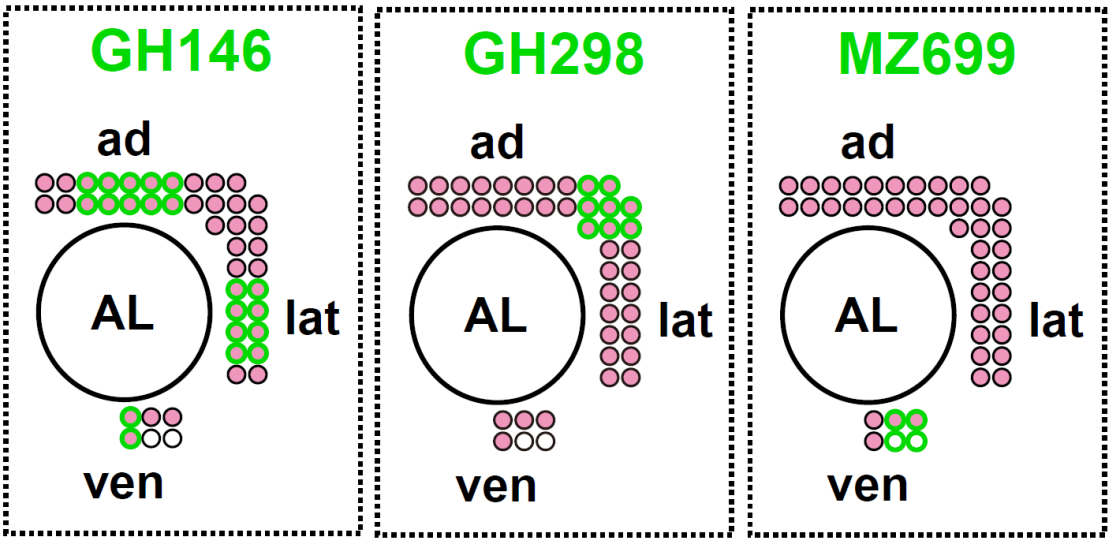
GH146
ad
AL
lat
ven
GH298
ad
AL
lat
ven
MZ699
ad
AL
lat
ven

Figure 6. Expression of Hth in the anterodorsal and lateral progenitors.

Wild type clones at late 3rd instar stage. In both anterodorsal and lateral lineages, Hth (red) is expressed in the progenitors including the NBs (yellow dot circle) labeled with anti-Miranda (blue). Clones were induced at the 1st instar stage and labeled with *UAS-mCD8::GFP* (green) driven by *tubP-GAL4*. Optical sections. Scale bars: 20 μm.

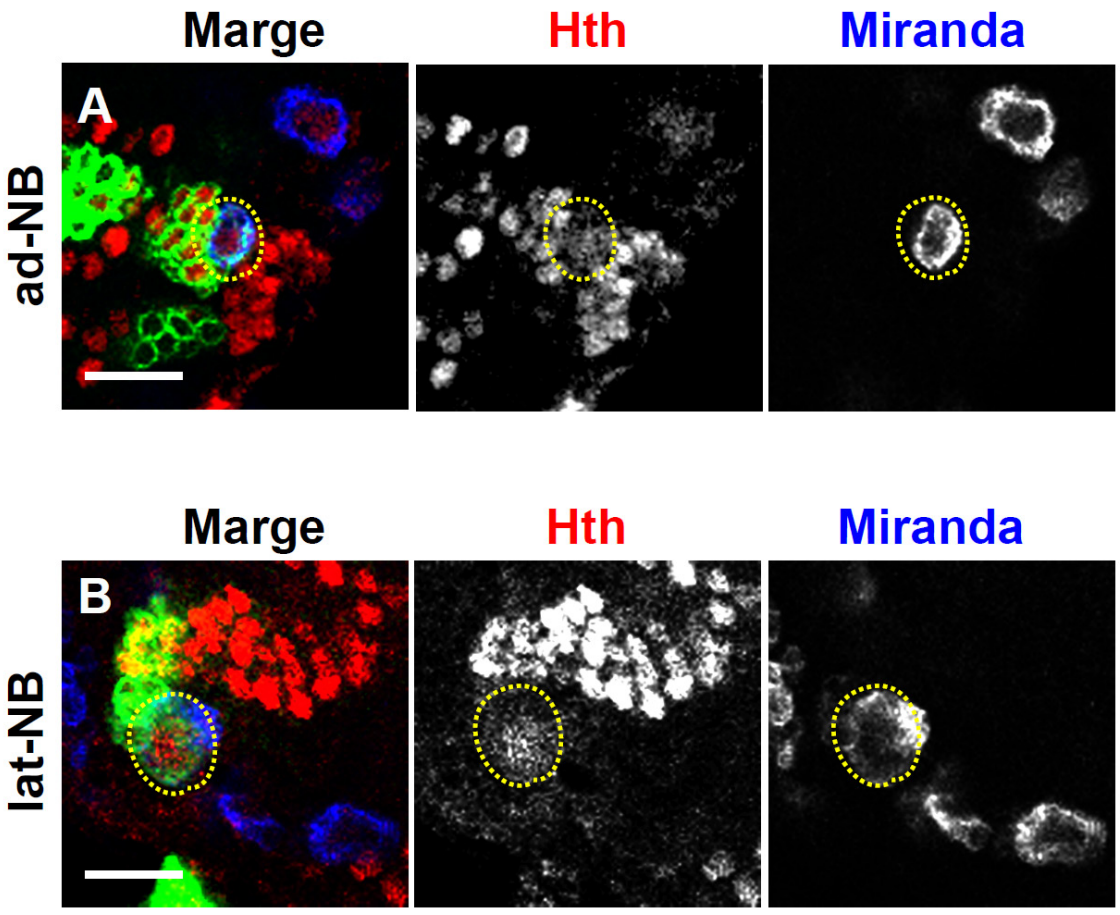
Marge
Hth
Miranda
A
ad-NB
Marge
Hth
Miranda
B
lat-NB

Figure 7. Expression of Ems was not altered by the loss of the *hth* activity.

(A) Expression of Ems in a $hth^{P1\text{-}K6\text{-}1}$ ad-NB clone. Note the expression of Ems (magenta) in the progenitors including the NB (yellow dot circle). (B) Expression of Ems in a $hth^{P1\text{-}K6\text{-}1}$ lateral NB clone rescued with p35. Note that Ems was expressed in the progenitors, including the NB (yellow dot circle), of the rescued lateral lineage. Clones were induced at the 1st instar stage and labeled with *UAS-mCD8::GFP* (green) driven by *tubP-GAL4*. Optical sections. Scale bars: 20 μm.

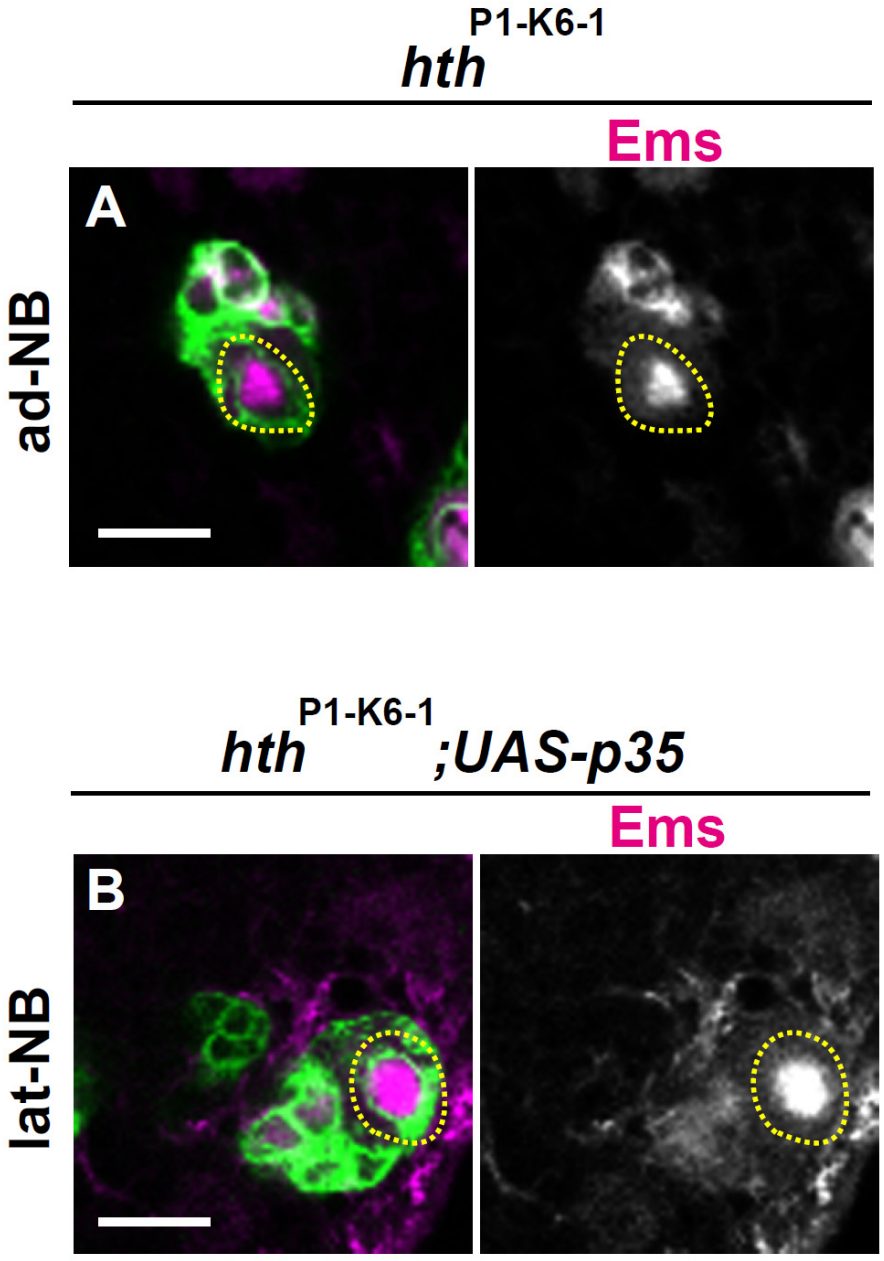
P1-K6-1
hth
Ems
A
ad-NB
P1-K6-1
hth ;UAS-p35
Ems
B
lat-NB

Figure 8. Dendritic targeting defects of *hth* ad-NB clones

Dendritic targeting phenotypes of wild-type (A1-A3), hth^{P2} (B1-B3) and $hth^{P1\text{-}K6\text{-}1}$ (C1-C3) ad-NB clones. Anterior (A1, B1, C1), middle (A2, B2, C2) and posterior (A3, B3, C3) parts of AL. Clones were induced by early 1st instar heat shock and labeled with *UAS-mCD8::GFP* driven by *GH146* (green). Neuropil was visualized with anti-nc82 (magenta). VA1d, VA1lm, VA3, VM2, DM6, D, DC3, DL1, and VM7 are the landmark glomeruli normally innervated by *GH146*-positive ad-PNs (yellow letters). VA2 glomerulus (white letters in A1) is innervated by ad-PNs born in the embryonic stage and, thus, uninnervated by the wild-type clone. DA1, DM5 and DM2 (white letters in A1-A3) are glomeruli normally innervated by lateral, but not ad-PNs. Yellow arrows in B1-B3 indicate the ad-type glomeruli with partial (D glomerulus) or no innervation (VA1lm, VA3 and DL1 glomeruli) in hth^{P2} ad-NB clones. White arrows in B1-B3 indicate ectopically innervated lateral-type glomeruli (DA1 and DM2) and the embryonic glomeruli (VA2) in hth^{P2} ad-NB clones.

The dendritic targeting by $hth^{P1\text{-}K6\text{-}1}$ ad-NB clones to the ad-type glomeruli were severely altered with partial (DM6, VA1d and D glomerulus) or no innervation (VA1lm, VA3, VM2, DL1 and VM7 glomeruli) (yellow arrows in C1-C3). $hth^{P1\text{-}K6\text{-}1}$ ad-NB clones also exhibit ectopic innervation in the lateral-type glomeruli (DA1) (white arrows in C1 and C2). The right side of the brain is shown. Medial is to the left and dorsal is up. Scale bars: 20 μm.

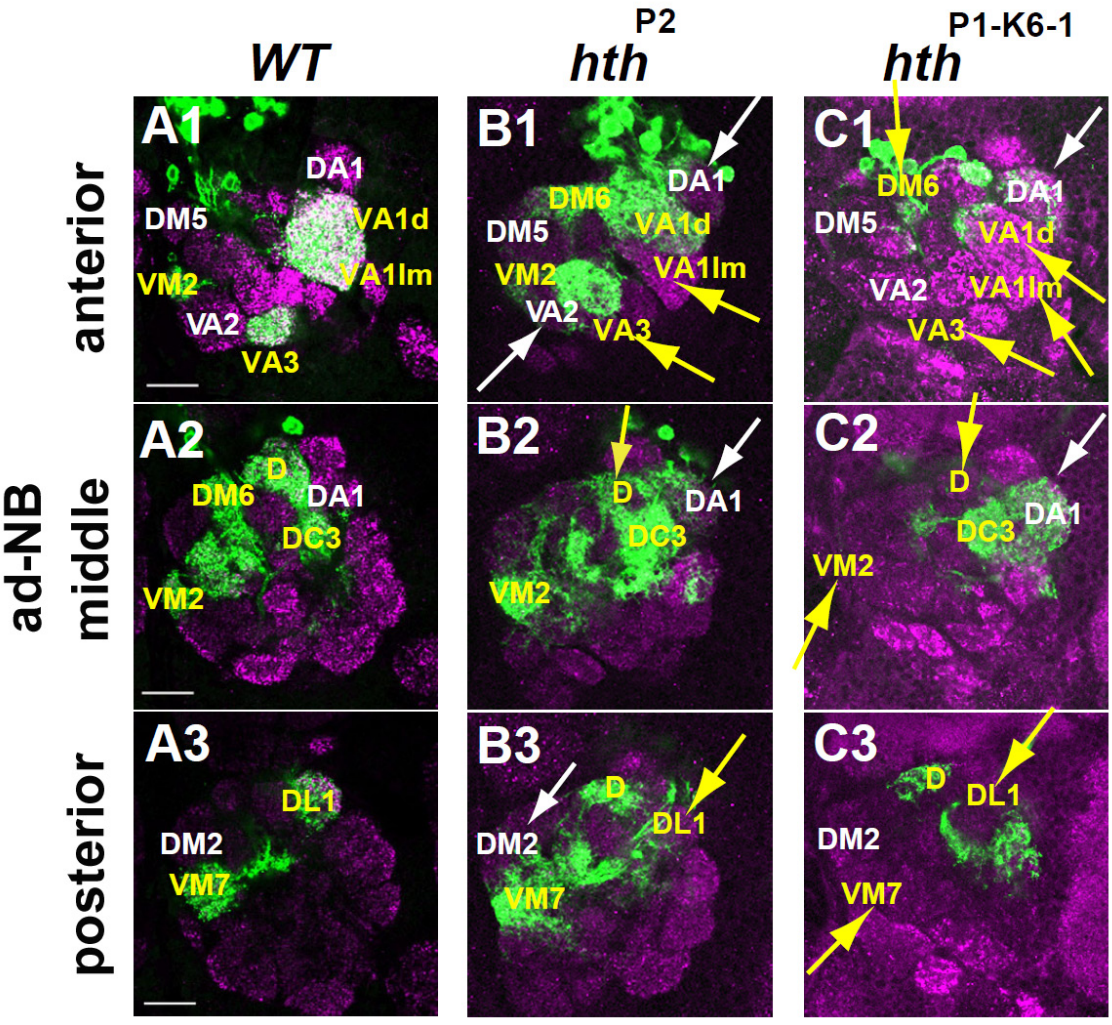
WT
hth
P2
hth
P1-K6-1
ad-NB
anterior
middle
posterior
A1
DA1
DM5
VA1d
VM2
VA1lm
VA2
VA3
B1
DA1
DM6
DM5
VA1d
VM2
VA1lm
VA2
VA3
C1
DM6
DA1
DM5
VA1d
VA2
VA1lm
VA3
A2
D
DM6
DA1
DC3
VM2
B2
D
DA1
DC3
VM2
C2
D
DA1
DC3
VM2
A3
DL1
DM2
VM7
B3
D
DL1
DM2
VM7
C3
D
DL1
DM2
VM7

Figure 9. Quantification of dendritic targeting defects of *hth* ad-NB clones

(A-C) Quantification of dendritic innervation in on-target glomeruli. For each sample, the extent of innervation in the target glomeruli was examined and classified to four classes. Dense, complete dense input all over the target glomerulus; moderate, irregular robust input all over the target glomerulus; sparse, partial weak input; no input. (D-F) Quantification of dendritic innervation in off-target glomeruli. Extent of innervation in the non-target glomeruli was classified to three classes. No input; sparse, weak input; moderate, irregular robust input. Number of samples is shown in the figure.

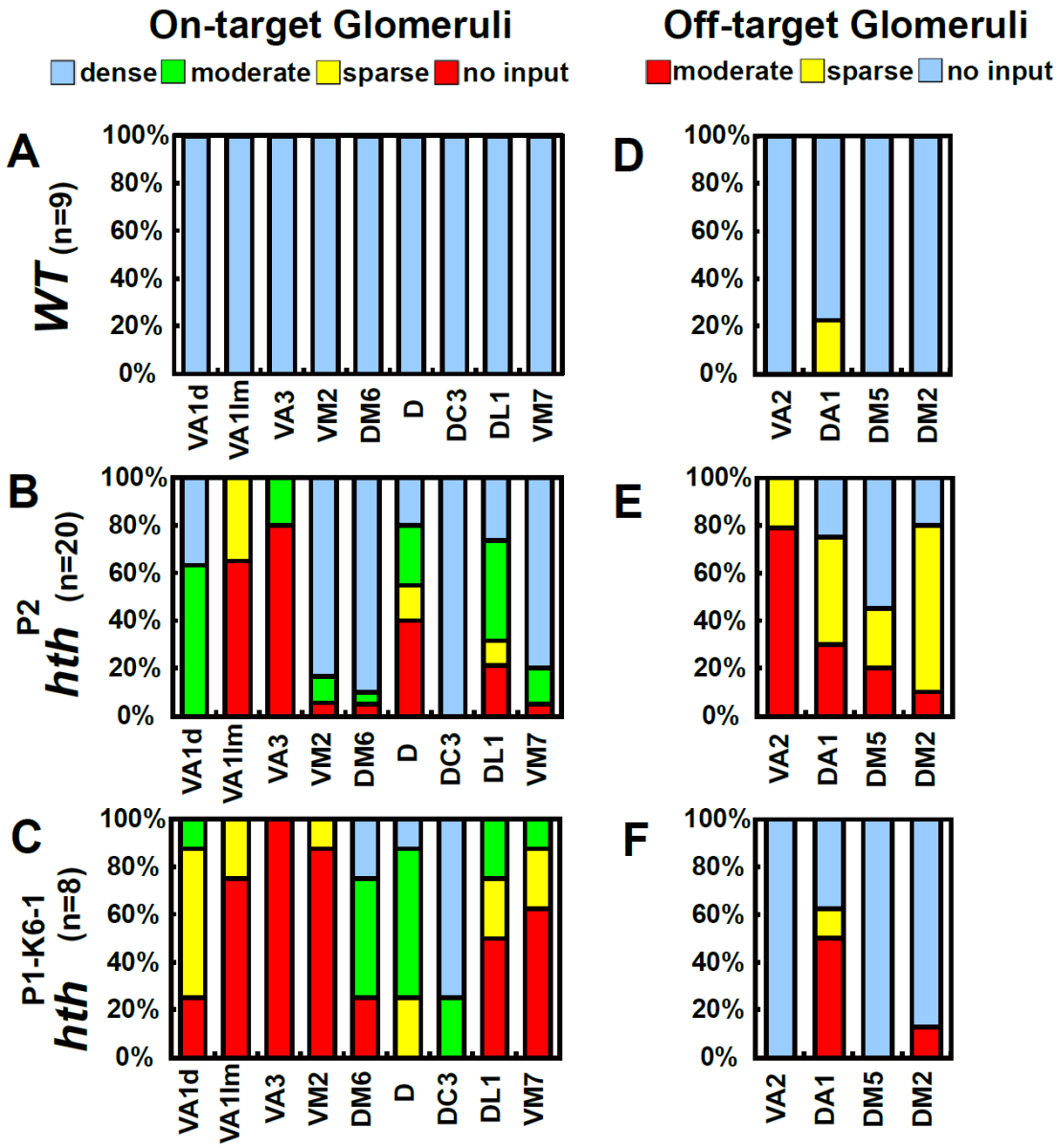
On-target Glomeruli
Off-target Glomeruli
dense
moderate
sparse
no input
A
WT (n=9)
B
P2 hth (n=20)
C
P1-K6-1 hth (n=8)
D
E
F
100%
80%
60%
40%
20%
0%
VA1d
VA1lm
VA3
VM2
DM6
D
DC3
DL1
VM7
VA2
DA1
DM5
DM2

Figure 10. Single and dual clone phenotypes of *hth* mutant PNs

AL glomerular defects with single and dual mutant clones. Reconstruction of optical sections of adult brain ALs. Immunostaining for Hth (magenta). The approximate outlines of the *hth* mutant clones, as deduced by the absence of Hth expression, are demarcated with yellow dotted circles. Yellow letters denote glomeruli normally innervated by ad-PNs. White letters denote glomeruli normally innervated by embryonic (VA2) or lateral PNs (DA1, DM5, DM2). Note the reduced AL size and the absence of the lateral-type glomeruli in C caused by the dual induction of the anterodorsal (ad) and lateral (lat) clones. Clones were induced by early 1st instar heat shock and labeled with *UAS-mCD8::GFP* driven by *GH146* (green). Scale bar: 20 μm.

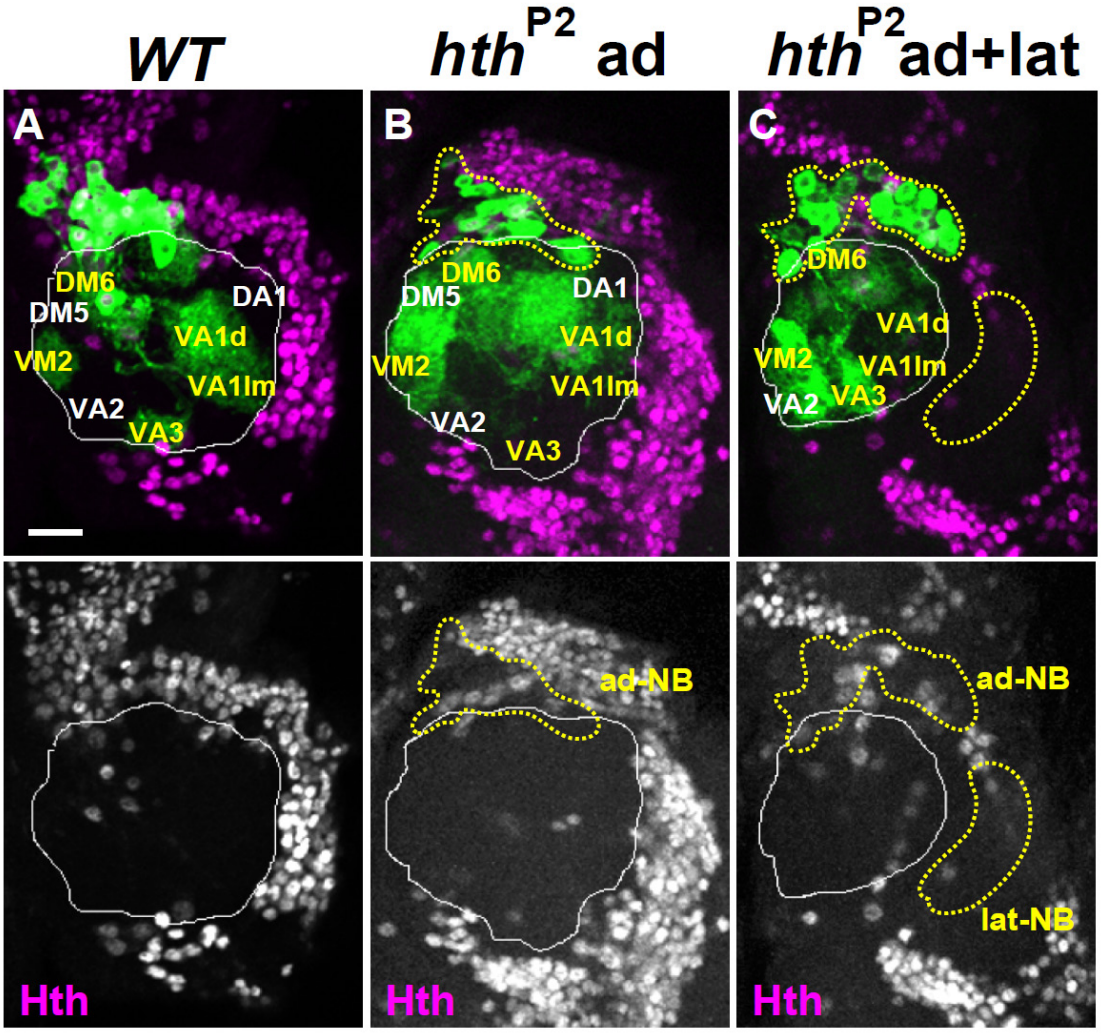
WT
hth P2 ad
hth P2 ad+lat
A
B
C
DM6
DM5
DA1
VA1d
VM2
VA1lm
VA2
VA3
ad-NB
lat-NB
Hth

Figure 11. Expression of N-Cadherin was not altered by the loss of the *hth* activity.

Expression of N-Cadherin (magenta) in wild-type and hth^{P2} ad-PN clones. 50h APF. (A, B) ALs with wild-type and hth^{P2} ad-PN clones. Yellow letters denote glomeruli innervated by ad-PNs. White letters denote glomeruli innervated by lateral or embryonic PNs. (C) Expression of N-Cadherin in the cell bodies. Note the expression of N-Cadherin in the mutant ad-PNs (arrowheads). Clones were induced by early 1st instar heat shock and labeled with *UAS-mCD8::GFP* driven by *GH146* (green). Scale bars: 20 μm.

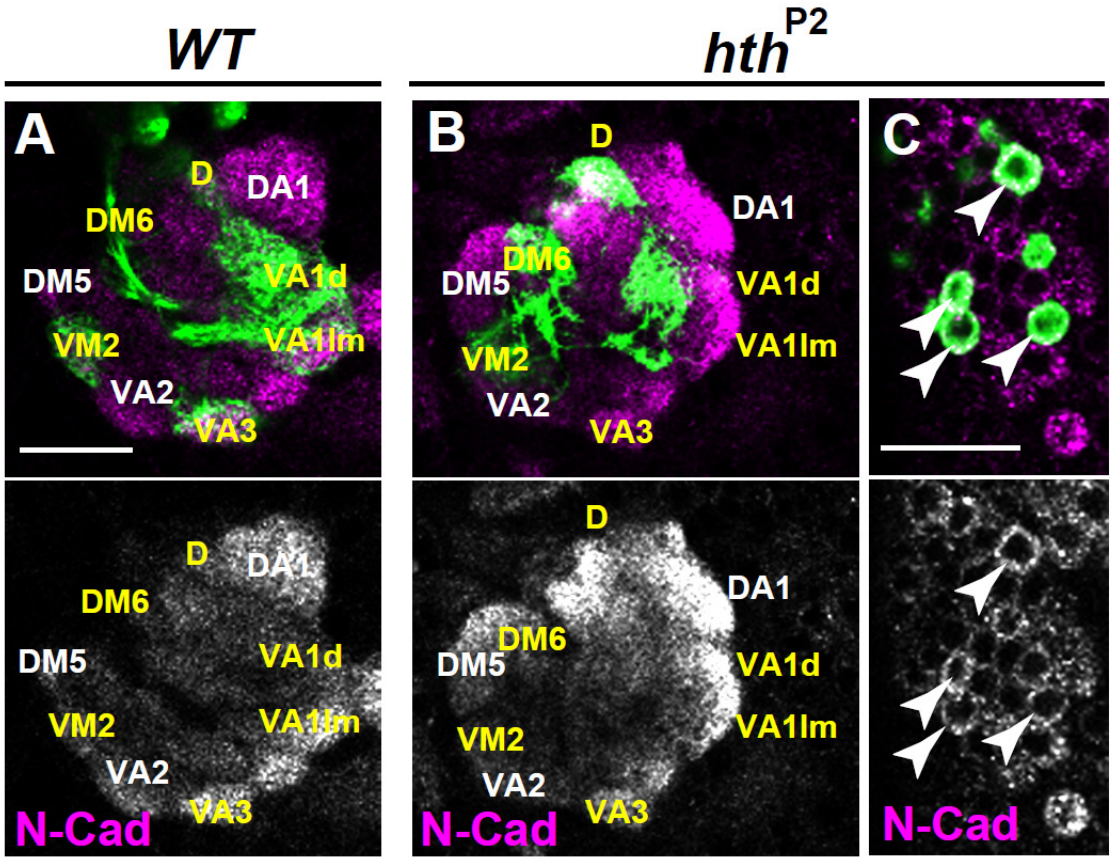
WT
hth P2
A
D
DA1
DM6
DM5
VA1d
VM2
VA1lm
VA2
VA3
B
D
DA1
DM6
DM5
VA1d
VM2
VA1lm
VA2
VA3
C
D
DA1
DM6
DM5
VA1d
VM2
VA1lm
VA2
VA3
N-Cad
D
DA1
DM6
DM5
VA1d
VM2
VA1lm
VA2
VA3
N-Cad
N-Cad

Figure 12. Dendritic targeting defects of *hth* DL1 single-cell clones.

(A-C) Dendritic targeting phenotypes of wild-type (A1, A2), hth^{P2} (B1, B2) and $hth^{P1\text{-}K6\text{-}1}$ (C1, C2) DL1 single-cell clones. Clones were induced by early 1st instar heat shock and labeled with *UAS-mCD8::GFP* driven by *GH146* (green). Optical sections of anterior (A1, B1, C1) and posterior (A2, B2, C2) parts of AL. Yellow dot circles show the DL1 glomeruli. Only DL1 was innervated by the wild-type single-cell clone (A1, A2), whereas targeting to the DL1 glomerulus was lost for the hth^{P2} and $hth^{P1\text{-}K6\text{-}1}$ single-cell clones (B1, B2, C1, C2) (yellow arrows). Instead, ectopic glomeruli, such as VA1d and DC3 (white arrows), were innervated. (D) Quantification of dendritic phenotypes of DL1 single-cell clones. DL1 innervation was classified for each sample to four classes. Dense, complete dense input all over the target glomerulus; moderate, irregular robust input all over the target glomerulus; sparse, partial weak input; no input. (E) Quantification of ectopic innervation phenotypes by DL1 single-cell clones. No input; sparse, weak input; moderate, irregular robust input. All the hth^{P2} and $hth^{P1\text{-}K6\text{-}1}$ DL1 clones showed ectopic innervation in non-DL1 glomeruli. Number of samples is shown in the bar. In A-C, Optical sections of the right side of the brain are shown. Medial is to the left and dorsal is up. Neuropil was visualized with anti-nc82 (magenta). Scale bars: 20 μm.

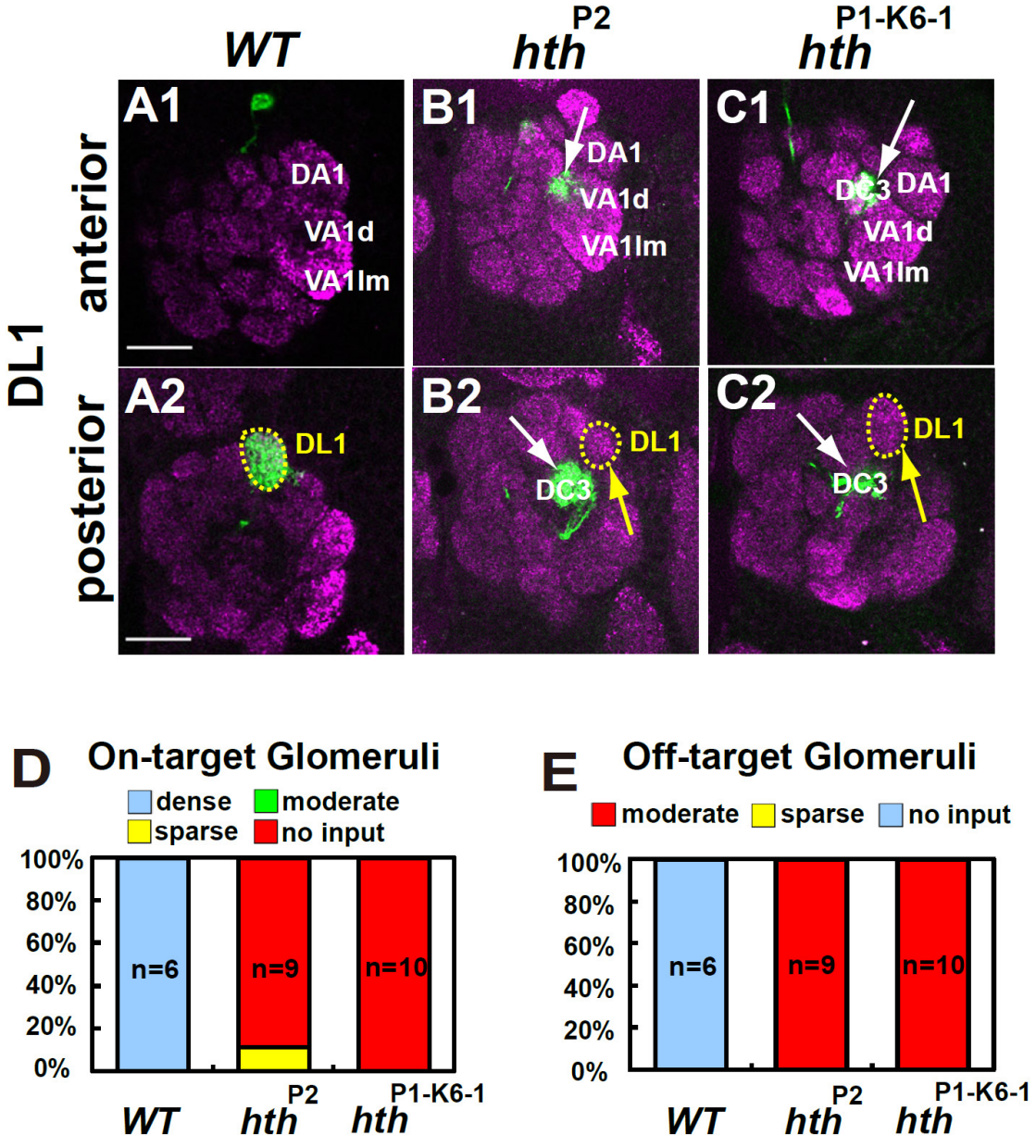
WT
hth P2
hth P1-K6-1
DL1
anterior
posterior
A1
B1
C1
A2
B2
C2
DA1
VA1d
VA1lm
DC3
DL1
D
On-target Glomeruli
dense
moderate
sparse
no input
100%
80%
60%
40%
20%
0%
n=6
n=9
n=10
WT
hth P2
hth P1-K6-1
E
Off-target Glomeruli
moderate
sparse
no input
100%
80%
60%
40%
20%
0%
n=6
n=9
n=10
WT
hth P2
hth P1-K6-1

Figure 13. Dendritic targeting defects of *hth MZ19* anterodorsal single-cell clones.

(A-D) Dendritic targeting phenotypes of wild-type (A, C) and $hth^{P1\text{-}K6\text{-}1}$ (B, D) *MZ19* anterodorsal single-cell clones. Clones were induced by heat shock at 24-48h after larval hatch and labeled with *UAS-mCD8::GFP* driven by *MZ19-GAL4* (green). Yellow dot circles show VA1d and DC3 glomeruli. Only the VA1d or DC3 glomerulus was innervated by the wild-type *MZ19* anterodorsal single-cell clones, whereas targeting to the VA1d and DC3 glomerulus was either absent or residual for $hth^{P1\text{-}K6\text{-}1}$ anterodorsal single-cell clones (yellow arrows). Instead, nearby ectopic glomeruli were innervated (white arrows). (E, F) Quantification of dendritic phenotypes of *MZ19* anterodorsal single-cell clones. Number of samples is shown in the bar. (E) Dendritic innervations in the on-target VA1d or DC3 glomerulus. For each sample, the extent of innervation in the on-target VA1d or DC3 glomerulus was examined and classified to four classes. Dense, complete dense input all over the target glomerulus; moderate, irregular robust input all over the target glomerulus; sparse, partial weak input; no input. (F) Ectopic innervation by *MZ19* anterodorsal single-cell clones. Ectopic innervation was classified for each sample to three classes. No input; sparse, weak input; moderate, irregular robust input. Note many of the $hth^{P1\text{-}K6\text{-}1}$ *MZ19* anterodorsal single-cell clones showed aberrant innervations in off-target glomeruli.

In A-D, optical sections of the right side of the brain are shown. Medial is to the left and dorsal is up. Neuropil was visualized with anti-nc82 (magenta). Scale bar: 20 μm.

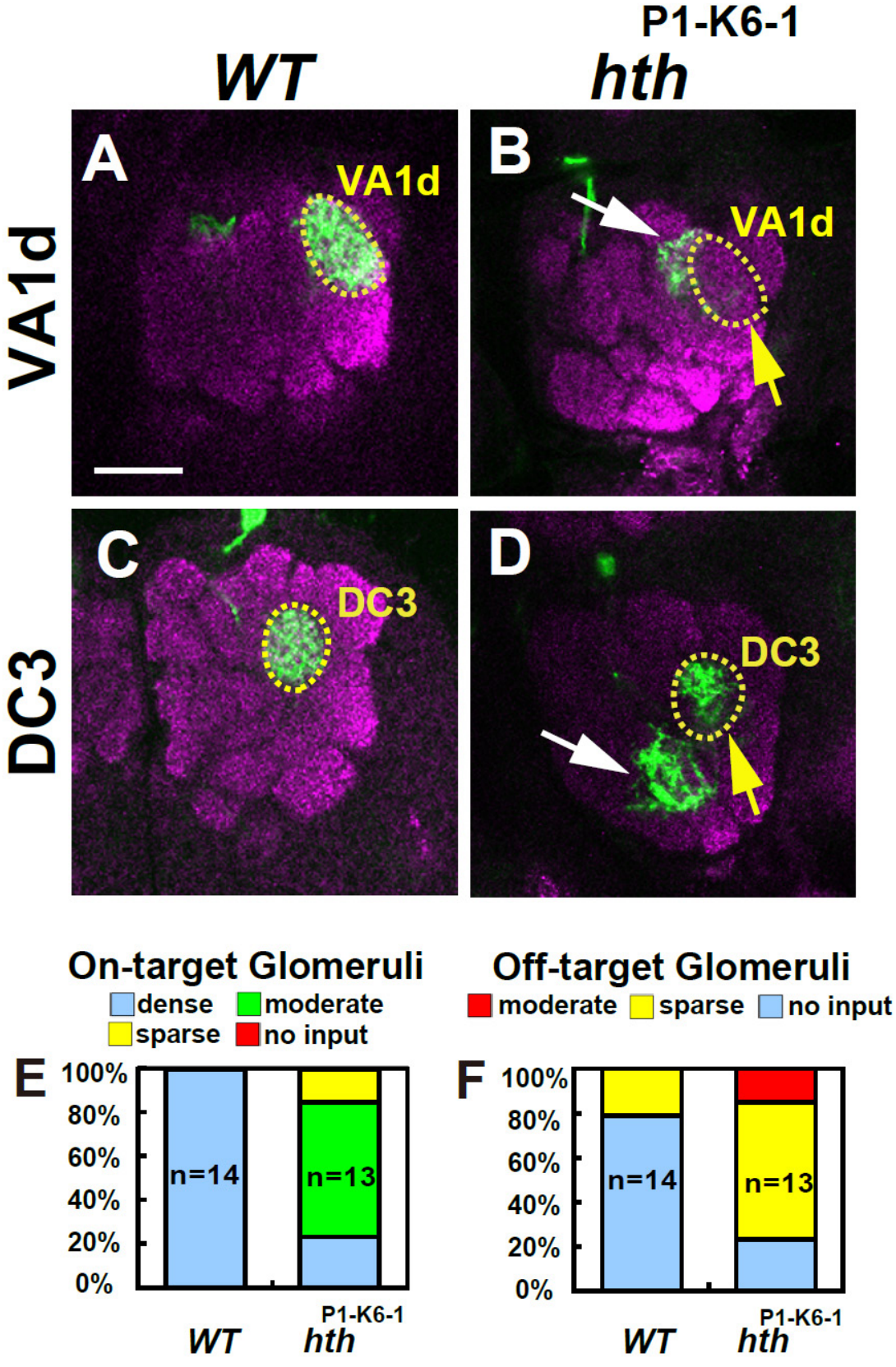
P1-K6-1
WT
hth
VA1d
DC3
A
B
C
D
VA1d
VA1d
DC3
DC3
On-target Glomeruli
dense
moderate
sparse
no input
Off-target Glomeruli
moderate
sparse
no input
E
F
100%
80%
60%
40%
20%
0%
n=14
n=13
n=14
n=13
WT
hth
P1-K6-1
WT
hth
P1-K6-1

Figure 14. Dendritic targeting defects of *hth* DA1 single-cell clones.

(A, B) Dendritic targeting phenotypes of wild-type (A) and $hth^{P1\text{-}K6\text{-}1}$ (B) DA1 single-cell clones. Clones were induced by heat shock at 24-48h after larval hatch and labeled with *UAS-mCD8::GFP* driven by *MZ19-GAL4* (green). Yellow dot circles show DA1 glomeruli. Only the DA1 glomerulus was innervated by the wild-type *MZ19* single-cell clones, whereas targeting to the DA1 glomerulus was residual for the $hth^{P1\text{-}K6\text{-}1}$ single-cell clone (yellow arrow). Instead, ectopic glomeruli were innervated (white arrow). (C, D) Quantification of dendritic phenotypes of DA1 single-cell clones. Number of samples is shown in the bar. (C) DA1 innervation was classified for each sample to four classes. Dense, complete dense input all over the target glomerulus; moderate, irregular robust input all over the target glomerulus; sparse, partial weak input; no input. (D) Ectopic innervation was classified for each sample to three classes. No input; sparse, weak input; moderate, irregular robust input. Note all of the $hth^{P1\text{-}K6\text{-}1}$ DA1 single-cell clones showed ectopic innervation in off-target glomeruli.

In A and B, optical sections of the right side of the brain are shown. Medial is to the left and dorsal is up. Neuropil was visualized with anti-nc82 (magenta). Scale bar: 20 μm.

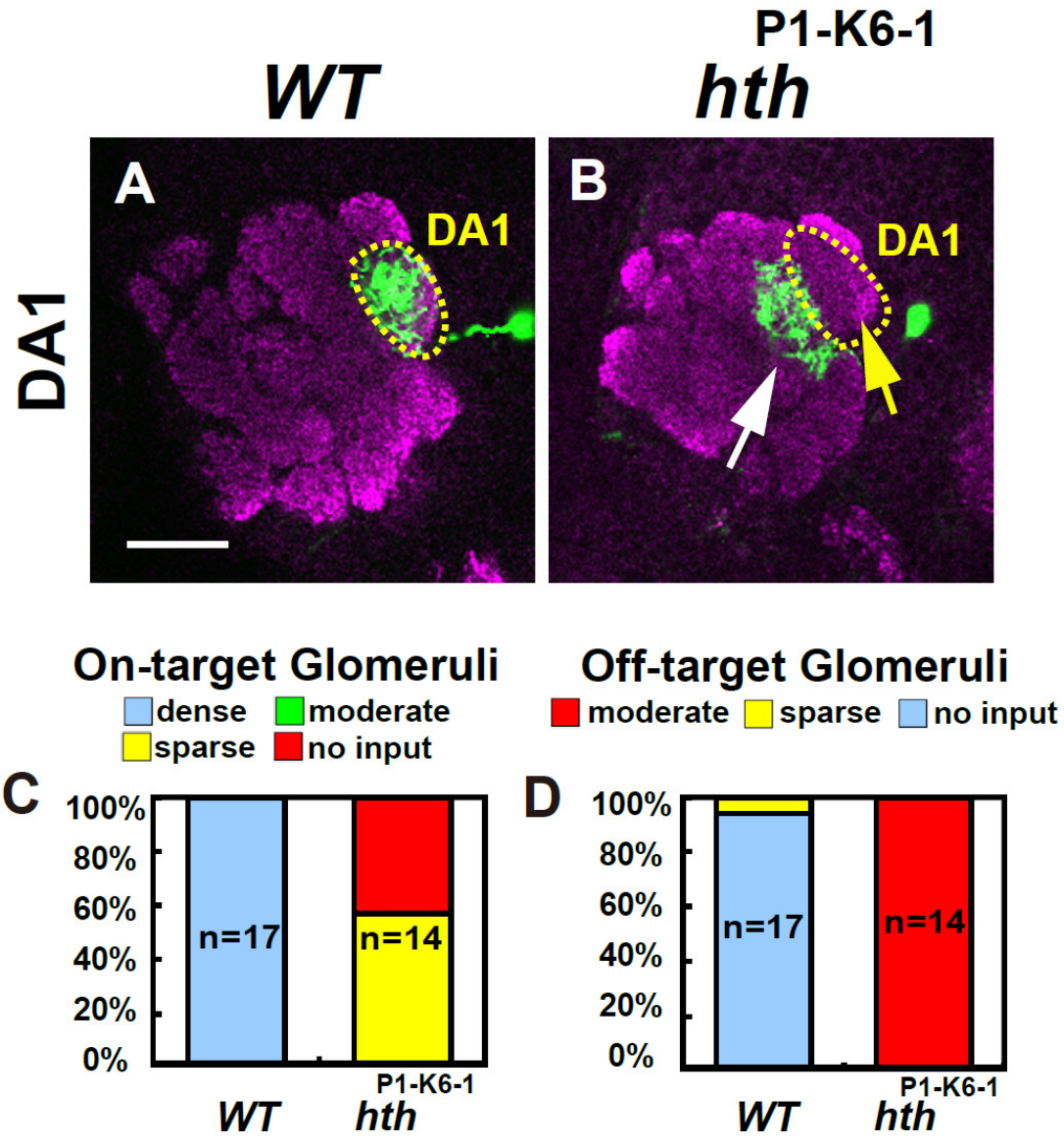
P1-K6-1
WT
hth
DA1
A
DA1
B
DA1
On-target Glomeruli
dense
moderate
sparse
no input
Off-target Glomeruli
moderate
sparse
no input
C
100%
80%
60%
40%
20%
0%
n=17
n=14
WT
hth
P1-K6-1
D
100%
80%
60%
40%
20%
0%
n=17
n=14
WT
hth
P1-K6-1

Figure 15. Axonal targeting defects of *hth* ad-NB clones.

(A–C) Axonal targeting phenotypes of wild-type (A), hth^{P2} (B) and $hth^{P1\text{-}K6\text{-}1}$ (C) ad-NB clones in the adult brain. Clones were induced by early 1st instar heat shock and labeled with *UAS-mCD8::GFP* driven by *GH146* (green). Neuropil was visualized with anti-nc82 (magenta). White dot lines demarcate MB calyx and LH. White arrows in (B) indicate spurious hth^{P2} axons that failed to fasciculate with the major bundle (yellow arrow). Note severe defasciculation and the detour of mutant axons from the wild-type path. In addition, *hth* PNs showed ectopic extensions in the ventrolateral brain (arrowhead in B, C). (D–F) Quantification of axonal phenotypes of ad-NB clones. Number of samples is shown in the bar. (D) Fasciculation of PN axons. Integrity of PN fasciculation was classified to the following four classes. Normal, fasciculation in a single bundle; mild, partially defasciculated; medium, defasciculated into several bundles; severe, complete defasciculation. Note that axons of 85% of the hth^{P2} and all of the $hth^{P1\text{-}K6\text{-}1}$ ad-NB clones failed normal fasciculation. (E) Axonal routing on the MB calyx. Axonal routing via the MB calyx was classified to the following three classes. Normal, all axons routing on the calyx; mild, partial routing on the calyx; severe, complete loss of routing on the calyx. Axons of 33% of the hth^{P2} and all of the $hth^{P1\text{-}K6\text{-}1}$ ad-NB clones detoured from the wild-type MB path. Note that the branching patterns of the mutant clones were aberrant even though they routed on the MB calyx. (F) Ectopic extension in the ventrolateral brain was classified in the following three classes. Normal, no axons extending ventrolaterally; mild, subsets of axons extending ventrolaterally; or severe, majority of axons extending ventrolaterally. Note the majority of the hth^{P2} (20/21) and all of the $hth^{P1\text{-}K6\text{-}1}$ ad-NB clones showed ectopic extensions in the ventrolateral brain. Scale bar: 50μM.

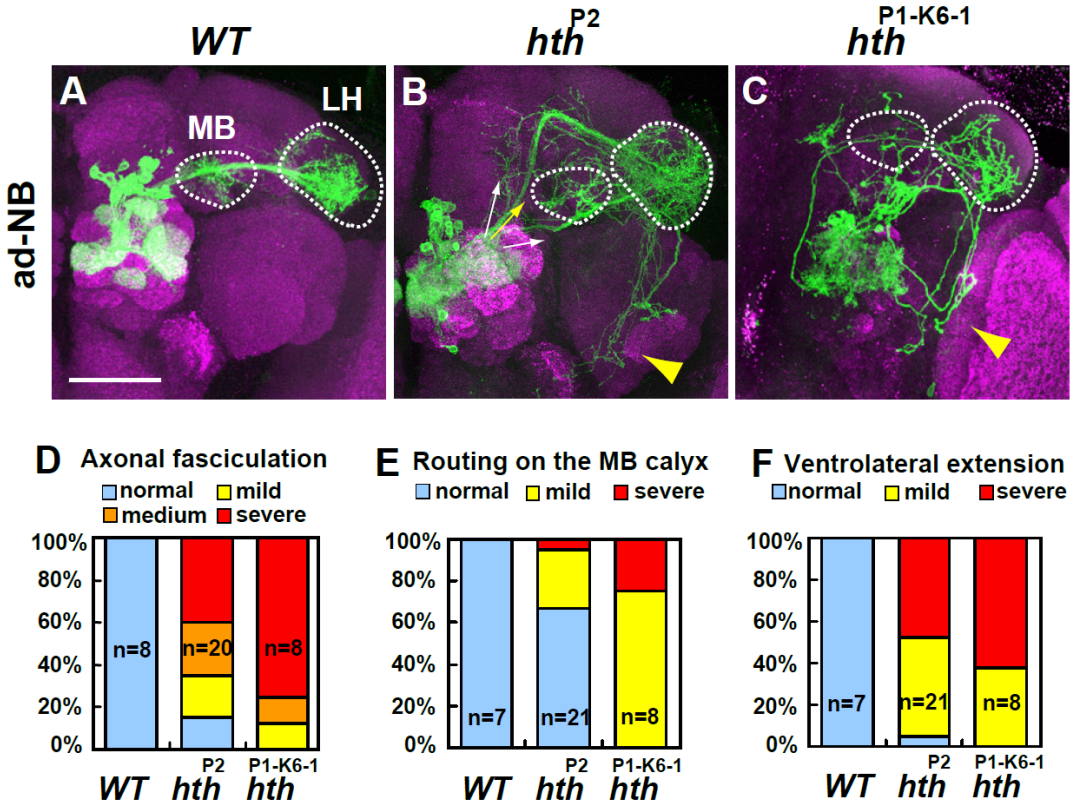
WT
hth P2
hth P1-K6-1
ad-NB
A
MB
LH
B
C
D Axonal fasciculation
normal
mild
medium
severe
100%
80%
60%
40%
20%
0%
n=8
n=20
n=8
WT
hth P2
hth P1-K6-1
E Routing on the MB calyx
normal
mild
severe
n=7
n=21
n=8
F Ventrolateral extension
normal
mild
severe
n=7
n=21
n=8

Figure. 16 Expression of Fas II was detected only faintly on *hth* mutant axons.

Expression of Fas II (magenta) in the axons of hth^{P2} ad-PN clones. 50h APF. Fas II was expressed in the inner antenno-cerebral tract that consists of the axons of anterodorsal and lateral PNs. While the axonal tract contributed by the normal lateral PNs (yellow arrow) expressed Fas II, the axonal tract of hth^{P2} ad-PN clone (white arrow) only faintly expressed Fas II. Clones were induced by early 1st instar heat shock and labeled with *UAS-mCD8::GFP* driven by *GH146* (green). Scale bar: 10μm.

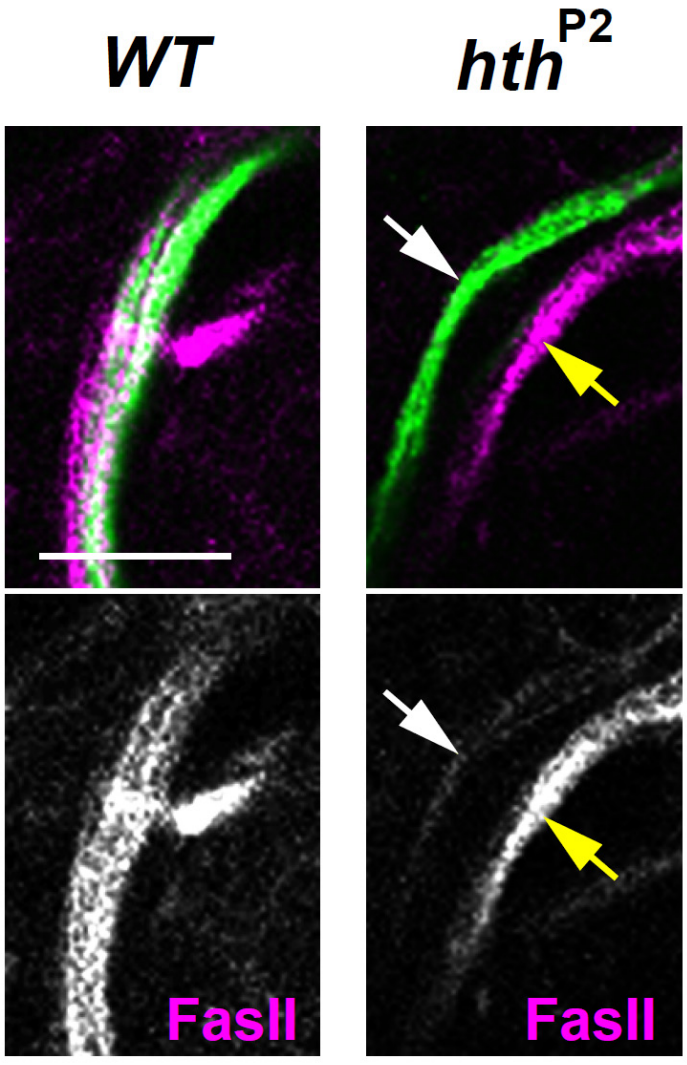
WT
hth P2
FasII
FasII

Figure 17. Axonal targeting defects of *hth* DL1 single-cell clones

(A-C) Axonal targeting phenotypes of wild-type (A), hth^{P2} (B) and $hth^{P1\text{-}K6\text{-}1}$ (C) DL1 single-cell clones. Clones were induced by early 1st instar heat shock and labeled *UAS-mCD8::GFP* driven by *GH146* (green). White dot lines demarcate the MB calyx and LH. Note that the hth^{P2} and $hth^{P1\text{-}K6\text{-}1}$ clones showed aberrant arborization in LH (yellow arrows in B, C). On the other hand, most hth^{P2} and $hth^{P1\text{-}K6\text{-}1}$ DL1 single-cell clones retained normal axonal routing via the MB calyx. (D-F) Quantification of axonal phenotypes of DL1 single-cell clones. Number of samples is shown in the bar. (D) Routing on the MB calyx. (E) Number of boutons on the MB calyx. (F) Number of branches in the LH. Note the increased branch number of hth^{P2} (12.9 ± 1.5) and $hth^{P1\text{-}K6\text{-}1}$ (14.5 ± 1.3) as compared to the wild type (8.0 ± 0.3). *$p < 0.05$ and ***$p < 0.001$ by Student's t-test. Scale bar: 50 μm.

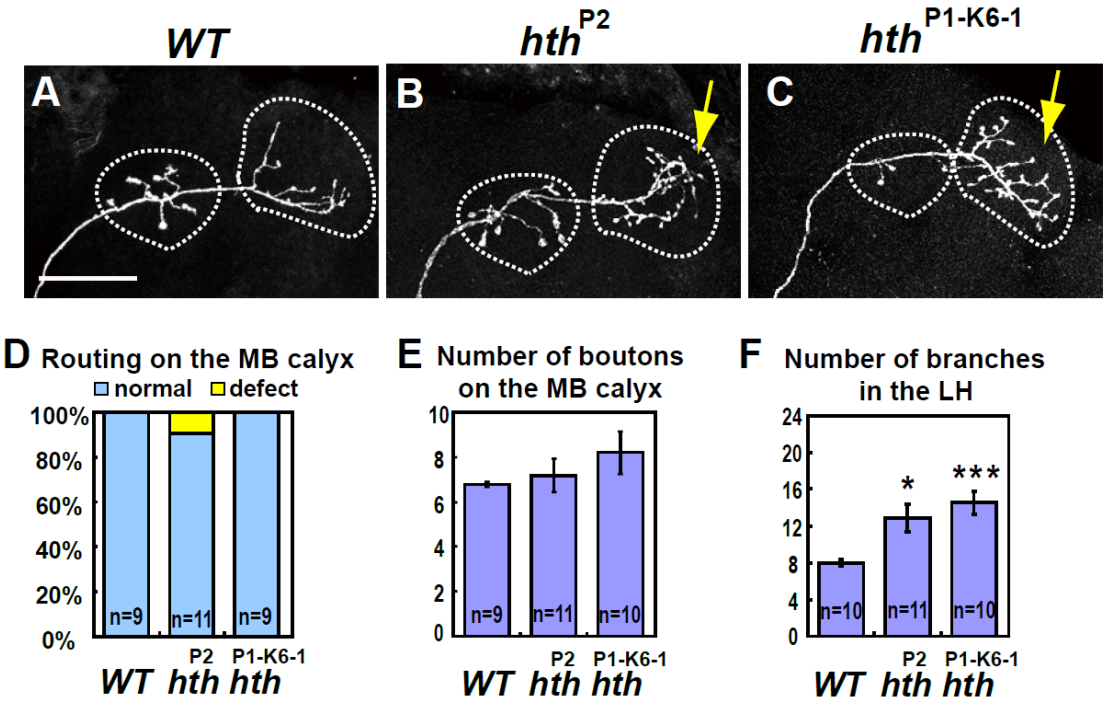
WT
hth P2
hth P1-K6-1
A
B
C
D Routing on the MB calyx
normal
defect
100%
80%
60%
40%
20%
0%
n=9
n=11
n=9
WT hth P2 hth P1-K6-1
E Number of boutons on the MB calyx
10
8
6
4
2
0
n=9
n=11
n=10
WT hth P2 hth P1-K6-1
F Number of branches in the LH
24
20
16
12
8
4
0
*
***
n=10
n=11
n=10
WT hth P2 hth P1-K6-1

Figure 18. Axonal targeting defects of *hth* DA1 single-cell clones

(A, B) Axonal targeting phenotypes of wild type (A) or $hth^{P1\text{-}K6\text{-}1}$ (B) DA1 single-cell clones. Clones were induced by heat shock at 24-48h after larval hatch and labeled with *UAS-mCD8::GFP* driven by *MZ19-GAL4*. White dot lines demarcate the MB calyx and LH. Note that the $hth^{P1\text{-}K6\text{-}1}$ clone shows a reduction in the number of boutons on the MB calyx (yellow arrowhead in B) and an increase in branch length in LH (yellow arrow in B). On the other hand, most $hth^{P1\text{-}K6\text{-}1}$ DA1 single-cell clones retained normal axonal routing via the MB calyx. (C-E) Quantification of axonal phenotypes of DA1 single-cell clones. Number of samples is shown in the bar. (C) Axonal routing on the MB calyx. (D) Number of boutons on the MB calyx. Note that $hth^{P1\text{-}K6\text{-}1}$ clones show a reduction in the number of boutons on the MB calyx (2.36 ± 2.1), as compared to the wild type (3.40 ± 0.3). (E) Maximum branch length in the LH. As an indicator of LH branching patterns, the longest terminal branch was measured for each clone. $hth^{P1\text{-}K6\text{-}1}$ clones show a significant increase in maximum branch length (50.8 ± 8.3), as compared to the wild type (26.2 ± 3.3). *$p < 0.05$ and ***$p < 0.001$ by Student's t-test. Scale bar: 50 μm.

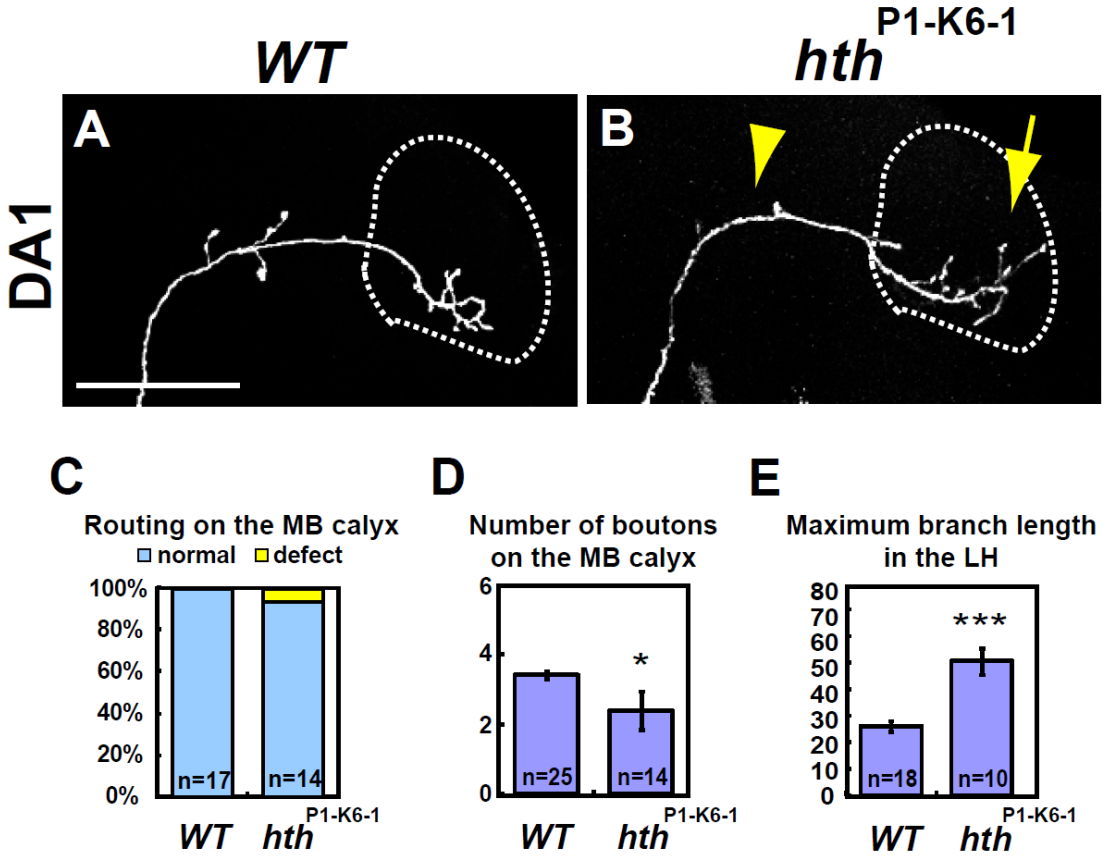
WT
hth P1-K6-1
DA1
A
B
C
Routing on the MB calyx
normal
defect
100%
80%
60%
40%
20%
0%
n=17
n=14
WT
hth P1-K6-1
D
Number of boutons on the MB calyx
6
4
2
0
*
n=25
n=14
WT
hth P1-K6-1
E
Maximum branch length in the LH
80
70
60
50
40
30
20
10
0
***
n=18
n=10
WT
hth P1-K6-1

Figure 19. Partial rescue phenotypes of ad-NB clones by *GH146*-mediated *hth* expression.

(A-D) Axonal and dendritic phenotypes of wild type (A), hth^{P2} (B) and *GH146*- mediated rescue (C, D) ad-NB clones. (C) Wild-type like clones. (D) Aberrant clones. Arrows in B and D indicate ectopic extensions in the ventrolateral brain. White dot lines demarcate the MB calyx and LH. (E) Quantification of ectopic extension in the ventrolateral brain. NB-clones. Only 27% (3/11) of the hth^{P2} NB clones restored wild-type like axonal pattern by *GH146*-mediated *hth* expression. Clones were induced by early 1st instar heat shock and labeled with *UAS-mCD8::GFP* driven by *GH146-GAL4* (green). Neuropil was visualized with anti-nc82 (magenta). Scale bar: 50 μm.

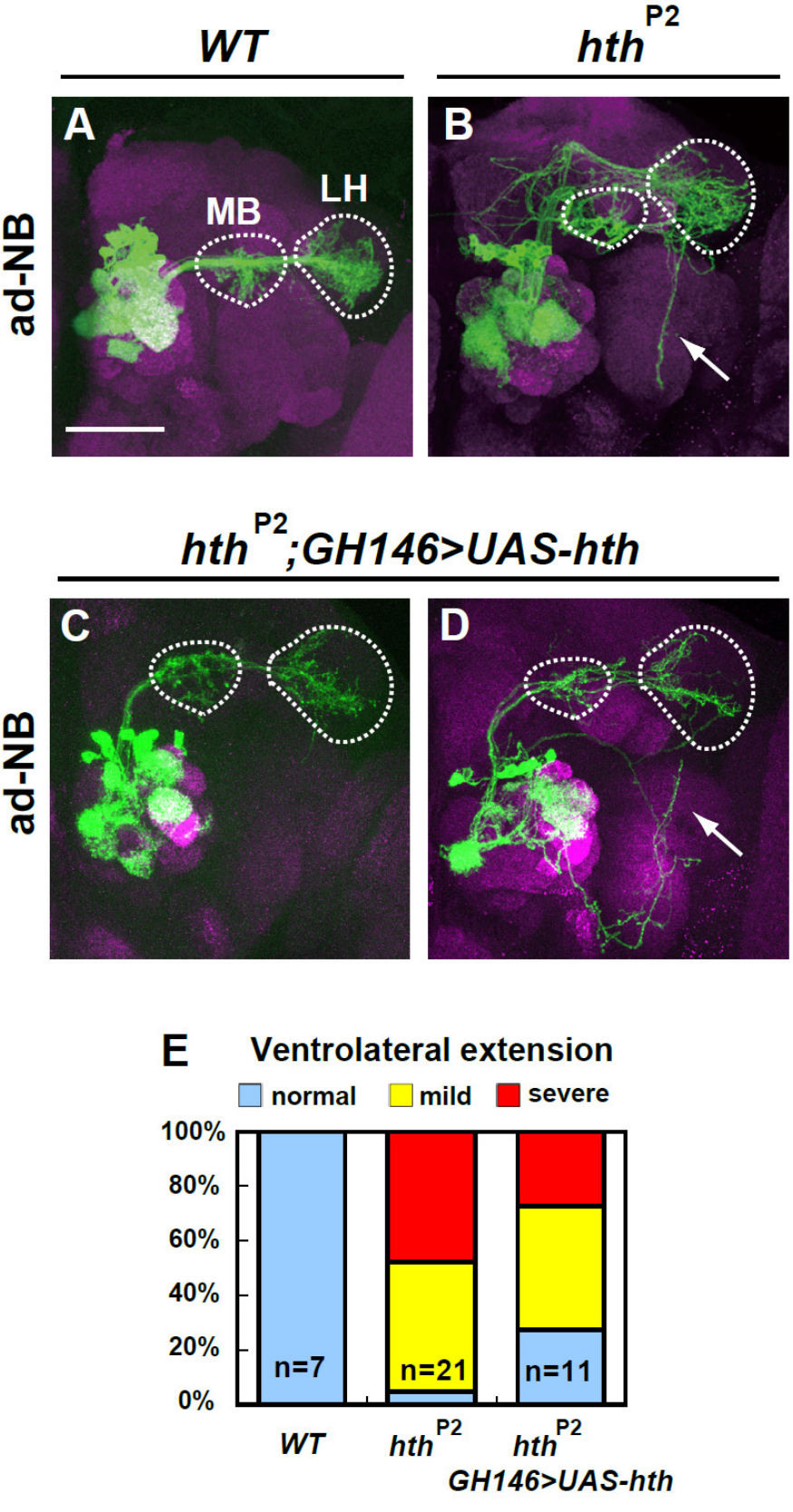
WT
hth P2
A
B
MB
LH
ad-NB
hth P2;GH146>UAS-hth
C
D
ad-NB
E
Ventrolateral extension
normal
mild
severe
100%
80%
60%
40%
20%
0%
n=7
n=21
n=11
WT
hth P2
hth P2
GH146>UAS-hth

Figure 20. Partial rescue of dendritic targeting phenotype by *GH146*-mediated *hth* expression

(A-D) Dendritic targeting phenotypes of wild-type (A), hth^{P2} (B) and *GH146*-mediated rescue (C and D) clones. Dendritic patterns of ad-NB clones in the anterior (A1-D1), middle (A2-D2) or posterior (A3-D3) parts of the AL in the adult brain. C and D are examples of varying rescue phenotypes. Yellow letters denote glomeruli normally innervated by ad-PNs. White letters denote glomeruli normally innervated by embryonic ad-PNs (VA2) or lateral PNs (DA1, DM5, DM2). Yellow arrows indicate wild-type like glomeruli. White arrows indicate aberrant glomeruli. Wild-type like innervation was restored only in a subset of glomeruli (yellow arrows). (E, F) Quantification of dendritic innervation by *GH146*-mediated rescue clones. (E) Quantification of dendritic innervation in on-target glomeruli. For each sample, the extent of innervation in the target glomeruli was examined and classified to four classes. Dense, complete dense input all over the target glomerulus; moderate, irregular robust input all over the target glomerulus; sparse, partial weak input; no input. (F) Quantification of dendritic innervation in off-target glomeruli. Extent of innervation in the non-target glomeruli was classified to three classes. No input; sparse, weak input; moderate, irregular robust input. Clones were induced by early 1st instar heat shock and labeled with *UAS-mCD8::GFP* driven by *GH146-GAL4* (green). Neuropil was visualized with anti-nc82 (magenta). Scale bar: 20 μm.

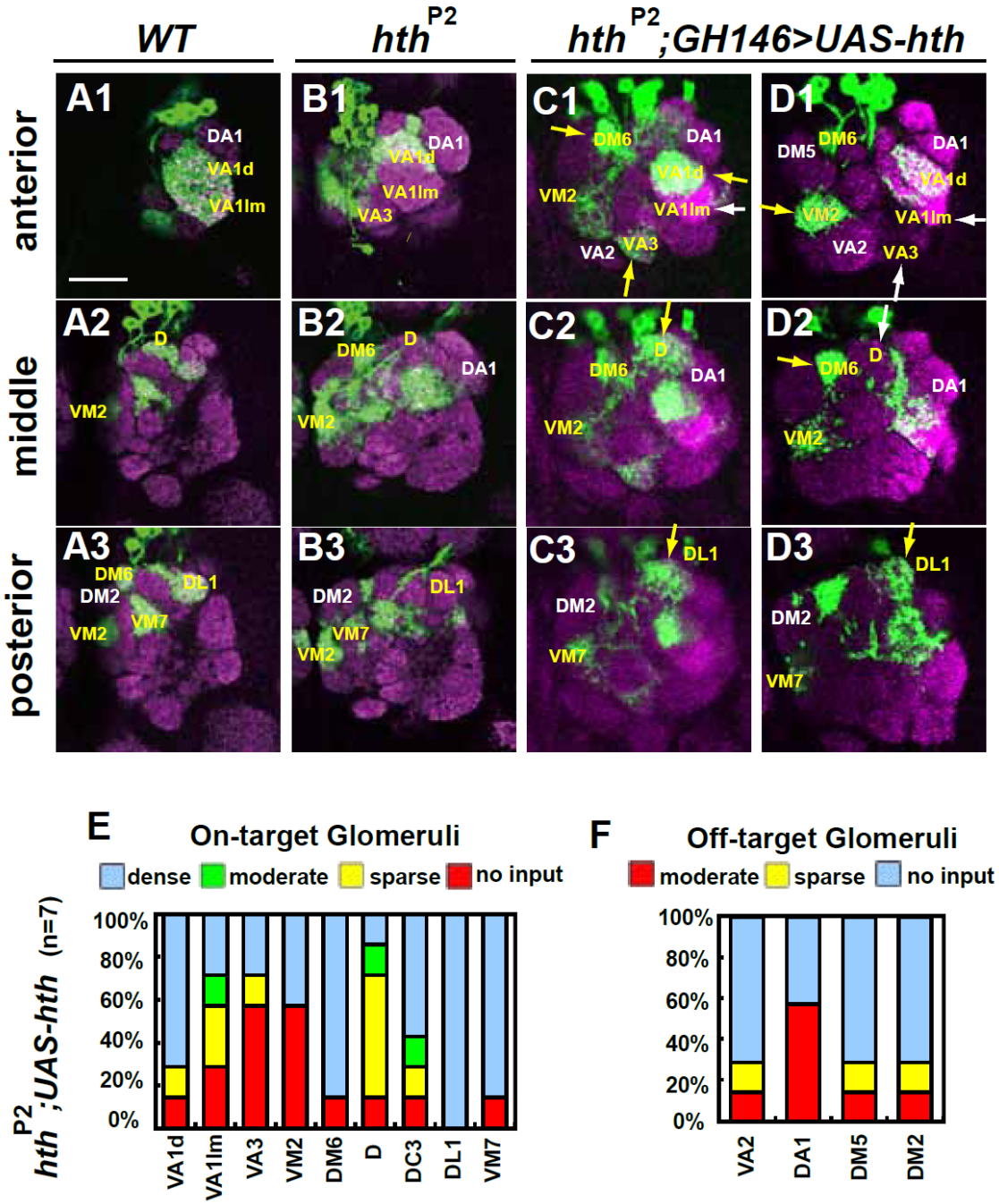
WT
hth P2
hth P2;GH146>UAS-hth
anterior
middle
posterior
A1
DA1
VA1d
VA1lm
B1
DA1
VA1d
VA1lm
VA3
C1
DM6
DA1
VA1d
VM2
VA1lm
VA2
VA3
D1
DM5
DM6
DA1
VA1d
VM2
VA1lm
VA2
VA3
A2
D
VM2
B2
DM6
D
DA1
VM2
C2
D
DM6
DA1
VM2
D2
D
DM6
DA1
VM2
A3
DM6
DL1
DM2
VM2
VM7
B3
DM2
DL1
VM7
VM2
C3
DL1
DM2
VM7
D3
DL1
DM2
VM7

E
On-target Glomeruli
dense
moderate
sparse
no input
hth P2;UAS-hth (n=7)
100%
80%
60%
40%
20%
0%
VA1d
VA1lm
VA3
VM2
DM6
D
DC3
DL1
VM7
F
Off-target Glomeruli
moderate
sparse
no input
100%
80%
60%
40%
20%
0%
VA2
DA1
DM5
DM2

Figure 21. Partial rescue phenotypes of DL1 single-cell clones by *GH146*-mediated *hth* expression.

(A-D) Axonal and dendritic phenotypes of wild type (A), hth^{P2} (B) and *GH146*- mediated rescue (C, D) clones. (C) Wild-type like clones. (D) Aberrant clones. White dot lines demarcate the MB calyx and LH. (E) Quantification of DL1 targeting in single-cell clones. Note that half of the hth^{P2} single-cell clones restored moderate (2/6) or dense (1/6) DL1 targeting by *GH146*-mediated *hth* expression. (F) Quantification of the number of LH branches in single-cell clones. Note suppression of the excess terminal branches by the *GH146*-mediated *hth* expression. * $p < 0.05$ by Student's t-test. Clones were induced by early 1st instar heat shock and labeled with *UAS-mCD8::GFP* driven by *GH146-GAL4* (green). Neuropil was visualized with anti-nc82 (magenta). Scale bar: 50 μm.

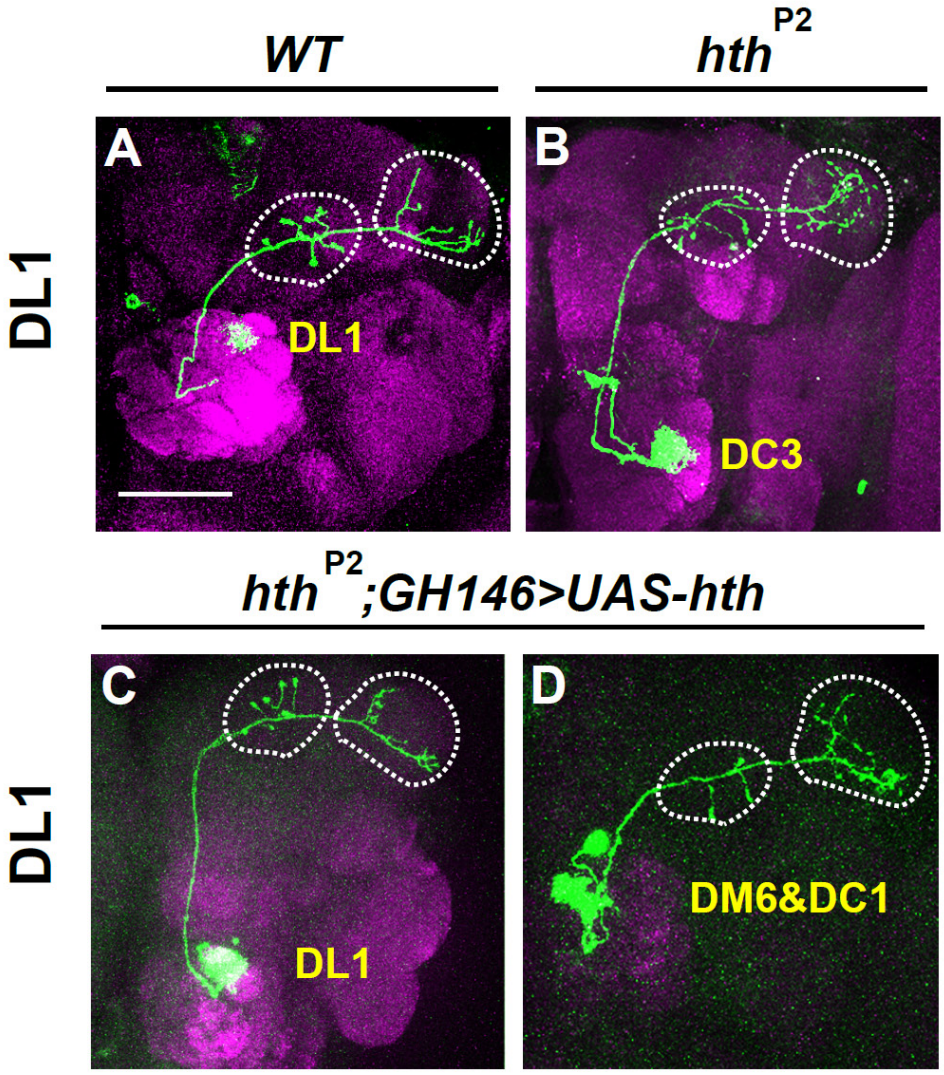
WT
hth P2
A
B
DL1
DL1
DC3
hth P2;GH146>UAS-hth
C
D
DL1
DL1
DM6&DC1

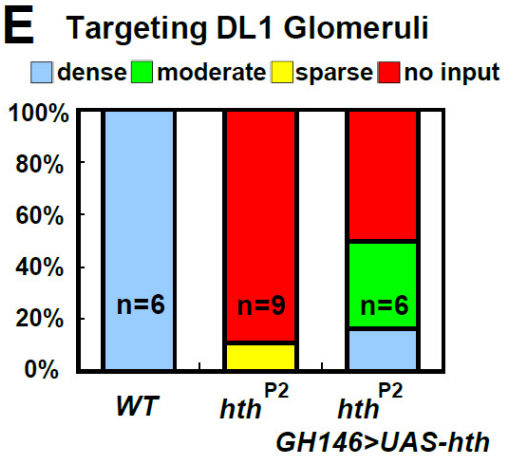
E Targeting DL1 Glomeruli
dense
moderate
sparse
no input
100%
80%
60%
40%
20%
0%
n=6
n=9
n=6
WT
hth P2
hth P2
GH146>UAS-hth

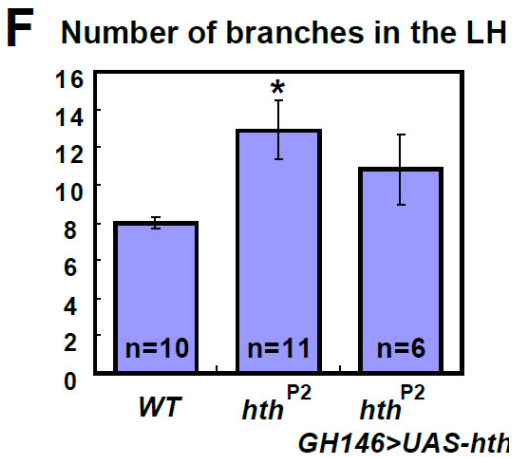
F Number of branches in the LH
16
14
12
10
8
6
4
2
0
*
n=10
n=11
n=6
WT
hth P2
hth P2
GH146>UAS-hth

Figure 22. Restoration of axonal and dendritic defects by *hth* driven by *elav-GAL4*

(A–C) Axonal targeting phenotypes of wild-type (A), hth^{P2} (B) and rescued (C) ad-NB clones in the adult brain. Clones were induced by early 1st instar heat shock and labeled with *UAS-mCD8::GFP* driven by *elav-GAL4* (green). Neuropil was visualized with anti-nc82 (magenta). White dot lines demarcate the MB calyx and LH. White arrow in (B) indicates aberrant hth^{P2} axonal routing. Note the wild type-like axonal projection by the rescued clone. Scale bar, 50 μm. (D–F) Dendritic targeting phenotypes of wild-type (D), hth^{P2} (E) and rescued (F) ad-NB clones. Wild-type *elav-GAL4* clones showed preferential dendritic targeting to the DL2dv glomerulus (yellow dot circles). Most hth^{P2} clones dendrites exhibited fuzzy innervation in DL2dv with ectopic innervation in nearby glomeruli (yellow arrow). Note the wild type-like DL2dv targeting by the rescued clone. Scale bar, 20 μm. (G) Quantification of axonal phenotypes of the *elav-GAL4* mediated NB clones. While many of the hth^{P2} clones (12/15) showed axonal defects, normal axonal projection pattern was restored in most of the rescued clones (9/11). (H) Quantification of DL2dv targeting phenotypes. DL2dv innervation was classified for each sample to three classes. Dense, complete dense input all over the target glomerulus; moderate, irregular robust input all over the target glomerulus; sparse, partial weak input; no input. While most of the hth^{P2} clones (14/15) failed to show complete innervation in DL2dv, wild type-like targeting was restored in most of the rescued clones (9/11). (I) Quantification of aberrant DL1 targeting phenotypes. Aberrant DL1 innervation was classified for each sample to three classes. No input; sparse, weak input; moderate, irregular robust input. While most of the hth^{P2} clones (14/15) showed aberrant DL1 innervation, ectopic targeting was suppressed in most of the rescued clones (10/11).

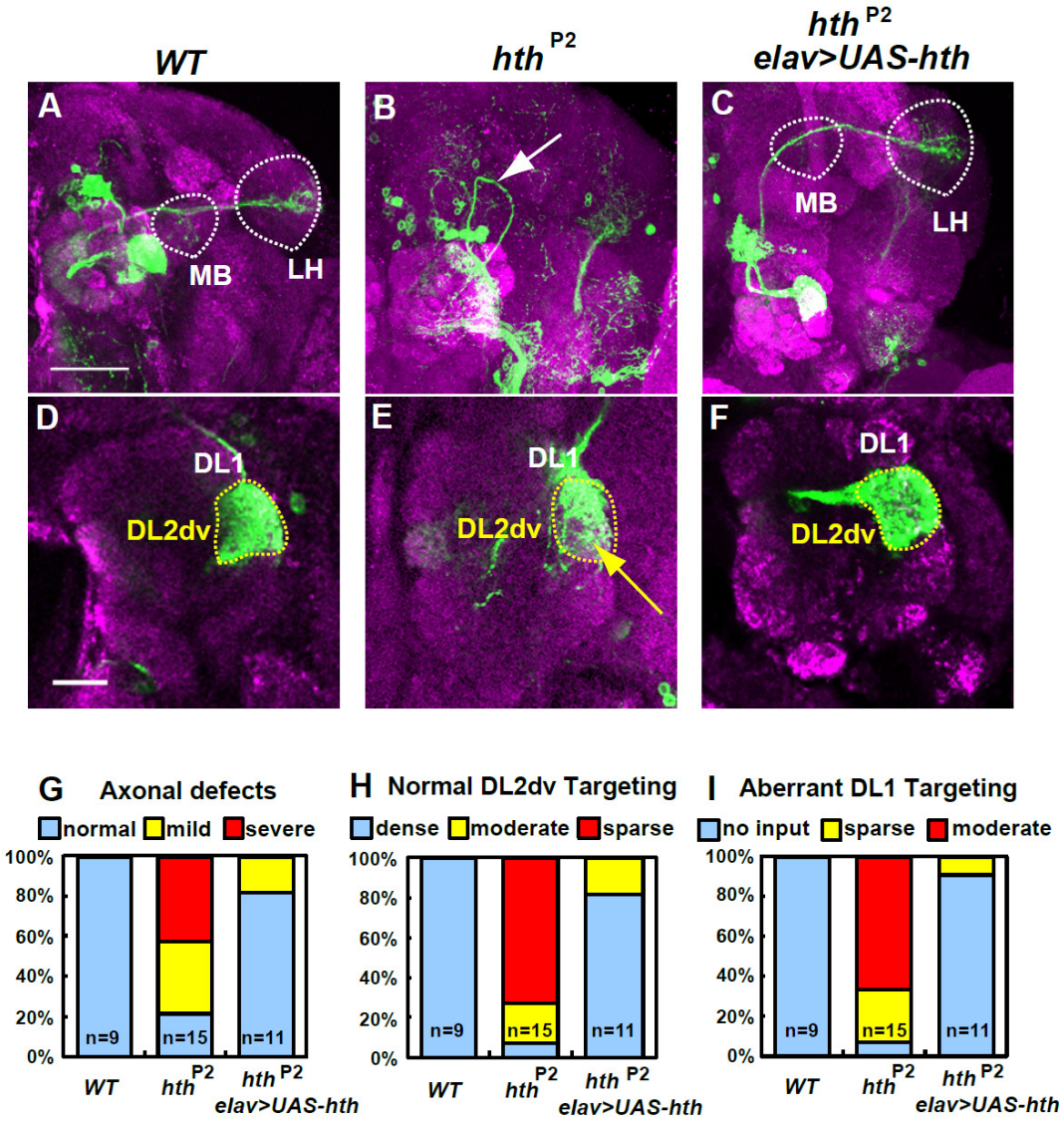
WT
hth P2
hth P2
elav>UAS-hth
A
B
C
MB
LH
MB
LH
D
E
F
DL1
DL2dv
DL1
DL2dv
DL1
DL2dv
G Axonal defects
normal
mild
severe
100%
80%
60%
40%
20%
0%
n=9
n=15
n=11
WT
hth P2
hth P2
elav>UAS-hth
H Normal DL2dv Targeting
dense
moderate
sparse
n=9
n=15
n=11
WT
hth P2
hth P2
elav>UAS-hth
I Aberrant DL1 Targeting
no input
sparse
moderate
n=9
n=15
n=11
WT
hth P2
hth P2
elav>UAS-hth

Figure 23. Dendritic phenotypes of ad-NB clones caused by over expression of *hth.*

(A, B) Dendritic targeting phenotypes of wild-type (A1-A3) and *hth* GOF (B1-B3) ad-NB clones. Dendritic patterns of ad-NB clones in the anterior (A1, B1), middle (A2, B2) and posterior (A3, B3) parts of AL. Yellow letters denote glomeruli normally innervated by ad-PNs. White letters denote glomeruli normally innervated by embryonic ad-PN (VA2) or lateral PNs (DA1, DM5, DM2). Note the absence of dendritic innervation in VA3 (yellow arrow in B2). (C) Quantification of dendritic innervation in on-target glomeruli. For each sample, the extent of innervation in the target glomeruli was examined and classified to four classes. Dense, complete dense input all over the target glomerulus; moderate, irregular robust input all over the target glomerulus; sparse, partial weak input; no input. VA3 innervation was lost in ~60% (5/8) of the GOF clones. (D) Quantification of dendritic innervation in off-target glomeruli. Extent of innervation in the non-target glomeruli was classified to three classes. No input; sparse, weak input; moderate, irregular robust input. Number of samples is shown in the figure. Clones were induced by early 1st instar heat shock and labeled with *UAS-mCD8::GFP* driven by *GH146* (green). Neuropil was visualized with anti-nc82 (magenta). The right side of the brain is shown. Medial is to the left and dorsal is up. Scale bar: 20 μm.

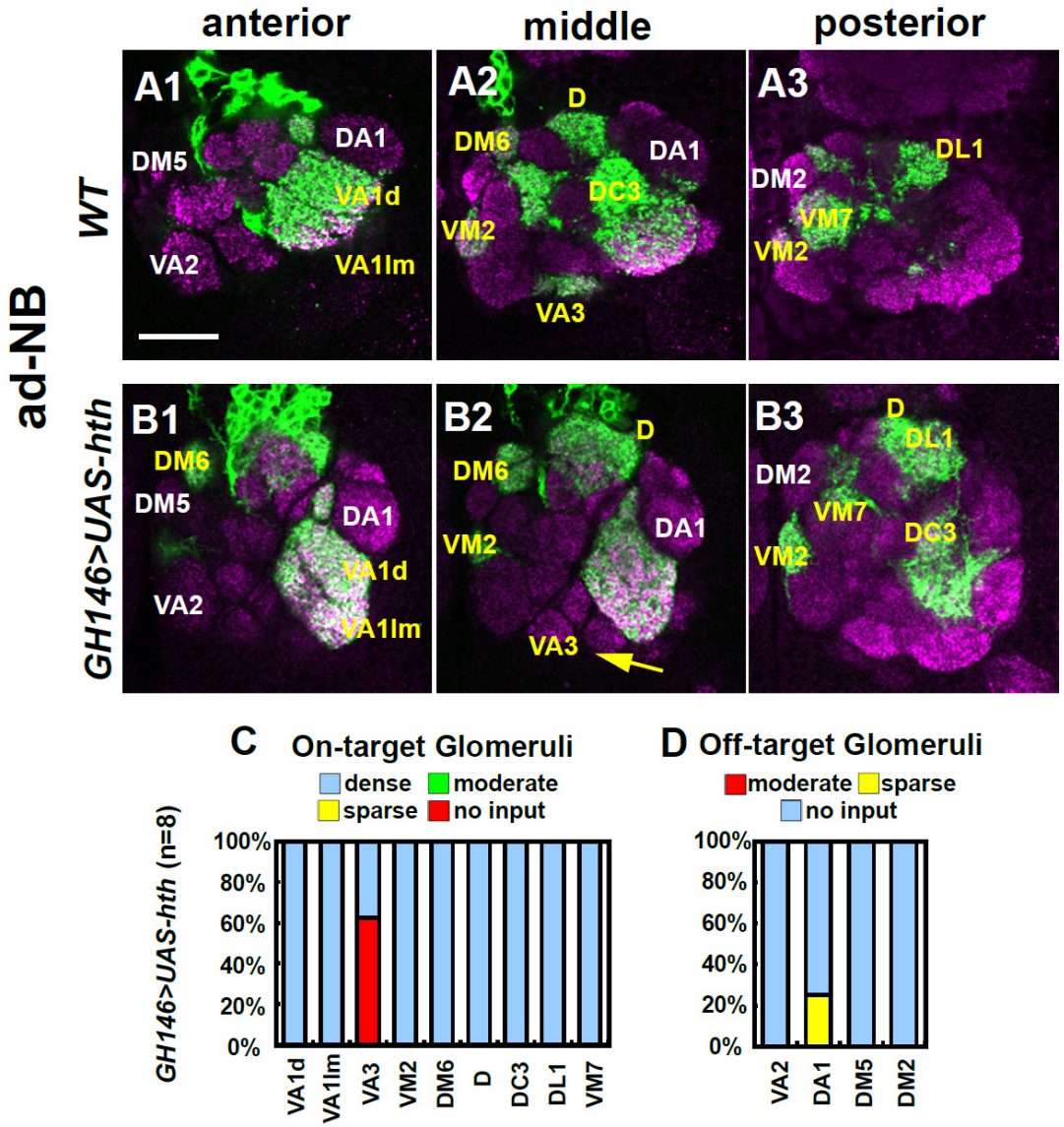
anterior
middle
posterior
ad-NB
WT
GH146>UAS-hth
A1
DA1
DM5
VA1d
VA2
VA1lm
A2
D
DM6
DA1
DC3
VM2
VA3
A3
DL1
DM2
VM7
VM2
B1
DM6
DM5
DA1
VA1d
VA2
VA1lm
B2
D
DM6
VM2
DA1
VA3
B3
D
DL1
DM2
VM7
DC3
VM2
C On-target Glomeruli
dense
moderate
sparse
no input
GH146>UAS-hth (n=8)
100%
80%
60%
40%
20%
0%
VA1d
VA1lm
VA3
VM2
DM6
D
DC3
DL1
VM7
D Off-target Glomeruli
moderate
sparse
no input
100%
80%
60%
40%
20%
0%
VA2
DA1
DM5
DM2

Figure 24. Dendritic phenotypes of single-cell clones caused by over expression of *hth*.

(A, B) Dendritic targeting phenotypes of wild-type (A) and *hth* GOF (B) single-cell clones. Yellow dot circles show DL1 glomeruli. DL1 targeting was not affected in GOF clones. (C, D) Quantification of dendritic phenotypes of DL1 single-cell clones. (C) DL1 innervation was classified for each sample to four classes. Dense, complete dense input all over the target glomerulus; moderate, irregular robust input all over the target glomerulus; sparse, partial weak input; no input. (D) Ectopic innervation was classified for each sample to three classes. No input; sparse, weak input; moderate, irregular robust input. Number of samples is shown in the bar. Clones were induced by early 1st instar heat shock and labeled with *UAS-mCD8::GFP* driven by *GH146* (green). Neuropil was visualized with anti-nc82 (magenta). The right side of the brain is shown. Medial is to the left and dorsal is up. Scale bar: 20 μm.

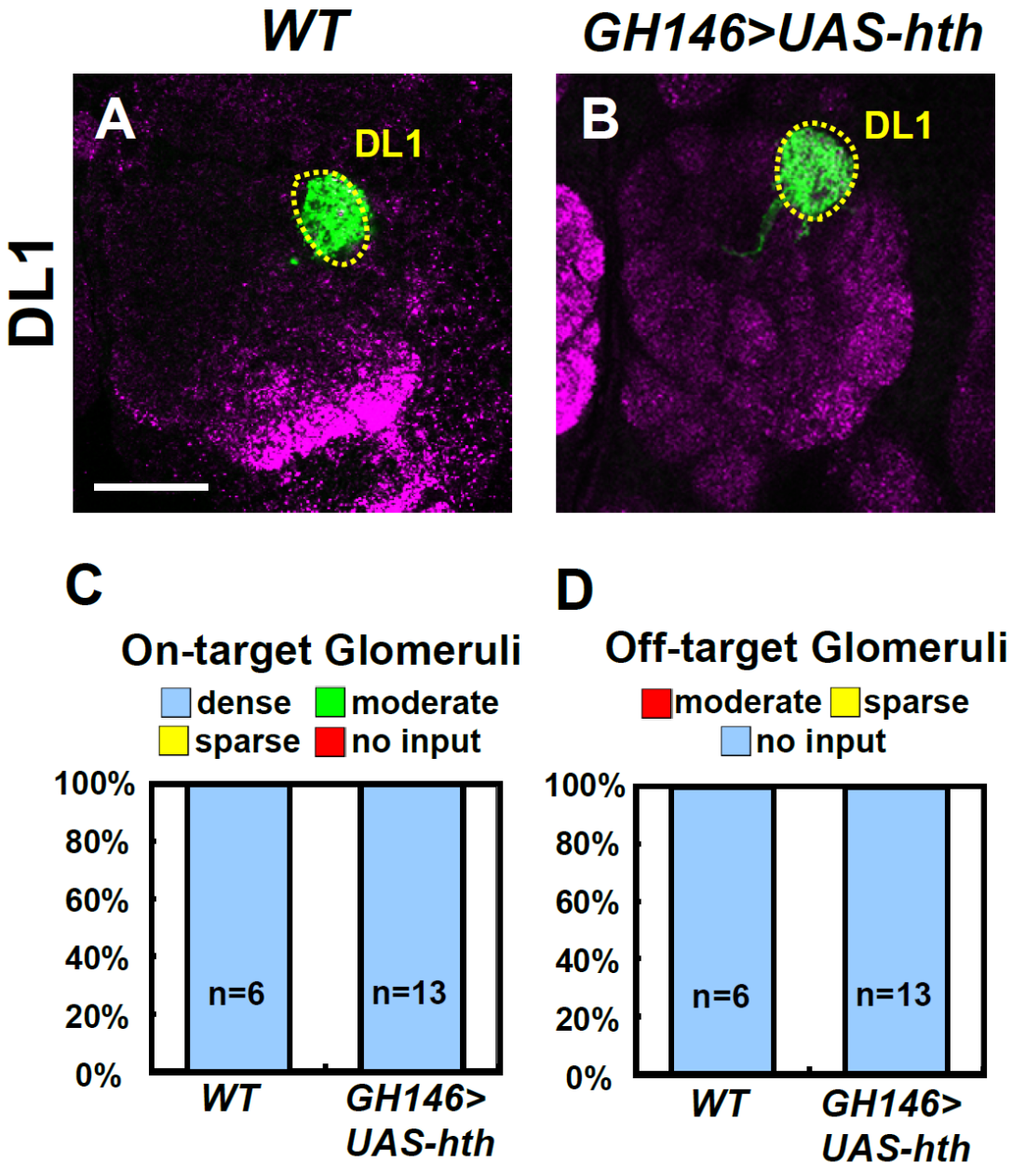
WT
GH146>UAS-hth
DL1
A
DL1
B
DL1
C
On-target Glomeruli
dense
moderate
sparse
no input
100%
80%
60%
40%
20%
0%
n=6
n=13
WT
GH146>
UAS-hth
D
Off-target Glomeruli
moderate
sparse
no input
100%
80%
60%
40%
20%
0%
n=6
n=13
WT
GH146>
UAS-hth

Figure 25. Axonal phenotypes of ad-NB clones caused by over expression of *hth*

Axonal targeting phenotypes of wild-type (A) and *hth* overexpression (B) ad-NB clones. White dot lines demarcate the MB calyx and LH. Arrow in B indicate aberrant branching in the LH. Clones were induced by early 1st instar heat shock and labeled with *UAS-mCD8::GFP* driven by *GH146* (green). Neuropil was visualized with anti-nc82 (magenta). The right side of the brain is shown. Medial is to the left and dorsal is up. Scale bar: 50 μm.

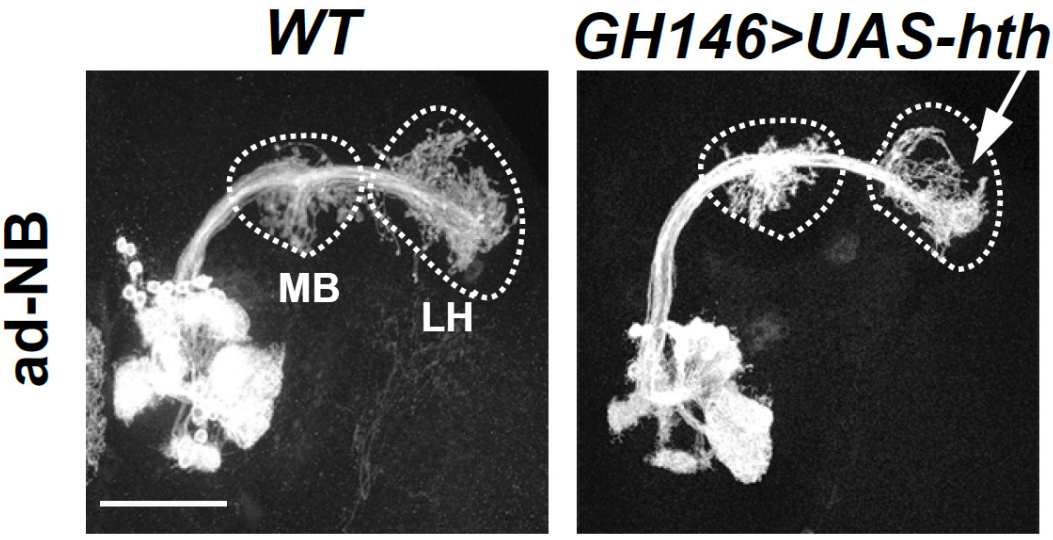
WT
GH146>UAS-hth
ad-NB
MB
LH

Figure 26. Axonal phenotypes of single-cell clones caused by over expression of *hth*

(A, B) Axonal targeting phenotypes of wild-type (A) and *hth* overexpression (B) single-cell clones. White dot lines demarcate the MB calyx and LH. Arrow in B indicate aberrant branching in the LH. (C, D) Quantification of axonal phenotypes of single-cell clones. (C) Number of boutons on the MB calyx. (D) Number of branches in the LH. *** $p < 0.001$ by Student's t-test. Number of samples is shown in the bar. Clones were induced by early 1st instar heat shock and labeled with *UAS-mCD8::GFP* driven by *GH146* (green). Neuropil was visualized with anti-nc82 (magenta). The right side of the brain is shown. Medial is to the left and dorsal is up. Scale bar: 50 μm.

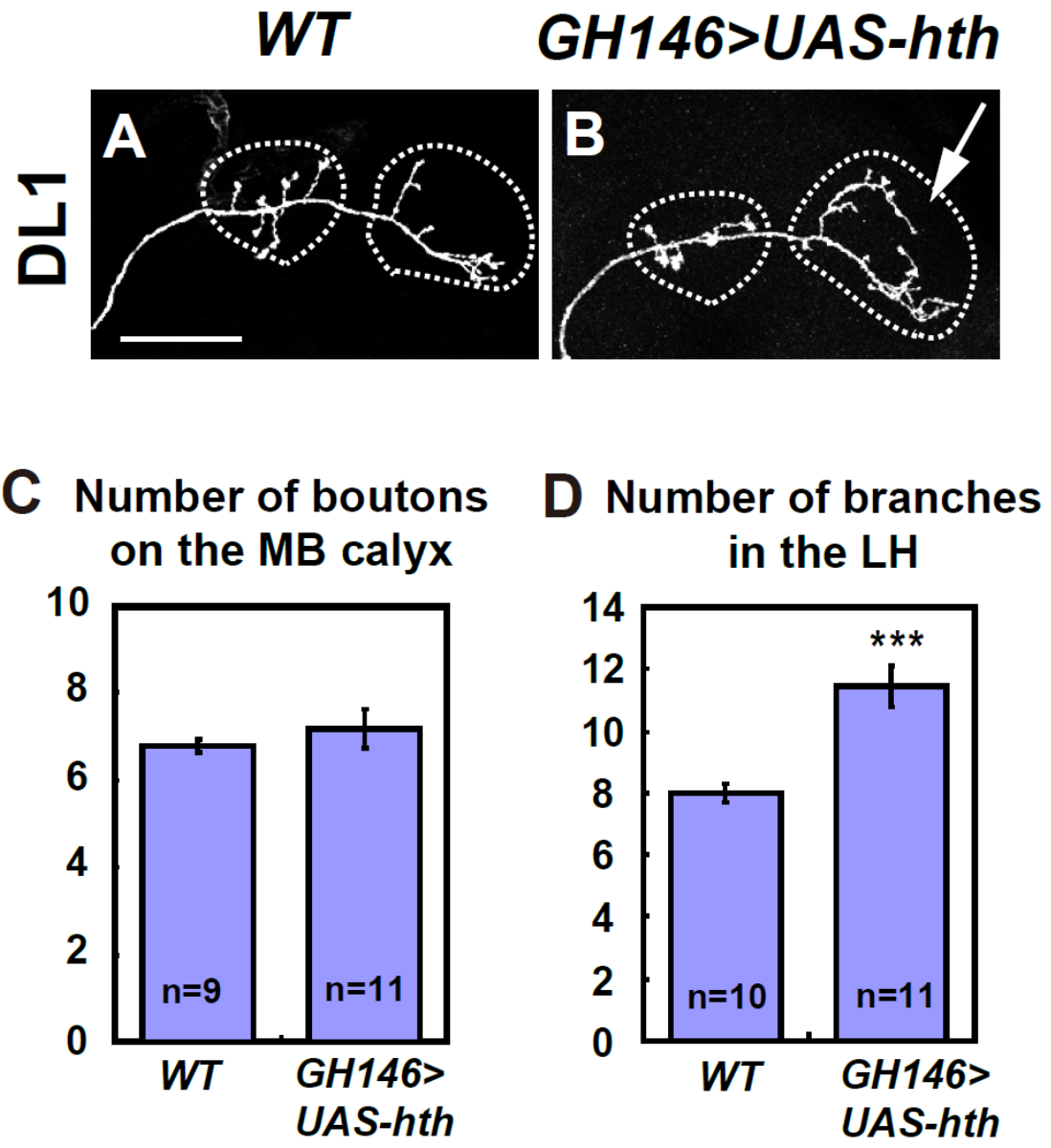
WT
GH146>UAS-hth
DL1
A
B
C Number of boutons on the MB calyx
10
8
6
4
2
0
n=9
n=11
WT
GH146> UAS-hth
D Number of branches in the LH
14
12
10
8
6
4
2
0
***
n=10
n=11
WT
GH146> UAS-hth

Figure 27. Dendritic targeting defects of *exd* mutant ad-NB clones.

(A, B) Dendritic targeting phenotypes of wild-type and *exd*^{1} ad-NB clones. Dendritic targeting patterns of ad-NB clones in the anterior (A1, B1), middle (A2, B2) or posterior (A3, B3) parts of AL. Yellow letters denote the landmark glomeruli normally innervated by *GH146*-positive ad-PNs. White letters denote ectopic glomeruli that are not innervated by the wild-type ad-PNs. Yellow arrows indicate on-target glomeruli with partial or no innervation by *exd*^{1} clones. White allows indicate off-target glomeruli ectopically innervated by the *exd*^{1} clone. (C) Quantification of dendritic innervation in on-target glomeruli. For each sample, the extent of innervation in the target glomeruli was examined and classified to four classes. Dense, complete dense input all over the target glomerulus; moderate, irregular robust input all over the target glomerulus; sparse, partial weak input; no input. (D) Quantification of dendritic innervation in off-target glomeruli. Extent of innervation in the non-target glomeruli was classified to three classes. No input; sparse, weak input; moderate, irregular robust input. Number of clones is indicated in the figure. Clones were induced by early 1st instar heat shock and labeled with *UAS-mCD8::GFP* driven by *GH146* (green). Neuropil was visualized with anti-nc82 (magenta). Scale bar: 20 μm.

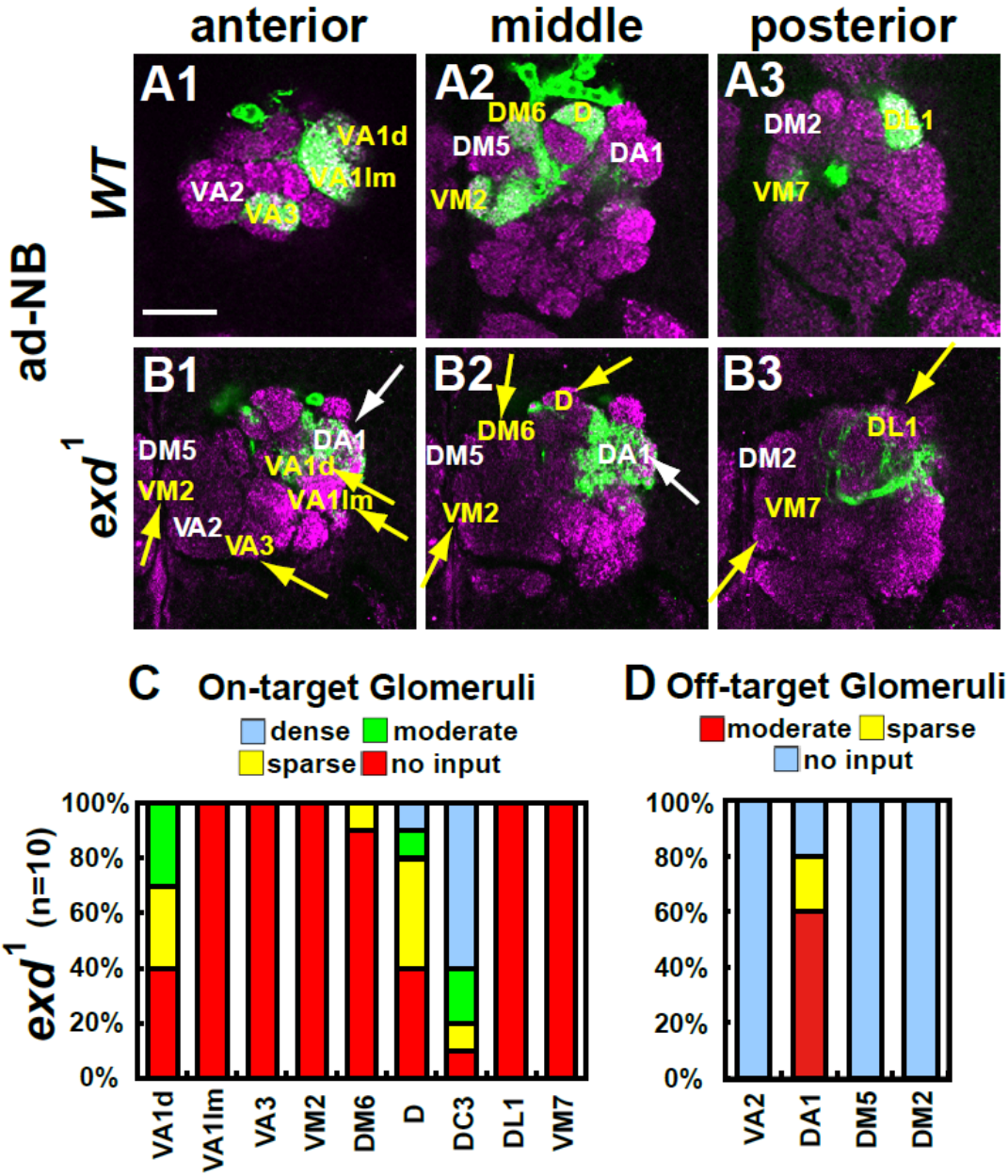
anterior
middle
posterior
ad-NB
WT
exd1
A1
A2
A3
B1
B2
B3
VA1d
VA1lm
VA2
VA3
DM6
D
DM5
DA1
VM2
DM2
DL1
VM7
C On-target Glomeruli
dense
moderate
sparse
no input
exd1 (n=10)
100%
80%
60%
40%
20%
0%
VA1d
VA1lm
VA3
VM2
DM6
D
DC3
DL1
VM7
D Off-target Glomeruli
moderate
sparse
no input
VA2
DA1
DM5
DM2

Figure 28. Dendritic targeting defects of *exd* mutant single-cell clones.

(A, B) Dendritic targeting phenotypes of wild-type and *exd*^{1} single-cell clones. Optical sections of anterior (A1, B1) and posterior (A2, B2) parts of AL. Yellow dot circles demarcate the DL1 glomeruli. Only DL1 was innervated by the wild-type single-cell clones (A1, A2). Note loss of innervation in the DL1 glomerulus (yellow arrow) for the *exd*^{1} single-cell clone (B1, B2). (C) Quantification of on-target innervation phenotypes of the DL1 single-cell clones. DL1 innervation was classified for each sample to four classes. Dense, complete dense input all over the target glomerulus; moderate, irregular robust input all over the target glomerulus; sparse, partial weak input; no input. (D) Quantification of ectopic targeting phenotypes of the DL1 single-cell clones. Ectopic innervation was classified for each sample to three classes. No input; sparse, weak input; moderate, irregular robust input. Number of clones is indicated in the bar. Clones were induced by early 1st instar heat shock and labeled with *UAS-mCD8::GFP* driven by *GH146* (green). Neuropil was visualized with anti-nc82 (magenta). Scale bar: 20 μm.

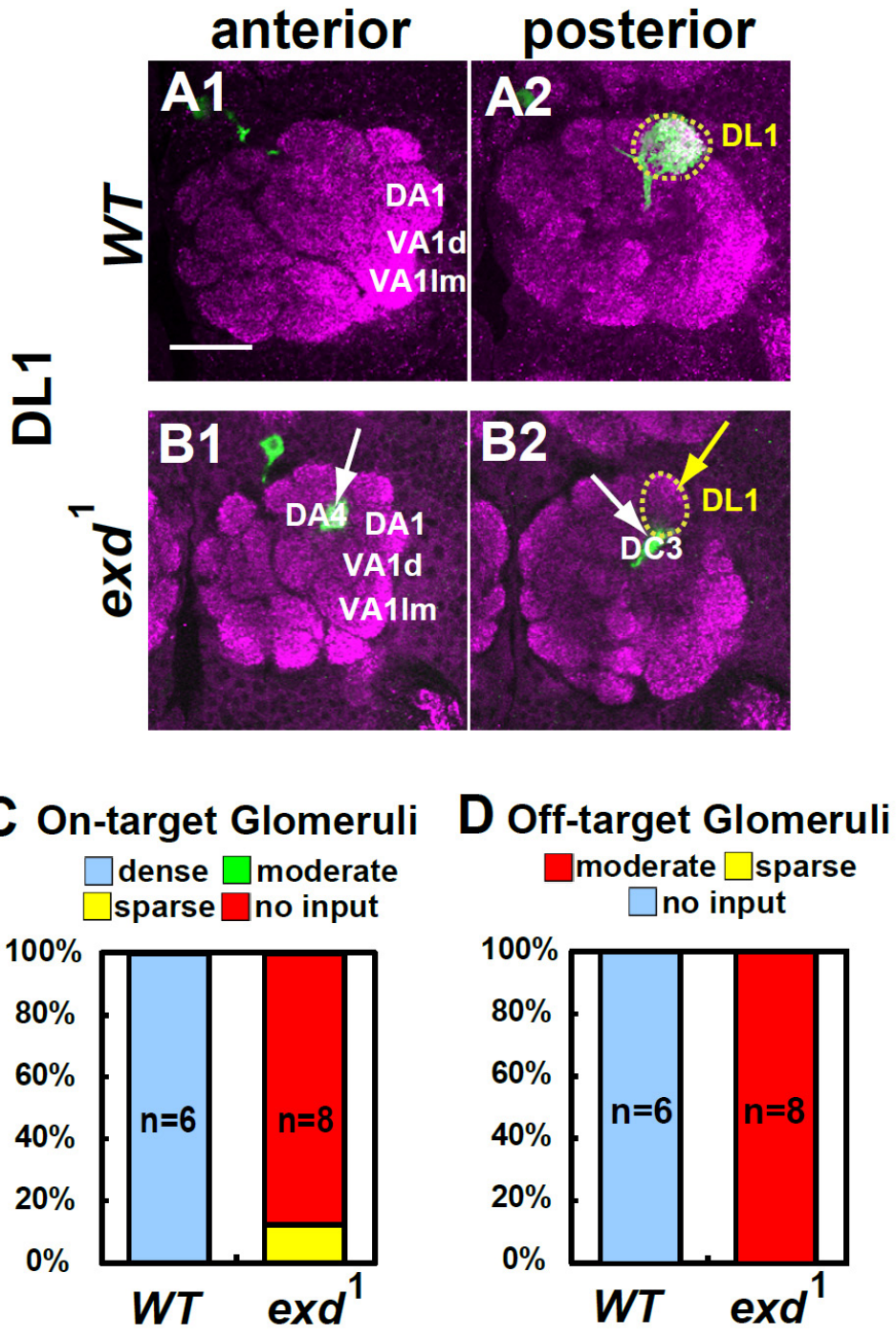
anterior
posterior
A1
A2
DL1
WT
DA1
VA1d
VA1lm
DL1
B1
B2
exd1
DA1
DA1
VA1d
VA1lm
DL1
DC3
C On-target Glomeruli
dense
moderate
sparse
no input
100%
80%
60%
40%
20%
0%
n=6
n=8
WT
exd1
D Off-target Glomeruli
moderate
sparse
no input
100%
80%
60%
40%
20%
0%
n=6
n=8
WT
exd1

Figure 29. Axonal targeting defects of *exd* mutant ad-NB clones.

(A, B) Axonal targeting phenotypes of wild-type and *exd*^{1} ad-NB clones. White dot lines demarcate the MB calyx and LH. White arrow in B indicates aberrant *exd*^{1} axons that failed to fasciculate with the major bundle (yellow arrow). Arrowhead in B indicates an ectopic extension of *exd*^{1} PNs in the ventrolateral brain. (C–E) Quantification of axonal phenotypes of *exd*^{1} ad-NB clones. Number of samples is shown in the bar. (C) Fasciculation of ad-PN axons. Note that axons of 8/9 (89%) of the *exd*^{1} ad-NB clones failed to show normal fasciculation. (D) Axonal routing on the MB calyx. Note that axons of 67% (6/9) of the *exd*^{1} ad-NB clones failed to rout on the MB calyx. (E) Ectopic extension in the ventrolateral brain. Note that 67% (6/9) of the *exd*^{1} ad-NB clones showed ectopic extensions. Clones were induced by early 1st instar heat shock and labeled with *UAS-mCD8::GFP* driven by *GH146* (green). Neuropil was visualized with anti-nc82 (magenta). Scale bar: 50 μm.

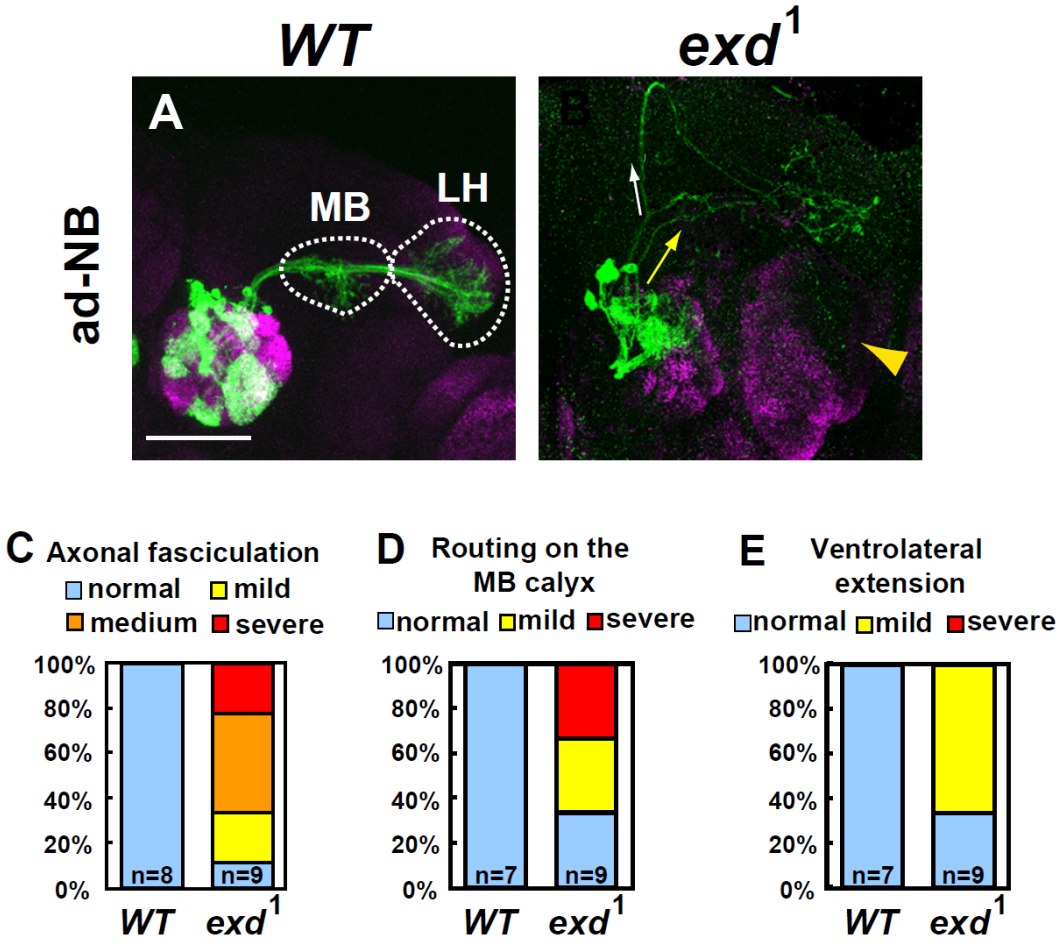
WT
exd1
A
B
ad-NB
MB
LH
C Axonal fasciculation
normal
mild
medium
severe
100%
80%
60%
40%
20%
0%
n=8
n=9
WT
exd1
D Routing on the MB calyx
normal
mild
severe
n=7
n=9
E Ventrolateral extension
normal
mild
severe
n=7
n=9

Figure 30. Axonal targeting defects of *exd* mutant single-cell clones.

(A, B) Axonal targeting phenotypes of wild-type and exd^{1} single-cell clones. White dot lines demarcate the MB calyx and LH. Note that exd^{1} clones showed aberrant branching pattern in LH (yellow arrow in B). (C) Quantification of axonal routing phenotypes. (D) Quantification of the numbers of boutons on the MB calyx. (E) Quantification of the number of branches in the LH. *** $p < 0.001$ by Student's *t*-test. Number of samples is shown in the bar. Clones were induced by early 1st instar heat shock and labeled with *UAS-mCD8::GFP* driven by *GH146*. Scale bar: 50 μm.

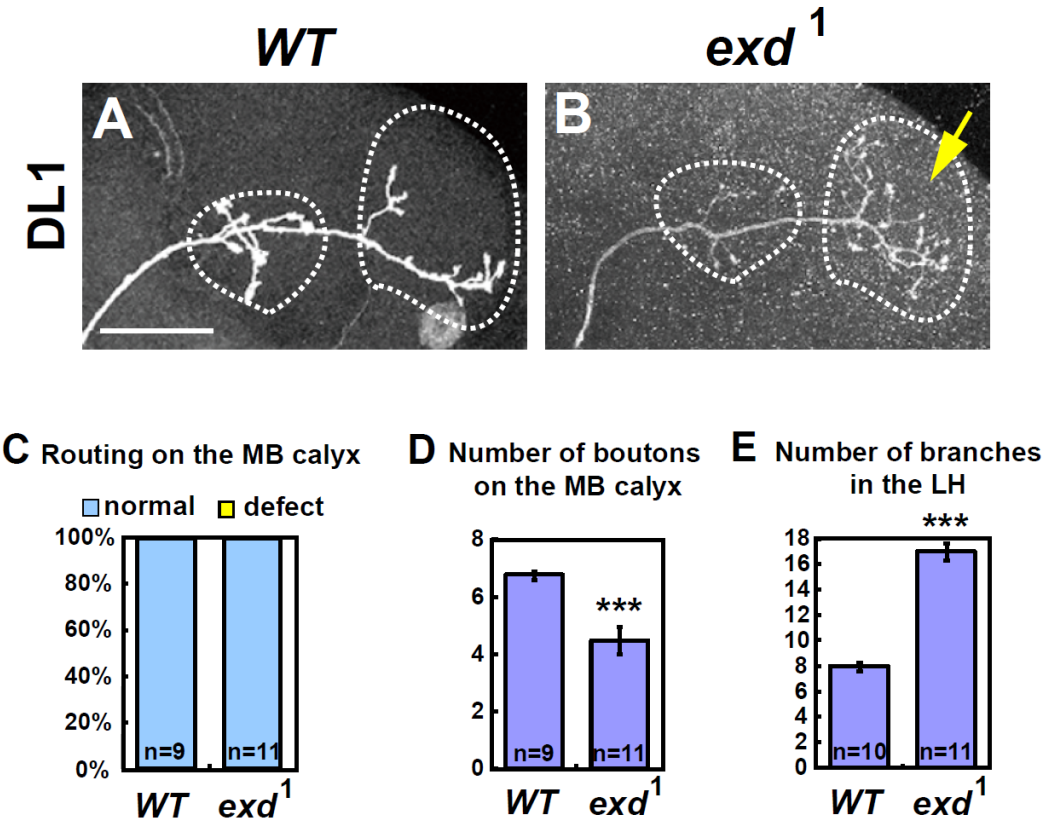
WT
exd 1
DL1
A
B
C Routing on the MB calyx
normal
defect
100%
80%
60%
40%
20%
0%
n=9
n=11
WT
exd 1
D Number of boutons on the MB calyx
8
6
4
2
0
***
n=9
n=11
WT
exd 1
E Number of branches in the LH
***
18
16
14
12
10
8
6
4
2
0
n=10
n=11
WT
exd 1

Figure 31. Expression of Hth and Exd in wild-type PNs.

(A) Expression of Hth and Exd in the adult AL neurons. Hth (red) and Exd (blue) are co-expressed in many of the AL neurons, including anterodorsal (ad), lateral (lat) and ventral (ven) PNs. (B–D) Double immunostaining for Hth and Exd in the larval, pupal and adult ad-PNs. Optical sections. Note that Hth and Exd are co-expressed in most of the developing and adult ad-PNs. PNs were labeled by mCD8::GFP driven by *GH146* (green). Scale bars: 20 μm.

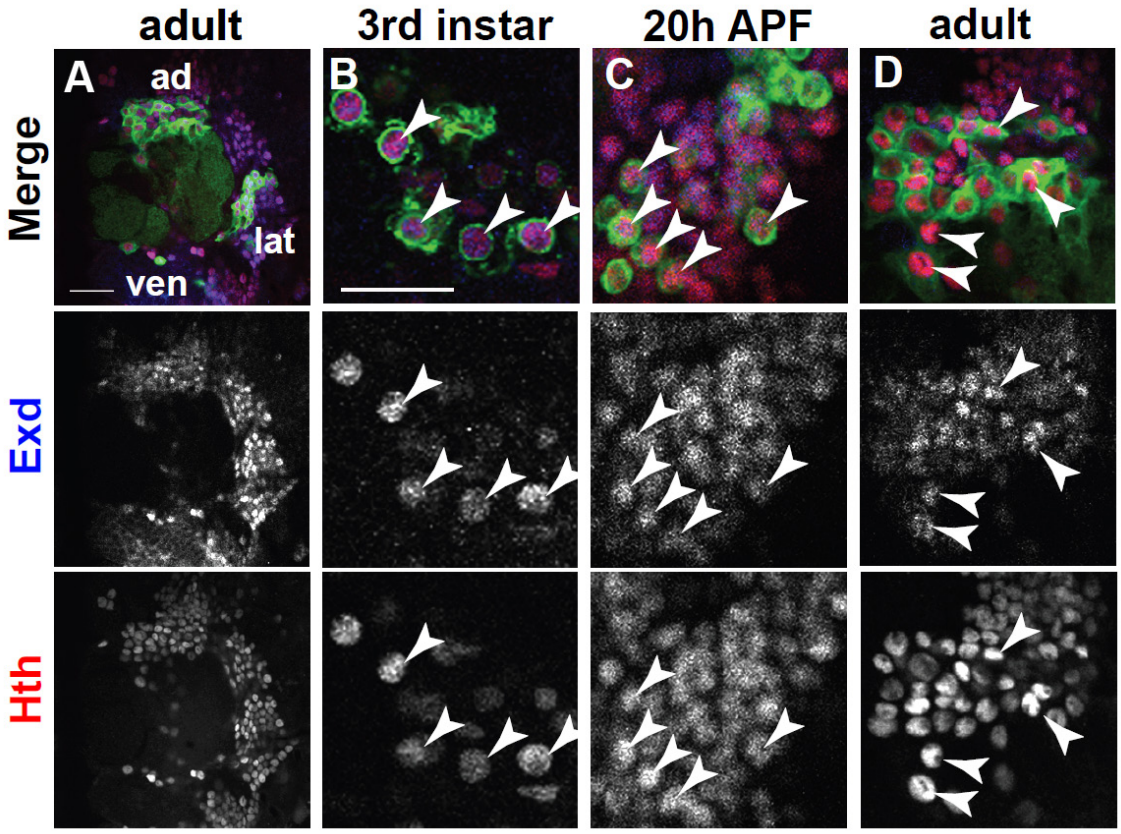
adult
3rd instar
20h APF
adult
A
ad
lat
ven
B
C
D
Merge
Exd
Hth

Figure 32. Hth and Exd were expressed in the anterodorsal and lateral progenitors at the larval stage.

Expression of Hth and Exd in the anterodorsal and lateral progenitors at the 3rd instar stage. NBs are demarcated with dotted circles. Scale bars: 20 μm.

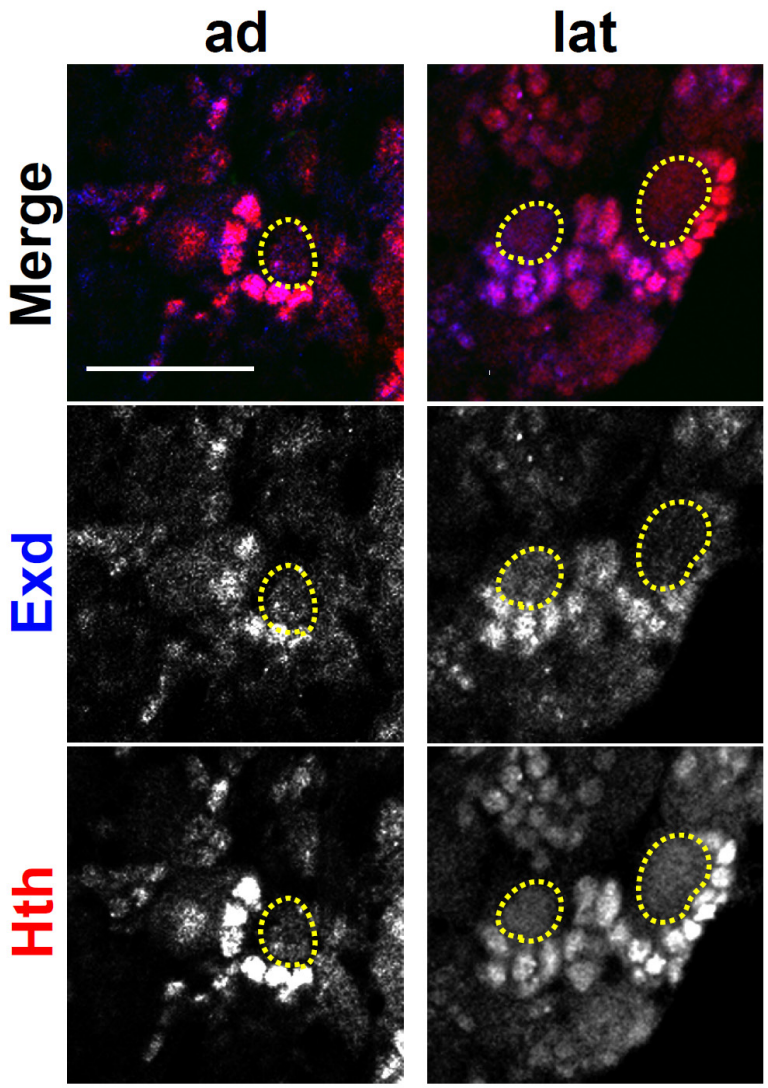
ad
lat
Merge
Exd
Hth

Figure 33. Expression of Exd in *hth* mutant clones.

(A, B) Expression of Exd in hth^{P2} mutant ad-NB clone at the 20 h APF (A) and adult (B). Note the absence of Exd expression in the hth^{P2} cells (arrowheads in A, B). (C, D) Expression of Exd in DL1 single-cell clones at the adult stage. Exd is expressed in the wild-type but not in the hth^{P2} clone (arrowheads in C, D). Clones were induced by early 1st instar heat shock and labeled with mCD8::GFP driven by *GH146*. Scale bars: 20 μm for A, 10 μm for C. Optical sections.

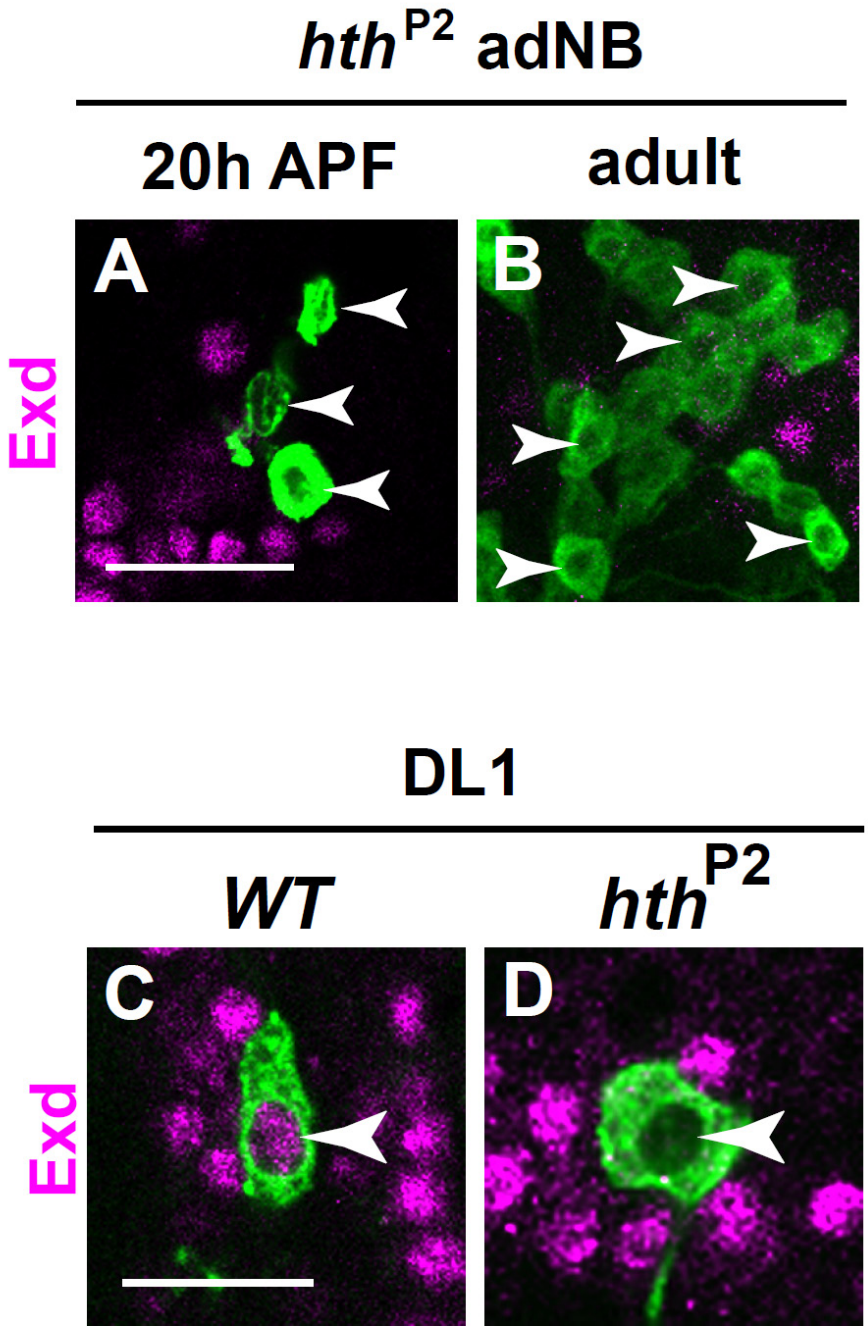
hth P2 adNB
20h APF
adult
A
B
Exd
DL1
WT
hth P2
C
D
Exd

Figure 34. Expression of Hth in *exd* mutant clones.

(A, B) Expression of Hth in exd^{1} mutant ad-NB clones at 20 h APF (A) and adult (B). Note the absence of Hth expression in the exd^{1} cells (arrowheads in A, B). (C, D) Expression of Hth in DL1 clone. Hth is expressed in the wild-type but not in the exd^{1} clone (arrowheads in C, D). Clones were induced by early 1st instar heat shock and labeled with mCD8::GFP driven by *GH146*. Scale bars: 20 μm for A, 10 μm for C. Optical sections.

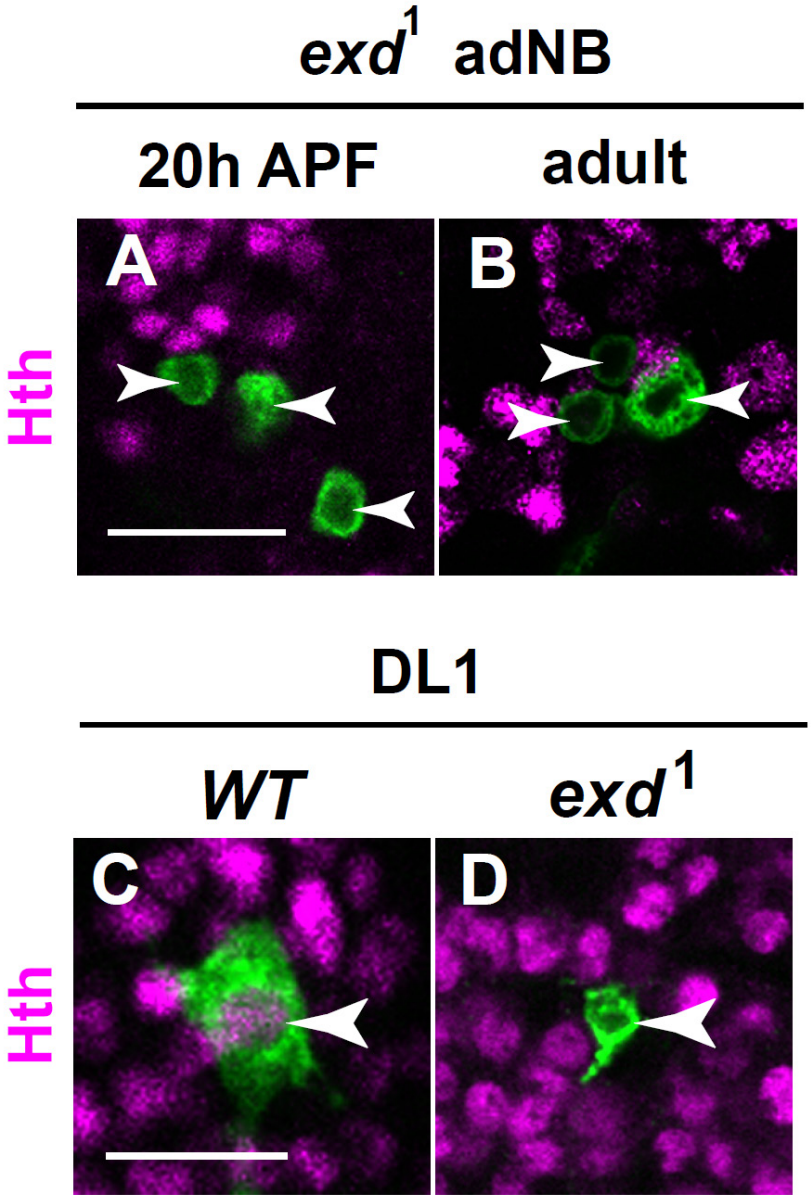
exd1 adNB
20h APF
adult
A
B
Hth
DL1
WT
exd1
C
D
Hth

Figure 35. Expression of Acj6 in wild-type PNs.

(A–C) Double immunostaining for Hth and Acj6 in ad-PNs. Optical sections. Hth (red) and Acj6 (blue) were co-expressed in ad-PNs (arrowheads) at the larval, pupal and adult stages. PNs are labeled with *mCD8::GFP* driven by *GH146* (green). Scale bar: 20 μm.

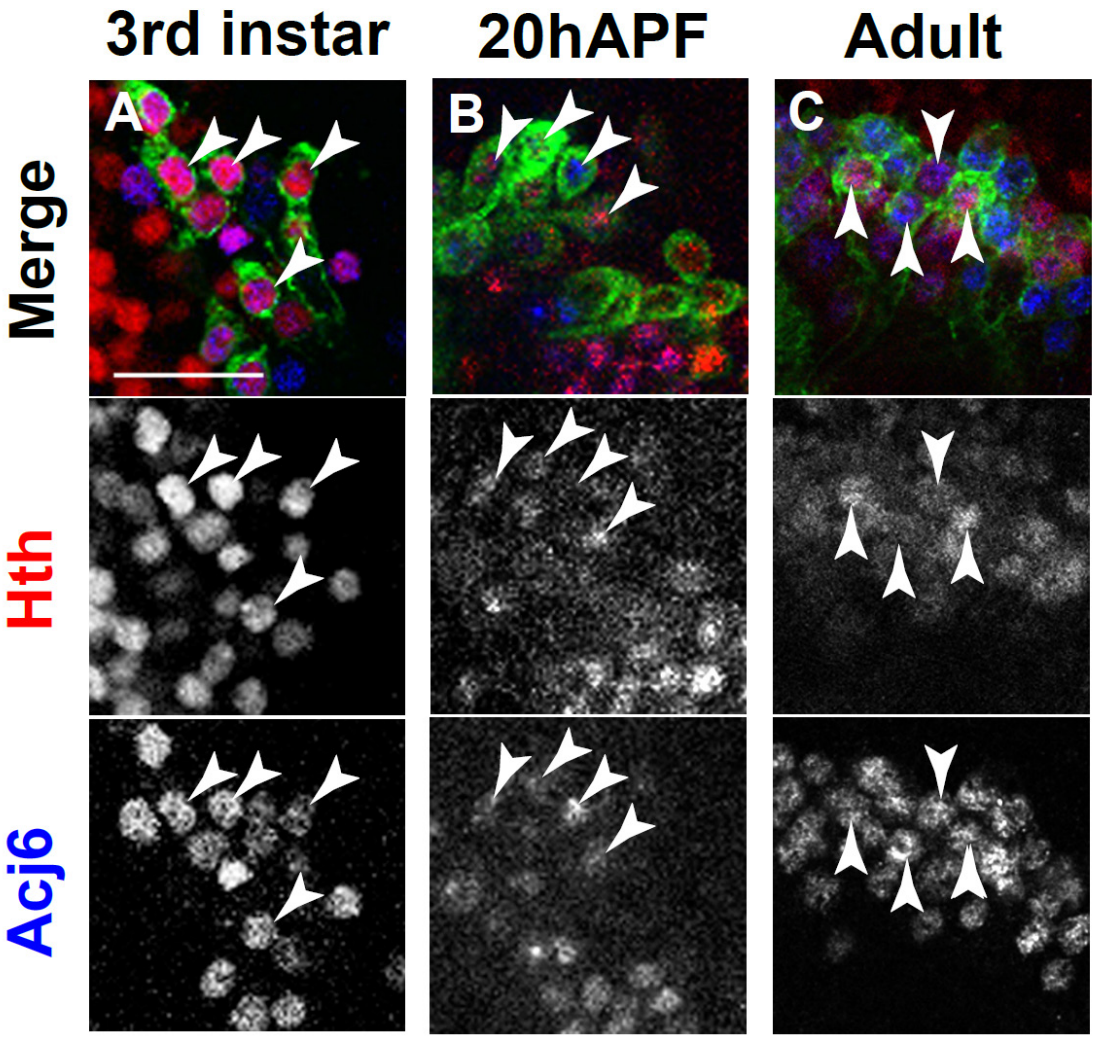
3rd instar
20hAPF
Adult
A
B
C
Merge
Hth
Acj6

Figure 36. Expression of Acj6 was not altered in the *hth* mutant PNs and vice versa.

(A) Expression of Acj6 in a hth^{P2} mutant clone. (B) Expression of Hth in an $acj6^{6}$ mutant clone. Adult brains. Optical sections. Expression of Acj6 was retained in hth^{P2} mutant PNs (arrowheads in A), and the expression of Hth was retained in $acj6^{6}$ mutant PNs (arrowheads in B). Mutant clones were induced by early 1st instar heat shock and labeled with *mCD8::GFP* driven by *GH146* (green). Scale bar: 20 μm.

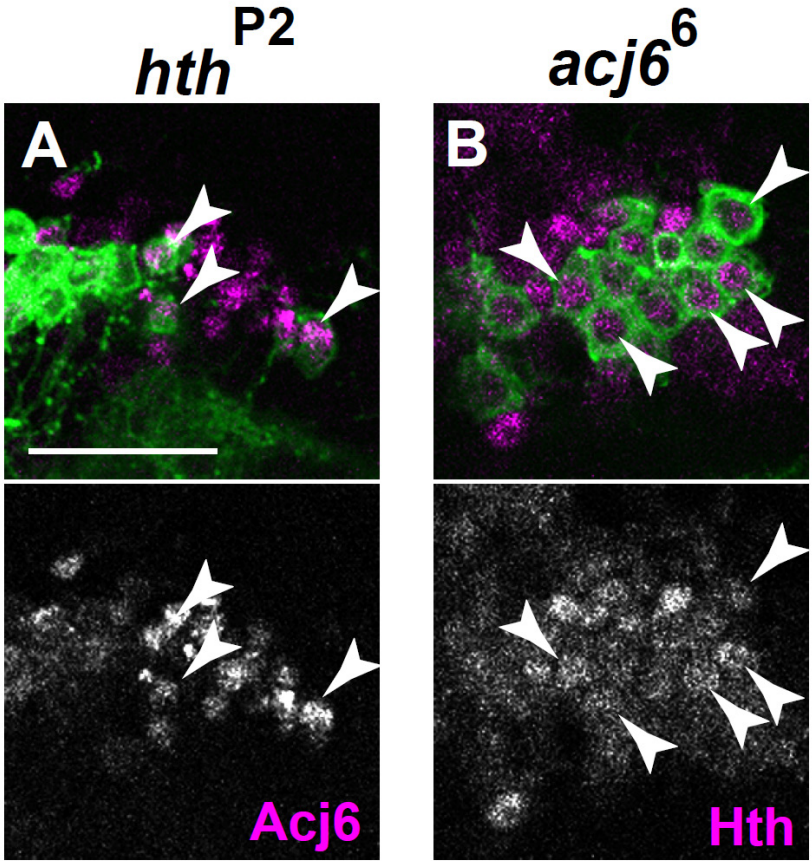
hth P2
acj6 6
A
B
Acj6
Hth

Figure 37. Expression of Lola in wild-type PNs.

(A-C) Double immunostaining for Hth and Lola in ad-PNs. Optical sections. Hth (red) and Lola (blue) were co-expressed in ad-PNs (arrowheads) at the larval, pupal and adult stages. PNs were labeled with *mCD8::GFP* driven by *GH146* (green). Scale bar: 20 μm.

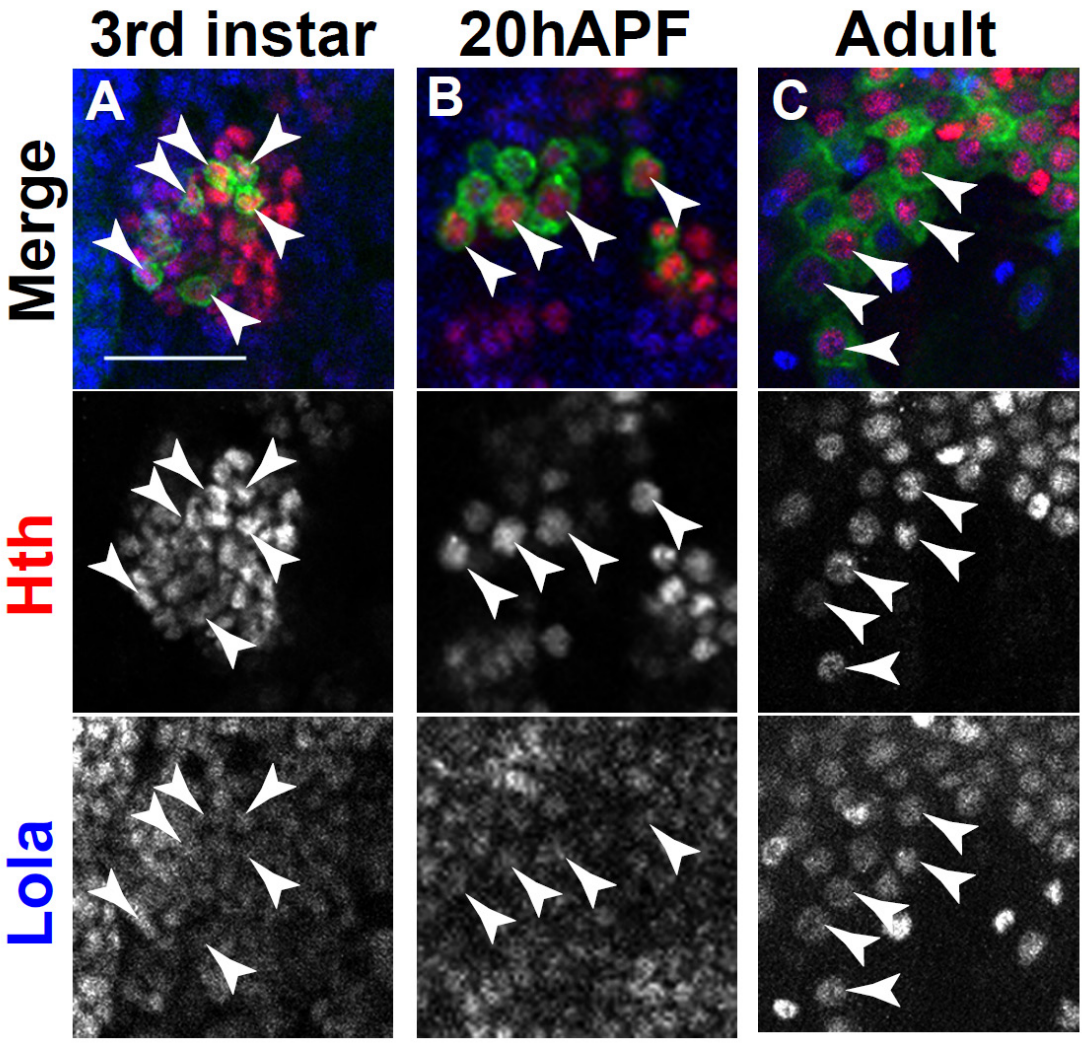
3rd instar
20hAPF
Adult
A
B
C
Merge
Hth
Lola

Figure 38. Expression of Lola was not altered in the *hth* mutant PNs and vice versa.

(A) Expression of Lola in a hth^{P2} mutant clone. (B) Expression of Hth in a $lola^{ore76}$ mutant clone. Adult brains. Optical sections. Expression of Lola was retained in hth^{P2} mutant PNs (arrowheads in A), and the expression of Hth was retained in $lola^{ore76}$ mutant PNs (arrowheads in B). Mutant clones were induced by early 1st instar heat shock and labeled with *mCD8::GFP* driven by *GH146* (green). Scale bar: 20 μm.

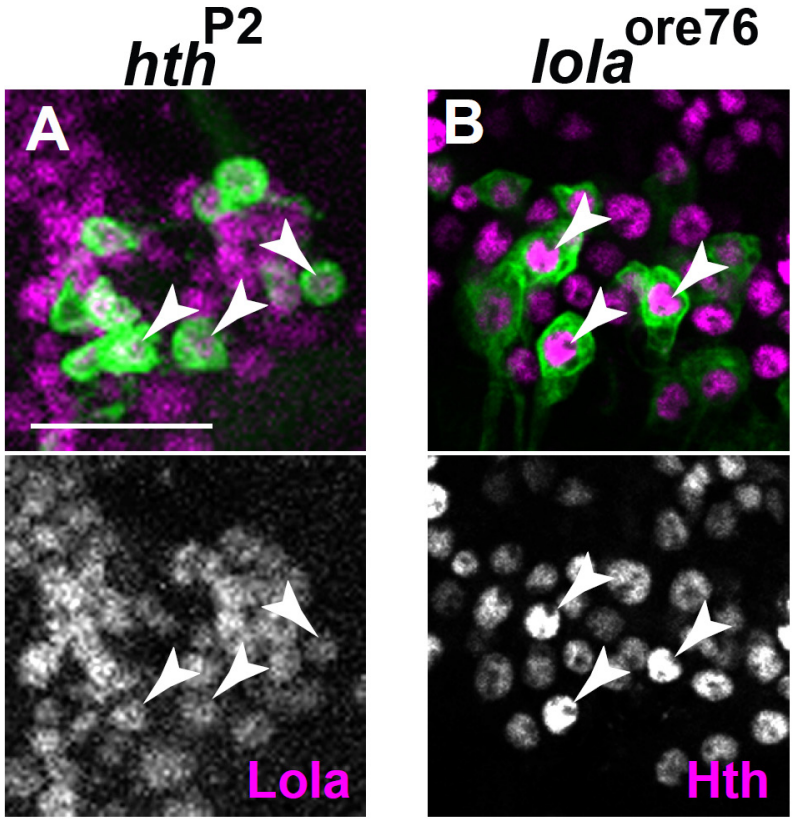
hth P2
lola ore76
A
B
Lola
Hth